Flexural Behaviour of Unreinforced Alternative Masonry Walls

by

Jean-Pierre Daniel Jooste

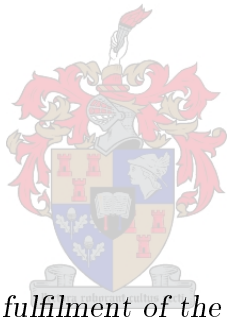

Thesis presented in partial fulfilment of the requirements for the degree of Master of Engineering in the Faculty of Engineering at Stellenbosch University

Supervisor: Dr Wibke de Villiers

December 2020

Declaration

By submitting this thesis electronically, I declare that the entirety of the work contained therein is my own, original work, that I am the sole author thereof (save to the extent explicitly otherwise stated), that reproduction and publication thereof by Stellenbosch University will not infringe any third party rights and that I have not previously in its entirety or in part submitted it for obtaining any qualification.

Date: December 2020 .....

Abstract

Flexural Behaviour of Unreinforced Alternative Masonry Walls

J.D. Jooste

Department of Structural Engineering,
University of Stellenbosch,
Private Bag X1, Matieland 7602, South Africa.

Thesis: MEng (Civil)

December 2020

Over two million households in South Africa reside in informal housing. In an effort to provide adequate formal housing to these citizens, government subsidised 40m^2 houses are being constructed, referred to collectively as low-income housing (LIH). The walling systems of these structures are predominantly unreinforced masonry (URM) constructed out of conventional masonry units (CMUs). In South Africa, fired clay brick and concrete blocks are the CMUs of choice. The environmental performance of these materials is poor due to the high temperatures required to manufacture fired clay brick and cement. Furthermore, the chemical reaction that produces cement clinker releases CO_2 regardless of the source used to heat it.

To reduce the environmental impact of providing LIH, it has been proposed that these structures could be built using alternative masonry units (AMUs) with lower embodied carbon values and improved thermal performance. The ongoing adoption of the performance-based European masonry building code (Eurocode 6) provides an avenue for AMUs to gain access into the local housing market. However, to facilitate the development of AMU-specific performance based regulations, the minimum mechanical requirements of AMUs need to be determined.

According to the South African loading code (SANS 10160 - Parts 1, 3 and 4) buildings must be able to withstand wind and, in certain areas, seismic loads. The walls of LIH must be able to withstand the out-of-plane (OOP) application of these loads through flexure. This thesis is an experimental investigation into the flexural behaviour of URM walls constructed out of AMUs. It forms part of an effort by a research group at Stellenbosch University to determine the minimum mechanical requirements of a broad spectrum of AMUs. This spectrum is represented by units composed of geopolymer (GEO), compressed stabilised earth (CSE) and adobe (ADB). One CMU, composed of concrete (CON) acts as a benchmark across all of the studies.

To determine the flexural behaviour of walls constructed from these materials, a large quantity of the aforementioned units were manufactured in such a way as to closely match those produced by other members of the research group. Two cement-sand mortars with target strengths of 7MPa and 20MPa were developed for the construction of masonry specimens. Thereafter, a flexural strength test setup was developed and used to conduct tests on small walls constructed out of these units and mortars. To supplement the flexural wall strength results, the compressive strength and modulus of elasticity of the masonry, units and mortar was also tested. Further tests were also conducted on the unit dry density and on the mortar consistency and flexural strength.

The developed test setup successfully tested walls constructed out of 20MPa and 7MPa mortar for each unit-type investigated. The flexural strengths of the CON, GEO and CSE walls were equivalent to or greater than design flexural strengths proposed by local design standards for equivalent CMUs. This implies that these materials are strong enough to withstand relevant OOP loading in standard design configurations. The data produced from this test and the supplementary tests are suitable for use in numerical modelling and contributes to the existing body of literature on AMUs. This further contributes to the cause of developing performance-based standards for AMUs.

Uittreksel

Flexural Behaviour of Unreinforced Alternative Masonry Walls

J.D. Jooste

Departement Struktuur Ingenieurswese,
Universiteit van Stellenbosch,
Privaatsak X1, Matieland 7602, Suid Afrika.

Tesis: MIng (Siviel)

Desember 2020

Meer as twee miljoen huishoudings in Suid-Afrika maak gebruik van informele behuising. In 'n poging om voldoende formele behuising aan hierdie burgers te verskaf, word regeringsgesubsidieerde 40 m^2-huise gebou wat gesamentlik as lae-inkomste-behuising (LIH) bekendstaan. Die muursisteme van hierdie strukture is hoofsaaklik onbewapende messelwerk (URM) wat uit konvensionele messelwerkeenhede (CMU's) bestaan. In Suid-Afrika word gebrande kleibakstene en betonblokke die algemeenste as CMU's gekies. Die omgewingsimpak van hierdie materiale is hoog as gevolg van die hoë temperature wat vereis word om kleibakstene en sement te vervaardig. Verder stel die chemiese reaksie wat sementklinker produseer ook CO^2 vry, ongeag die bron wat gebruik is om dit te verhit.

Om die omgewingsimpak van LIH te verminder, is daar voorgestel dat hierdie struktuur gebou kan word met behulp van alternatiewe messelwerkeenhede (AMU's) met laer koolstof inhoud en verbeterde termiese gedrag. Die voortdurende gebruik van die prestasiegebaseerde Europese messelwerkboukode (Eurocode 6) bied 'n weg vir AMU's om toegang tot die plaaslike huismark te kry. Om die ontwikkeling van AMU-spesifieke prestasiegebaseerde regulasies te vergemaklik, moet die minimum meganiese vereistes van AMU's egter bepaal word.

Volgens die Suid-Afrikaanse laskode moet geboue wind en, in sekere gebiede, seimiese lasgevalle kan weerstaan. Die mure van LIH moet die uit-vlak (OOP) aanwending van hierdie laste deur middel van buiging kan weerstaan. Hierdie tesis is 'n eksperimentele ondersoek na die buiggedrag van URM-mure wat uit AMU's bestaan. Dit vorm deel van 'n poging deur 'n navorsingsgroep aan die Universiteit Stellenbosch ten doel om die minimum meganiese vereistes van 'n wye spektrum AMU's te bepaal. Hierdie spektrum word voorgestel deur eenhede wat uit geopolymer (GEO), saamgeperste gestabiliseerde grond (CSE) en adobe (ADB) bestaan. Een CMU, saamgestel uit beton (CON), dien as die maatstaf vir al die studies/eksperimente.

Om die buiggedrag van mure wat uit hierdie materiale bestaan te bepaal, is 'n groot hoeveelheid van die bogenoemde eenhede op so 'n manier vervaardig dat dit goed ooreenstem met dié wat deur ander lede van die navorsingsgroep vervaardig word. Twee sement-sandmortels met teikensterktes van 7MPa en 20MPa is ontwikkel vir die konstruksie van messelwerkmonsters. Daarna is 'n opstelling vir buigsterkte-toetsing ontwikkel en gebruik om toetse op klein mure uit te voer wat uit hierdie eenhede en mortels bestaan. Om die buigsterkte-resultate aan te vul, is die druksterkte en elastisiteitsmodulus van die messelwerk, eenhede en mortel getoets. Verdere toetse is ook uitgevoer op die droë digtheid van die eenheid en op die mortel se bestendigheid en buigsterkte.

Die ontwikkelde toetsopstelling het mure wat uit 20M en 7M mortel gebou is, suksesvol getoets vir elke eenheidstipe wat ondersoek is. Die buigsterkte van die CON-, GEO- en CSE-mure was dieselfde of beter as die buigsterkte wat deur plaaslike ontwerpstandaarde vir ekwivalente CMU's voorgestel is. Dit impliseer dat hierdie materiale sterk genoeg is om relevante OOP-laste in standaard ontwerpkonfigurasies te weerstaan. Die data van hierdie toets en die aanvullende toetse is geskik vir gebruik in numeriese modellering en dra by tot die bestaande literatuur oor AMU's. Dit dra ook verder by tot die ontwikkeling van prestasiegebaseerde standaarde vir AMU's.

Acknowledgements

This project could not have been completed alone. I would like to extend my heartfelt gratitude to:

- My supervisor, Dr Wibke De Villiers, for her invaluable insight, guidance, calm demeanour and patience - even at the most trying times.
- Johannes Fourie, Prince Shiso and Migal Schmidt upon whose knowledge this work depended.
- The technical staff of the Civil Engineering laboratories. This includes: Mr Johan van der Merwe for his role in the design and construction of many of the setups used in this project and who, together with Mr Viljoen, provided me with the necessary training.
- The support staff of the Civil Engineering laboratories. Especially Mr Ramat and Mr Jones of the Structural laboratory for assisting, training and guiding me throughout the entire experimental programme.
- Timothy Combrinck who worked tirelessly to make the unit manufacturing and setup construction possible.
- Kintu-Kisule Sebuyira, Hamzah Essa and Phathutshedzo Masindi who assisted in unit manufacturing and testing, for your diligence and interest.
- The laboratory management, Dr Stephen Zeranka and Jurie Visagie for training me to use the laboratory equipment and assisting me in conducting the tests.
- To all staff, fellow researchers and friends at the Civil Engineering laboratories who cooperated with me, worked alongside me and supported me.
- Mariska Bezuidenhout, for encouraging me and believing in me.
- My mother, father and sister. You laughed with me when I succeeded and picked me up when I fell. I could not have done this without you!

Contents

List of Figures

List of Tables

Nomenclature

Acronyms

Acronym	Expansion
AAC	alkali-activated cements
ADB	adobe
AMU	alternative masonry unit
ASTM	American Society for Testing and Materials
CMU	conventional masonry unit
CON	concrete
COV	coefficient of variation
CSE	compressed stabilized earth
DPC	damp proof course
ESLFM	equivalent static lateral force method
EN	European Norm
FA	fly ash
FV	flow value
GEO	geopolymer
GGBS	ground granulated blast-furnace slag
GGCS	ground granulated corex slag
GHG	greenhouse gasses
GSH	government-subsidised house
HDPE	high-density polyethylene
IPE	I-Profile Européennes (European I-Beam Profile)
NBR	National Building Regulations
LIH	low-income housing
LVDT	linear variable displacement transducer

LC	load cell
MSW	mine spoil waste
OOP	out-of-plane
OPC	ordinary Portland cement
OMC	optimum moisture content
PFC	parallel flange channel
SABS	South African Bureau of Standards
SANS	South African National Standards
SHS	square hollow section
URM	unreinforced masonry

Latin Symbols

Symbol	Unit	Description
b	mm	dimension of flexural wall perpendicular to span
C_{T_f}	-	factor used to determine fundamental period of vibration
E_{cu}	GPa	unit modulus of elasticity in compression
E_w	GPa	wallette modulus of elasticity in compression
E_m	GPa	mortar modulus of elasticity in compression
E_x, E_y	GPa	stiffness of masonry in the x and y directions
f_d	MPa	compressive strength of masonry in direction of thrust
f_{cm}	MPa	mortar compressive strength
f_{cu}	MPa	unit compressive strength
f_{cw}	MPa	wallette compressive strength
f_{xdi}	MPa	characteristic wall flexural strength, in the direction i
$f_{xd1,app}$	MPa	apparent characteristic wall flexural strength, in the vertical direction
$f_{x,m}$	MPa	mortar flexural strength
$f_{x,w}$	MPa	wall flexural strength
F_{max}	N	ultimate recorded force
h_t	m	height of a building from the foundation or from the top of a rigid basement
k	-	factor of the stiffness orthotropy of masonry
L	m	span of wall between supports for arch thrust equations
l	m	total wall length

l_1	mm	space between support bearings of flexural wall test
l_2	mm	space between load bearings of flexural wall test
l_3	mm	distance between support bearing and wall edge in flexural wall test
l_s	mm	dimension of wall in direction of span of flexural wall test
M_a	Nm	external, applied moment
$M_{Ed,i}$	Nm	applied design moment, in the direction i
M_i	Nm	component of the internal moments, in the direction i
M_{Rdi}	Nm	design value of the moment of resistance, in the direction i
p	MPa	pressure applied to the surface of a slab
q_{lat}	MPa	lateral load
$S_d(T_f)$	-	design spectrum for elastic analysis
T	kN	arch thrust
t	m	wall thickness
t_u	m	unit thickness
T_f	s	fundamental period of vibration
V_n	kN	design base shear force
W_{Ed}	Nm	applied horizontal pressure
W_n	kN	nominal sustained vertical load acting on a structure
z	mm	displacement of a slab
Z_i	mm^3	elastic section modulus, in the direction i

Greek Symbols

Symbol	**Unit**	**Description**
α_i	-	bending moment coefficient, in the direction i
δ	mm	midpoint wall deflection for arch thrust calculations
μ	-	orthogonal strength ratio of masonry
$\rho_{g,u}$	kg/m^3	unit dry density
σ_d	MPa	design compressive stress
θ	rad	angle of rotation

Chapter 1

Introduction

According to the most recent national census, approximately 2.1 million South African households reside in an informal dwelling (Statistics South Africa, 2016). Adequate housing is an internationally recognised fundamental need and human right. As stipulated by Section 26 of the South African Constitution (1996), the state must take measures to achieve this right. A number of approaches have been pursued to this end, including the provision of government-subsidised housing for low-income households. Typically this has taken the form of small, single-storey houses. These are usually built with masonry consisting of cementitious mortar and fired clay bricks or concrete blocks, collectively termed as conventional masonry units (CMUs).

The manufacture of CMUs requires that raw materials are subjected to high temperatures, which is mostly achieved by burning fossil fuels. The chemical reaction required to produce cement from limestone also releases carbon dioxide as a by-product (Domone and Illston, 2010). These activities contribute to green house gas (GHG) emissions and counteracts the nation's efforts to adhere to the Paris Agreement of which it became a part of in 2016.

It has been proposed that the aforementioned single storey low-income housing (LIH) could be constructed with alternative masonry units (AMUs) with less embodied carbon. This would potentially support both the efforts of housing and GHG emission reduction. The South African masonry industry is in the process of adopting the European design code, Eurocode 6, as SANS 51996 - Eurocode 6: Design of Masonry Structures. This standard is more performance-based than the standard it will replace, SANS 10164 - The Structural Use of Masonry. This could make the introduction of AMUs more viable than previously considered (De Villiers, 2019).

Research has been undertaken at Stellenbosch University to support the introduction of AMUs into the LIH market. A major objective of this research was to experimentally determine the mechanical properties of three AMUs and one CMU. This would enable comparisons to be drawn between the materials and contribute to our current understanding of their characteristics. The experimental data would also be made available to a separate study to validate a numerical model, to assess the structural performance of AMU walls.

One critical property of masonry walling is its ability to resist out-of-plane (OOP) loading. Various load-cases could result in OOP loading, but wind and earthquake loads are the most relevant scenarios for LIH. Due to the comparatively slender dimensions of contemporary masonry walling, OOP loads are generally resisted by some degree of bending. The aforementioned design standards allow the designers to designate flexural strengths for non-standard masonries based on standard quasi-static tests. This work seeks to experimentally determine the flexural characteristics of the aforementioned AMUs and CMU by applying such a test.

1.1 Aims

This study aims to determine the flexural behaviour of masonry walls composed of AMUs. This will be achieved experimentally, in such a way that the results might be used to validate a numerical model. Ultimately, the work is intended to contribute to the existing body of knowledge on the flexural behaviour of AMUs, while supporting the cause of providing LIH in a more environmentally sustainable manner.

1.2 Objectives and Methodology

Three main objectives were pursued in this study:

- Manufacture alternative and conventional masonry units that are similar to those produced in previous studies at Stellenbosch University.
- Design and construct a test setup that can test the flexural behaviour of alternative masonry.
- Experimentally assess the flexural behaviour of the alternative masonry so that the results may be used to validate a numerical model.

This thesis forms part of a group of research conducted at Stellenbosch University. Specifically, the same AMUs and CON unit used in this study were investigated by Fourie (2017), Shiso (2019) and Schmidt (2020). The AMUs that were investigated are geopolymer (GEO) units, compressed stabilised earth (CSE) units and adobe (ADB) units. The CMU, used as a benchmark, was chosen as a solid concrete (CON) unit. In achieving the first objective, the results produced by this study could be related to those presented by the group. This allows observations to drawn from the group as a whole. Furthermore, the numerical model would be able to obtain a wider range of parameters.

The unit compressive strength and secant elastic modulus was tested at an age of 28-days for the purposes of assessing the achievement of the first objective. The dry densities of the units were also tested after the completion of the masonry flexural behaviour tests. It should be noted that during the time of manufacturing the units of this study, only the work provided by Fourie (2017) and Shiso (2019) had been completed.

Achievement of the second objective was required before the aim of this study could be pursued. A literature review was conducted, partly so that existing tests methodologies and setups could be studied and inform the design of this setup. Based on the literature review, a setup was designed and constructed that was suitable given the constraints of the timeline and laboratory materials.

To achieve the third objective, masonry flexural strength tests were performed using the constructed test setup. However, the numerical model required input parameters unique to this study before it could produce results for validation. For this reason, a series of auxiliary unit, mortar and masonry tests were completed. These tests were all performed at an age as close as possible to that of the masonry flexural strength test so as to represent the parameters of the masonry specimens as closely as possible. The unit, mortar and masonry compressive strength and secant elastic modulus were tested for this reason. These tests along with the mortar consistency (flow table) tests were also completed as a means of quality control. The mortar flexural strength was tested as an additional auxiliary test. This parameter was not required by the model, but was investigated as an additional parameter against which the masonry flexural strengths could be compared.

The third main objective of this thesis also contributes to a larger, universal aim of experimental work in general, which is to contribute to the existing literature and provide experimental data to future researchers. The auxiliary tests were also performed for this purpose, so that future researchers might have a more complete data set from which to work. It should be noted that, although, according to the first objective, the units studied are of the same types produced by the aforementioned group of research, it was not possible to replicate the mechanical properties of these units exactly due to raw material variabilities.

1.3 Scope

The work presented in this study is limited to unreinforced masonry walls consisting of solid blocks and cementitious mortar. Dynamic loading is not covered - all material and structural strength tests were performed by applying monotonic, quasistatic loads.

1.4 Thesis Layout

The structure of this thesis is as follows. In Chapter 2, a background of the current topic is presented by briefly discussing the current regulatory framework surrounding the construction of LIHs and the use of CMUs in South Africa. This is followed by a brief description and discussion of the AMUs investigated in this study. Finally, a background on OOP loading and the manner in which masonry is designed to resist it is provided within a South African context.

In Chapter 3, a literature review is provided to present the effects of OOP loading on URM walls. This covers the different modes of failure that walls undergo and the parameters that affect the strength and load-displacement behaviour for each mode. Thereafter, a review of the types of OOP masonry tests is covered. Finally, the design and analysis techniques relevant to South Africa are presented as well as a brief description of techniques proposed by other authors and prescribed in other national codes.

The methods, materials and apparatus with which the units and mortar were manufactured are provided in Chapter 4. First, the relevant material properties of the material constituents are presented. Thereafter the manufacturing procedures, mix designs and curing conditions of the units are provided before the same is done for the mortar.

The experimental design of the study is presented in Chapter 5. This chapter first provides an overview of the experimental schedule. Thereafter, the specimens, apparatus and methods that were applied for tests are provided in separate sections. Greater detail is provided on the design and construction of the wall flexural strength tests.

The results of the experimental investigation are provided in Chapter 6. The individual or average results of each test are provided graphically and in tables accompanied by a description of the general trends therein. Additionally, the validity of the results and suitability of the applied test setups is also discussed.

Finally, the conclusions and recommendations of this thesis are presented in Chapter 7. These are based on the achievements of the aims and objectives of the study, but also include observations that were made throughout the experimental programme. The list of references and the appendices follow-on from this chapter.

Chapter 2

Background

2.1 LIH and Category 1 Buildings

The approval of construction plans and erection of all buildings are subject to the South African National Building Regulations and Building Standards Act (Act No. 103, 1977). The act stipulates which processes need to be followed and the responsibilities of parties involved, but does not provide any technical specifications. The National Building Regulations (NBR) provide technical guidance in applying the act. The design and assessment of all buildings are thus subject to the current version of the NBR, SANS 10400 (2010).

The NBR introduced a new standard of buildings, Category 1 buildings, in its 2004 edition, to reduce the cost of providing infrastructure in low-income communities. The cost-reduction is achieved by relaxing serviceability requirements. These include differences in allowable deflections, rain penetration and maintenance requirements when compared to non-Category 1 buildings. A building may be designed as Category 1 if it adheres to certain restrictions in terms of dimensions and occupancy.

As mentioned in Chapter 1, LIH is often provided in the form of small, single-storey masonry houses. These are referred to as government-subsidised houses (GSHs) and are typically simple constructions with short spans and small floor plans as seen in Figure 2.1. It is anticipated that most new GSHs will be designed as Category 1 buildings since the dimensional limits should easily be complied with given the spatial requirements of the building. Furthermore, the reduced cost would allow more housing units to be constructed.

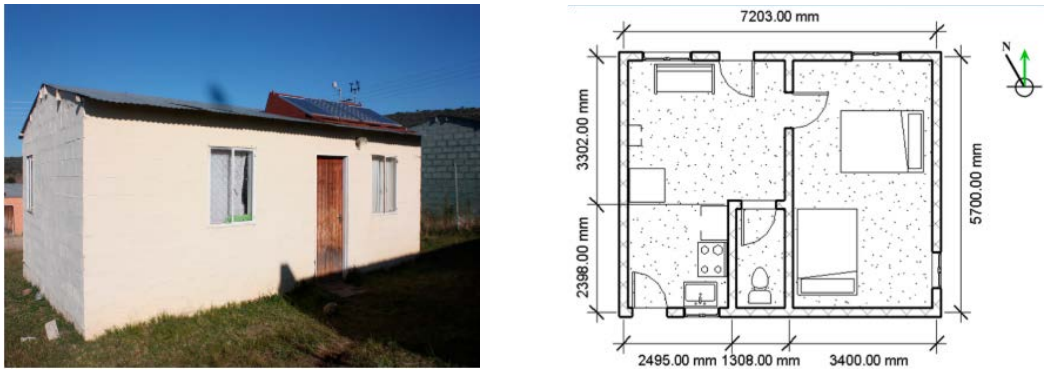

(a) (b)

Figure 2.1: Photo (a) and plan (b) of a typical GSH (Kelvin *et al.*, 2017, p. 6)

2.2 Conventional Masonry Units

Conventional masonry units (CMUs) can be defined more precisely as masonry units that are conventionally used and are regulated by the provision and application of standards (De Villiers, 2019). A summary of South African CMUs is provided in Table 2.1. The standards that have been provisioned for each unit-type are materials based standards that state requirements that need to be fulfilled by masonry unit manufacturers, such as dimensional tolerances and required compressive strengths as well as the methods that should be used to test for those parameters.

Table 2.1: South African CMUs and their relevant standards

CMU	Standard
Autoclaved Aerated Concrete Masonry Units	SANS 50771-4 (2007)
Burnt Clay Masonry Units	SANS 227 (2007)
Calcium Silicate Masonry Units	SANS 285 (2010)
Concrete Masonry Units	SANS 1215 (2008) SANS 50771-3 (2015)

The use of CMUs is also catered for in other regulatory documents. The current South African code of practice for The Structural Use of Masonry: SANS 10164 (1989) makes provision for CMUs. This takes the form of prescribing requirements that should be fulfilled at a structural design level (such as the use of movement joints) and on site to ensure good construction quality. Furthermore, the standard provides characteristic material strengths for masonry constructed with CMUs and common, qualifying mortars.

The wide-spread use and study of these CMUs have entrenched them within the building sector and within the minds of consumers - particularly in South Africa (De Villiers, 2019). However, their use does have environmental drawbacks. Concrete and burnt clay units in particular are large contributors of greenhouse gasses (GHGs) either through their required energy inputs or the chemical reactions of their raw materials. Furthermore, their production draws from a limited range of natural resources. These realizations in combination with the aforementioned climate and housing crises have led researchers to study the feasibility of using alternative masonry units (AMUs) for housing.

2.3 Alternative Masonry Units

In contribution to this research project, Fourie (2017) developed and characterised three AMUs with widely differing material properties and one CMU to act as a benchmark. The AMUs were chosen so that they consisted of materials that were readily available in South Africa. All subsequent experimental work by researchers within the same group was done with units that attempted to match the mix designs and properties of these units as closely as possible. This section will provide a background on each of the aforementioned AMUs.

2.3.1 Adobe Unit (ADB)

Adobe units, also referred to as "mud-bricks", consist of moist earth that has been moulded into shape and left to air-dry or sun-dry until hardened. This is often achieved by pressing the mixture into wooden moulds by hand, as seen in Figure 2.2. Organic material, such as straw, is sometimes also incorporated to improve their mechanical and thermal properties. Evidence of their use has been found world-wide and dates back to at least ten thousand years (Drysdale *et al.*, 1994). Adobe is attractive as an environmentally friendly alternative due to its low energy production requirements. Furthermore, adobe masonry has proven to be a superior thermal regulator due to its high specific heat value (Parra-Saldivar and Batty, 2006). Its components are widely available and can be recycled with basic tools, making it a popular choice for developing nations.

In designing adobe blocks, the parent soil should be analysed for suitability. The main characteristics to consider are the soil's composition, plasticity and optimum moisture content. The material should be composed of correct proportions of clay, silt and sand. While clay gives the finished unit cohesion, sand improves the unit's abrasion resistance and its inclusion helps to prevent harmfully high levels of water absorption. The soil's optimum moisture content should be measured to determine how much water should be mixed with the soil to provide the final product with the maximum density and strength (Norton, 1986).

Figure 2.2: Adobe brickmakers using a wooden mould (Horn, 2006)

Adobe masonry is generally of low to moderate strength. To counteract this, most forms of adobe walls are thick, massive (solid) structures. This requires larger wall volumes with more material consumption. However, the consequential higher thermal mass is thought to be one of the main contributors to earth building's superior thermal-regulatory properties - potentially reducing the energy use of the inhabitants. Unfired earth absorbs large quantities of water and can soften under prolonged exposure to moisture. Furthermore, its thermal conductivity increases linearly under increased humidity. This makes adobe most suitable for warm, dry regions with little rainfall (Olukoya Obafemi and Kurt, 2016).

2.3.2 Compressed Stabilized Earth Unit (CSE)

The alteration of a soil's composition or properties to fulfil an engineering requirement can be defined as stabilization. This practice was initiated by geotechnical practitioners to construct road bases, and subsequently adopted for the production of masonry units in the 1940s (Venkatarama Reddy, 2012). With regards to earth based blocks, three main stabilization techniques have been identified: chemical, mechanical and physical stabilization, although colloquially, the term 'stabilization' is often associated with chemical additives (Rigassi, 1985).

Chemical stabilization implies altering the chemistry of a unit through the addition of reactive compounds. A variety of materials such as bitumen, iron mine spoil waste (MSW), blast furnace slag and fly ash (FA) have been investigated as stabilizing agents (or partial replacements thereof) (Nagaraj and Shreyasvi, 2017). However, Ordinary Portland cement (OPC) and lime are the most commonly used in practise (Malkanthi *et al.*, 2020). Both increase the compressive strength durability of units through the formation of calcium-aluminate and calcium-silicate hydrate gels. These products form a matrix which binds the constituents of the unit together as it hardens (Venkatarama Reddy, 2012).

In cement stabilized blocks, these hydration products begin to form upon exposure to water. The hardening process of lime-stabilized units is generally slower and

results from the reaction of lime with clay minerals to form cementitious hydrates (Bell, 1996). Notably, the addition of ground granulated blast-furnace slag (GGBS) in conjunction with lime can result in faster setting times and stronger units when compared to cement-stabilized soils (Oti *et al.*, 2009). In general, the chosen additive should depend on the properties of the base soil and the required application. Soils that contain expansive clays (such as montmorillonite) require lime to prevent excessive strains and cracking brought about by moisture. Soils that have a smaller clay fraction with less expansive clays can readily be stabilized with cement (Venkatarama Reddy, 2012).

Improvement through altering the soil composition of a unit is known as physical stabilization. This usually involves the addition of clay or sand. Mechanical stabilization occurs through compressing a unit to a specified density or with a specified energy or pressure. Although adobes are often mechanically stabilized through hand-compaction, CSE units are typically compacted with greater energy to create a denser and hence stronger final product (Rigassi, 1985). In general, CSEs have improved mechanical and durability properties and similar thermal properties when compared to adobe units, while having a lower embodied energy compared to CMUs (Venkatarama Reddy, 2009).

2.3.3 Geopolymer Unit (GEO)

Geopolymers are a subset of a larger group of binders known as alkali-activated cements (AACs), which are manufactured by exposing an aluminosilicate to an alkali. This process produces a cementitious binder from a substance that generally is not cementitious of itself (Provis, 2014; Domone and Illston, 2010). Once set, geopolymers comprise mostly of aluminosilicate gels. This differs from other alkali-activated binders, which predominantly produce calcium silicate hydrate-based gels, such as those derived from slag (Provis and Van Deventer, 2009). The unit developed for this work may not strictly qualify as a geopolymer (GEO) due to the inclusion of slag in its mix design. Nevertheless, the units were referred to as GEO since this term is used ubiquitously in practice in lieu of AAC.

Alkali activation of blast-furnace slag was first demonstrated by Kühl in 1908 (Thomas *et al.*, 2016). Further work by Purdon (1940) and Glukhovsky (1965) supported the introduction of AACs into the building sector of the USSR, China and some European nations (Dakhane, 2016). Geopolymers on the other hand were initially developed in the 1980s by Davidovits as an alternative to fire-setting polymers before their worth as a construction material was realized (Provis and Van Deventer, 2009). The possibility of AAC to fulfil the role of OPC in a more environmentally friendly manner has brought more attention to the material in recent years. The aluminosilicate cementing components are generally sourced from industrial wastes and clays, making AACs less carbon intensive than OPC (Yang *et al.*, 2013).

AACs can be manufactured from a broad range of source materials. Domone and Illston (2010) list sodium hydroxide, sodium carbonate, sodium silicates and sodium sulphate as potential alkalis. Various slags (including GGBS, granulated phosphorous slag and steel slag) have been used as well as the pozzolans including fly ash (FA), condensed silica fume (CSF), metakaolin clay and volcanic ash as cementing components. AACs therefore exhibit a wide range of mechanical properties and manufacturing requirements that depend on their composition.

In a recent review, Ding *et al.* (2016) compared the engineering properties of three groups of AACs: alkali-activated slag concretes (AASC); alkali-activated fly ash concretes (AAFC) and alkali-activated slag-fly ash concretes (AASFC). In summary, all AAC products can achieve high compressive strengths. With AAFC, elevated curing temperatures are required, while AASC and AASFC can be cured at ambient temperature. The Young's modulus of AASC can be predicted from its compressive strength according to existing OPC models quite accurately, but the same models consistently overestimate the stiffness of the latter two binders. The existing data on the tensile splitting capacity of AAC correlates well with existing concrete codes, but more data is required to confirm the similarity between AAC and OPC in this area.

Jiao *et al.* (2019) performed an experimental investigation into masonry constructed with hollow AASC blocks and a slag-based AAC mortar. They found that the shear, flexural and tensile strengths of the masonry all increased with an increase in mortar compressive strength. However, the bond strength of the AAC assemblages was found to be weaker than what the relevant Chinese building code (GB 50003-2011) predicted for concrete masonry with cement-based mortar in the same compressive strength grade. This was attributed to the greater drying shrinkages exhibited by AAC mortars.

Domone and Illston (2010) state that AAC does have disadvantages such as the aforementioned drying shrinkage, raw material variability and an inadequate understanding of long-term properties . Research into the durability of AAC is ongoing, however, and has shown promising results (Hossain *et al.*, 2015). The alkalis used in producing AACs can be corrosive, presenting a real health and safety risk to construction workers. This makes the material more suitable for prefabricated concrete elements and factory produced masonry units. Nevertheless, AACs show promise as a contender in the production of more environmentally building materials.

2.4 Out-of-Plane Loads

All buildings are required to withstand some degree of out-of-plane (OOP) loading. Structurally, this implies that the laterally loaded walls of a building are required to transmit loading to the supporting foundation and walls adequately. The magnitude and type of OOP loading and the corresponding measures of design used to resist it are region-specific. This section briefly discusses the aforementioned issues with reference to Category 1 buildings in South Africa.

SANS 10400-B lists requirements that need to be fulfilled with regards to the structural design of buildings. Compliance with the SANS 10400-B needs to be demonstrated by the completion of a rational design or assessment. Furthermore, SANS 10400-B 4.2.1.2 requires that this is achieved in accordance to the criteria laid out in South Africa's loading code, SANS 10160. Further minimum requirements over and above the aforementioned codes are also demanded. This includes the accepted levels of damage per loading type, maintenance cycles and design lives of buildings.

Seismic and wind loads are deemed the most pertinent OOP loads for the design of walls in single-storey houses. A brief background of these loads is provided as well as a description of their treatment in design and analysis according local standards. Furthermore, the expected performance of Category 1 buildings against OOP loading is discussed.

2.4.1 Wind Loading

South Africa has a complex climate with 24 different identified climatic regions (Goliger *et al.*, 2013). The strongest winds typically originate from cold fronts along the south coast or convective thunderstorms on the interior parts of the country (Kruger, 2011). Severe winds have resulted in death and injury as well as the damage and destruction of buildings in South Africa. Figure 2.3 provides examples of substantial damage to buildings induced by severe wind events. More pertinently, 70% of wind-damage cases reported from 1948 to 2000 included the damage of houses or buildings (Goliger and Retief, 2007). This highlights the importance of designing for strong wind loads as well as the need to provide formal housing, since informal houses are generally thought to fail at lower wind speeds (Goliger and Retief, 2007). Category 1 buildings fall within the scope of SANS 10160-3 (2018), which stipulates how wind actions should be applied in the design of regular buildings with a height of less than 100m. The initial step in using the wind loading code is the calculation of design peak wind speeds. These are dependent on:

- the geographical location of the structure within South Africa,
- acceptable return period of the peak wind speed,
- the wind load's reference height above ground level,
- the obstruction provided by the surrounding terrain and
- the topography of the surrounding terrain.

Thereafter, the wind speed is converted into a pressure taking into account the density of the air dependent on the reference height of the wind load above sea level. Finally this pressure is applied to the building model in zones through the use of internal and external coefficients which take into account the geometry of the building, the effect of openings and the inclination of the wind.

Figure 2.3: Wind-damaged buildings in South Africa (Goliger *et al.*, 2013, p. 72)

Besides the application of SANS 10160-3, the NBR stipulates a set of minimum wind load requirements for dwelling houses. These include that the minimum pressure applied to the system as a whole and the structural elements must exceed 370 Pa and 450 Pa respectively. A table of minimum external and internal pressures that should be applied to each building component is also supplied.

2.4.2 Seismic Loading

Unreinforced masonry (URM) is especially vulnerable to catastrophic OOP failure during seismic events (Vaculik and Griffith, 2018). The nature of the OOP collapse of URM also makes it extremely hazardous for occupants as reported by numerous studies (Sorrentino *et al.*, 2017). Furthermore, many historically significant masonry buildings in seismically active areas are vulnerable to damage or even collapse. Due to these considerations, much of the work done on the OOP behaviour of URM is driven by seismic considerations.

Seismic activity occurs in certain parts of South Africa and can be described as moderate or stable as the country is located far from the nearest tectonic plate boundary (Brandt, 2011). Nevertheless, local seismic events have caused casualties and significant damage to buildings. The most damaging of which occurred near Tulbagh on 29 September 1969 and took the lives of 12 people and levelled parts of the town, displacing and injuring many others as seen in Figure 2.4. To reduce the aforementioned loss caused by earthquakes and tremors, structures built within seismically active zones must be designed to withstand the effects of seismic activity safely. Part B of the NBR, SANS 10400-B (2012), requires that this should be achieved through

conformance with SANS 10160-4 (2017).

Figure 2.4: Building damage and displaced citizens caused by the Tulbagh earthquake of 1969 (Midzi *et al.*, 2020)

According to SANS 10160-4 (2017), only buildings located within seismically active regions are subject to its regulation. These regions are defined in Figure 2.5 provided by the same standard and are classified according to two zones. Regions that experience natural activity only are classified as Zone I, while those that experience natural and mining-induced activity are categorized as Zone II. Buildings in Zone I are required to comply with all measures set out in the standard, while the regulation of a building in Zone II is dependent on its importance class. The importance class is a number in the range of one to five and indicates the importance of a building for public safety (in ascending order). In Zone II, those of importance class I, II and III are required only to comply with the minimum conceptual design and detailing requirements (which are prescriptive in nature), while those of importance classes IV and V are to be treated as buildings located in Zone I.

It has been argued that good conceptual design and detailing which provides buildings with adequate ductility should be emphasized over flawed and often ill-understood analysis techniques when considering seismic action (Wium, 2010; Mallin, 2019). For this reason, the standard requires that designers consider several specified principles in the design of all buildings in active zones.

For buildings that are multiple stories high, these principles include general considerations such as structural simplicity, the multi-directional and torsional behaviour of the structure as well as those pertaining to the adequate use of structural and non-structural building components. For single-storey buildings, conceptual guidance is provided on symmetry in the plan layout of the building and the positioning and size of openings in walls. Prescriptive specifications are also made with regards to the dimensions and materials used in building walls, roofs and chimneys. These conceptual design considerations are all prescriptive in nature and are simple to apply.

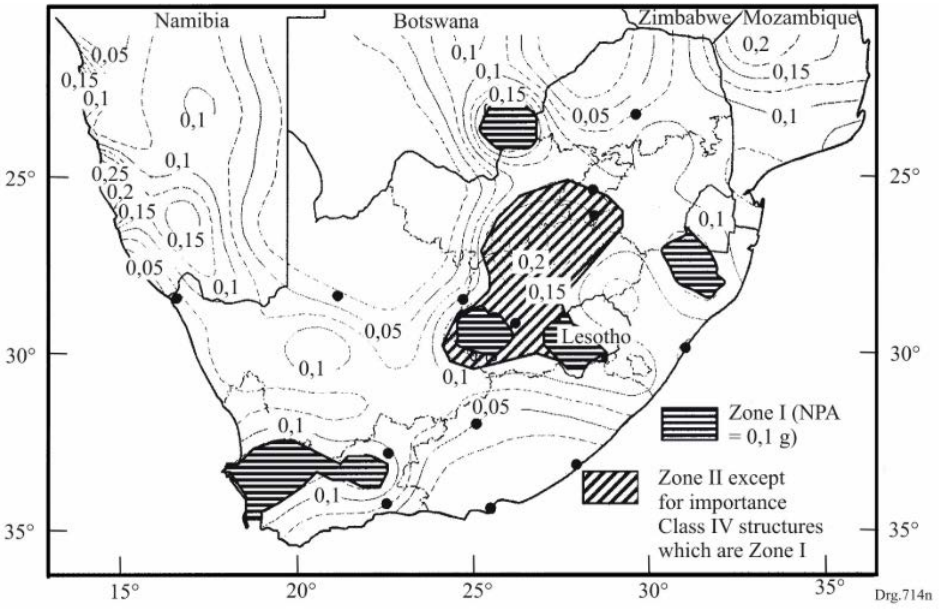

Figure 2.5: Regions subject to seismic loading provisions (SANS 10160-4, 2017)

In situations where analysis of the structural response is deemed necessary, SANS 10160-4 provides a simplified analysis method - the equivalent static lateral force method (ESLFM). This technique allows engineers to apply a series of lateral forces to a structure to assess its seismic performance in lieu of a dynamic analysis. ESLFM may be used if the fundamental period of vibration of the structure falls within specified bounds, the structure is not affected by higher modes of vibration and a set of conceptual and detailing guidelines are adhered to.

Following SANS 10160-4, the fundamental period of vibration of a building (T_f) can be estimated according to Equation (2.4.1), where C_{T_f} is an empirical factor depending on the material and structural system of the building and h_t is the height of the building from the foundation or the top of a rigid basement. The fundamental period of vibration is then used, in combination with correct ground type and behaviour factor to obtain a value from provided design response spectra graphs as shown in Figure 2.6.

$$T_f = C_{T_f} \times h_t^{\frac{3}{4}} \tag{2.4.1}$$

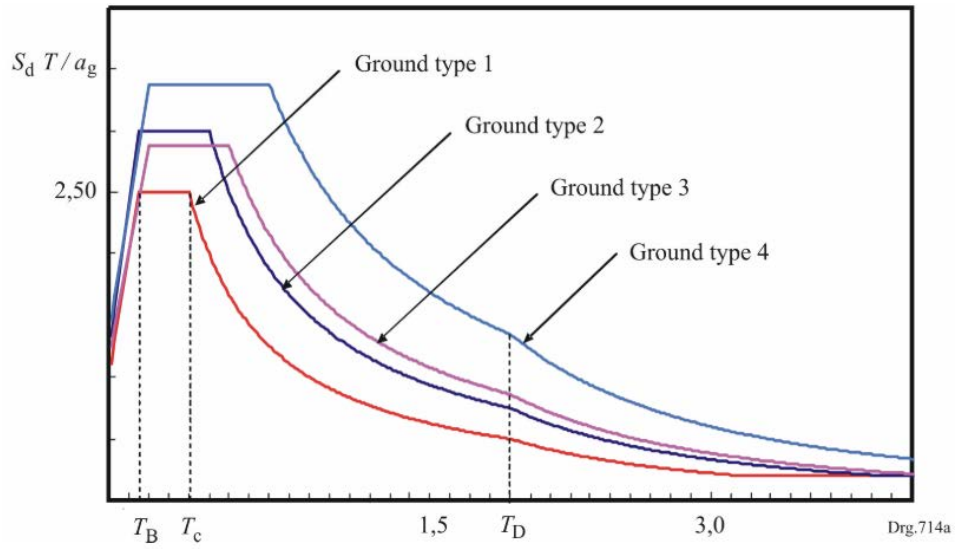

Figure 2.6: Design response spectra (SANS 10160, 2017)

The behaviour factor is included in the response spectra equations as a means of taking the plastic deformation and over strength characteristics of a building into account during the ESLFM analysis. The total base shear force (V_n), i.e. the lateral force applied to the base of the building is then determined according to Equation (2.4.2). In this equation, $S_d(T_f)$ is the non-dimensional value derived from the response spectrum and W_n is the nominal weight of the building sustained during the seismic event.

$$V_n = S_d(T_f) \times W_n \tag{2.4.2}$$

The design base shear is distributed to each storey in proportion to the weight it carries. The designer may then design the building as a linear elastic model with these lateral forces applied to the structure as stipulated in SANS 10160-1 (2018). Further guidance is provided on the distribution of the forces derived from the ESLF method to the structural and non-structural components of the building. Furthermore limitations are set on the permissible storey-drift of multi-storey buildings.

SANS 10160-4 also provides rules regarding the construction materials used. Specifications relevant to masonry buildings are provided in the code's annex. These include limitations on shear wall dimensions and aspect ratio as well as the minimum required bed joint reinforcement. Requirements for the allowance of shear distribution are also stipulated. Buildings that classify as "simple masonry buildings" are not required to be subjected to seismic analysis. To qualify, a building must have an importance class of lower than three, be lower than four storeys and comply with the stipulated conceptual design and dimensional requirements. It should be noted that these standards were developed for buildings constructed from conventional materials.

2.5 Summary

In this chapter, an introduction was made of the NBR and its relation to the construction industry. The role and limitations of Category 1 buildings as defined in the NBR in the provision of housing were also discussed. It is expected that most single-storey GSHs will be designed as Category 1 buildings.

Most single storey GSHs are constructed with CMUs in South Africa. Regulated CMUs were tabulated alongside their relevant materials-based standards. It is noted that CMUs have become entrenched within regulations and in the minds of consumers. The negative environmental aspects of CMUs in general are described briefly.

Various studies have been conducted to assess the feasibility of AMUs as a more environmentally friendly alternative to CMUs. Three AMUs and one CMU were developed by a previous student to be used in all subsequent studies involved in the current research project (including this one). The AMUs were manufactured from adobe, compressed stabilized earth and a geopolymer. The material constituents, manufacturing processes, and relevant engineering properties were briefly presented.

The dominant out-of-plane loads considered to be of relevance to this study were identified as wind pressure and seismic loading. The danger and prevalence of each load-type were discussed as well as the standards that regulate their consideration in the design of buildings. The design measures and assessment techniques provided by these standards were also presented as they pertain to the current study. In each case, it is found that simplified techniques enable designers to represent these loads as static out-of-plane forces or pressures for design.

Chapter 3

Literature Review

This chapter provides a brief review of the literature related to the flexural capacity of URM masonry. Specific attention is paid to solid masonry units bonded with cement-based mortar in single-leaf walls. The behaviour of walls subjected to out-of-plane (OOP) loads is described. Thereafter, a brief overview of the types of existing flexural strength tests is presented. Finally, a review of typical design and analysis practices is provided.

3.1 Out-of-Plane Behaviour of URM Walls

A horizontal load, applied to the face of a masonry wall, will cause that wall to bend out-of-plane. For brevity, such a wall will be referred to as a "flexural wall". A flexural wall that is laterally supported along its bottom and/or top only is said to be subjected to vertical flexure. If the same wall was laterally supported at either or both of its vertical edges, with no lateral restraint along its bottom edge, it would be subjected to horizontal flexure. Walls that are laterally restrained at vertical and horizontal edges are subjected to biaxial flexure. Figure 3.1 displays idealized cracking behaviour brought about by examples of each type of flexure for clarity. Since URM is much stronger in compression than it is in tension, flexural failure is usually commenced by cracking on the tension face of the wall. The processes that lead to ultimate failure (collapse of the wall), as well as the load resisting mechanisms, differ fundamentally for each case.

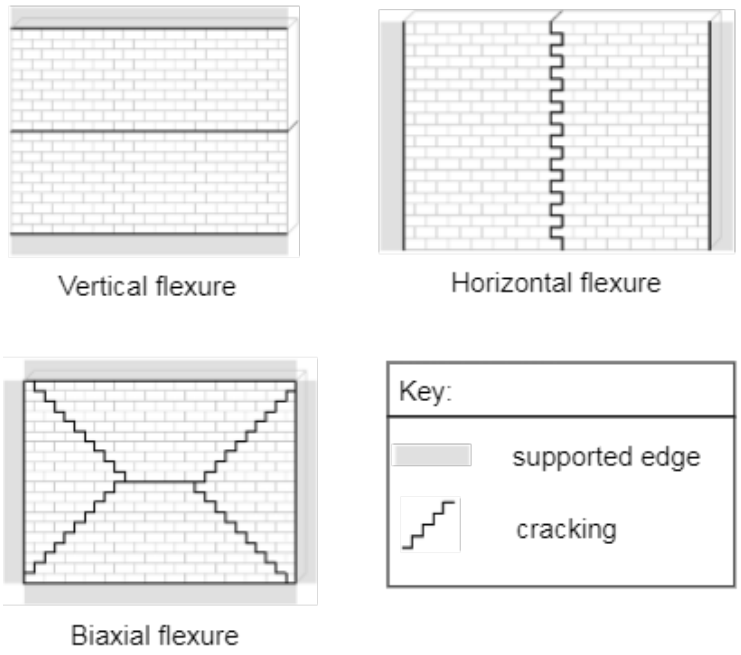

Figure 3.1: Walls subjected to different types of flexure. Adapted: Vaculik (2012, p. 3)

3.1.1 Vertical Flexure

A wall subjected to vertical flexure would resist OOP loading by bending about a horizontal neutral axis parallel with the bed joints. Cracking occurs where the tensile stresses overcome the wall's vertical flexural tensile strength. If the wall is laterally supported at the top and bottom, this usually takes place at the middle of the wall on the tension face and at the location of any fixed supports as shown in Figure 3.2. Vertical tensile stresses are resisted by the tensile capacities of the unit, mortar and the interface between them. In conventional masonry, however, failure almost invariably occurs within the interface along the bed joints, so that vertical flexural strength is usually controlled by the bond strength between the mortar and units (Grimm and Tucker, 1985, p. 1).

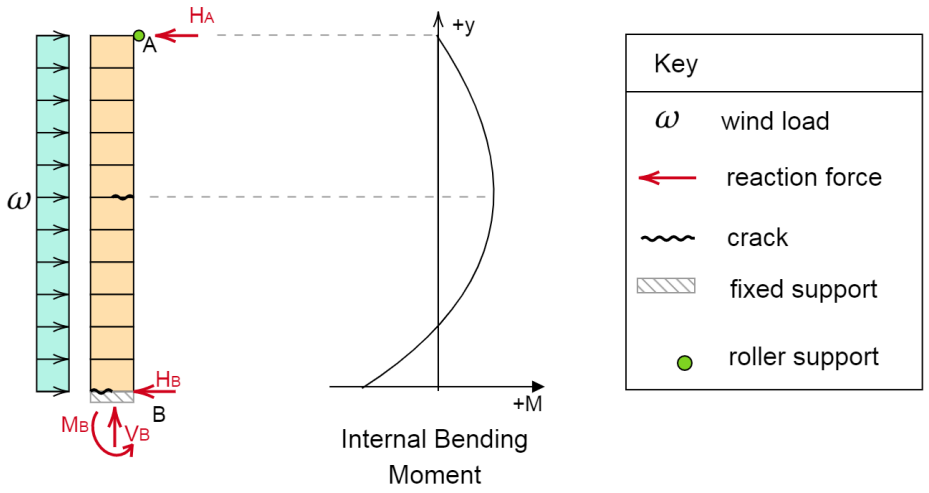

Figure 3.2: Crack pattern and bending moment of a wall in vertical flexure

Vertically applied axial compression directly counteracts flexural tension. In the case of single-storey low-income housing (LIH), this would take the form of the self-weight of the wall and the gravitational load applied by the roofing system resting above it. The axial compression can also counteract lateral loading through the development of a stabilizing moment.

Drysdale *et al.* (1994, p. 288-294) describe these load-resisting mechanisms through an example of a wall with a cracked base subjected to an increasing uniformly distributed wind load and supported laterally at the top as shown in Figure 3.2. In this example, it is argued that the bases of most masonry walls offer little to no tensile bond strength due to the presence of a damp-proof membrane or cracking caused by differential shrinkage between the wall and the foundation. Initially, the wall's own weight is enough to counteract the development of flexural tensile stresses at the base. However, with increasing wind load, a crack will open and lengthen from the windward side towards the leeward side at the base. This causes the vertical reaction to act at an eccentricity from the wall's centroid as displayed in Figure 3.3. The eccentricity between the line of action of the wall's gravitational load and its associated reaction create a couple moment that acts against the applied load. In the example, this moment would have a magnitude of the product of the walls own weight and the aforementioned eccentricity.

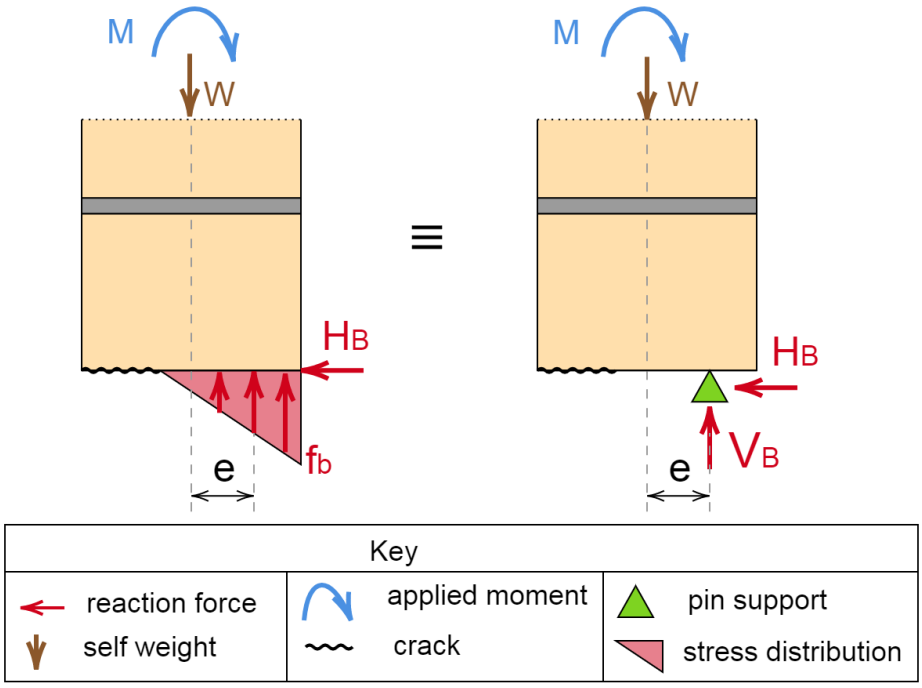

Figure 3.3: Eccentricity of the vertical reaction of a cracked base.

3.1.2 Horizontal Flexure

Horizontal flexure is resisted by bending about an axis normal to the bed joints. Pure horizontal flexure is rare in practice, since all walls must be supported along their base to resist gravity loading and even cracked bases would offer some lateral restraint due to friction. However, in some cases, portions of a wall can be considered to act in pure horizontal flexure, such as the top of a wall laterally supported along its base and sides, but not along its top. Once a wall has failed due to horizontal flexure, the resulting crack pattern can take the form of a straight, vertical line cutting through alternate head joints and units. This is known as 'line failure'. Alternatively, in what is known as 'stepped' or 'toothed' failure, the crack can form a jagged pattern, propagating through head joints and bed joints, but avoiding the masonry units. Both failure types are presented in Figure 3.4.

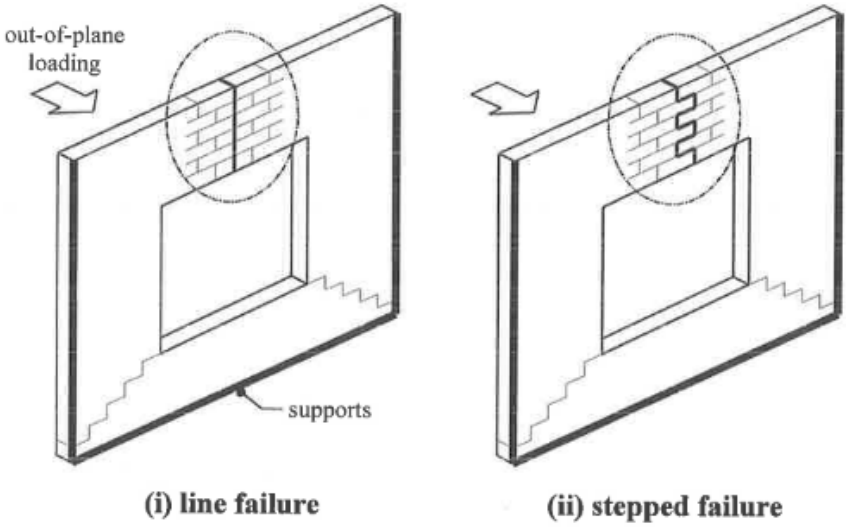

Figure 3.4: Line and stepped failure in horizontal flexure (Willis, 2004, p. 92)

The load resisting mechanisms and load-displacement behaviour can be described by considering the application of an increasing wind load to a wall laterally supported on its sides, with no lateral load resistance at its base or top. Figure 3.5 is provided for reference. Initially, the wall exhibits linear-elastic behaviour (Lawrence, 1995). At this stage, bending is resisted through the flexural strength of the units and mortar, and through the bond strength between the two. However, the bond strength of the head joints is usually the weakest of these load resisting mechanisms, so that cracks begin to form in the head joints well before the failure load is reached (Willis, 2004). The head joints continue to open with increasing load and provide little moment resistance after their initial cracking (Lawrence, 1995), reducing the stiffness of the wall as shown between Points b and c in Figure 3.5. In this range, the moment is resisted by the bed joints and units, until the ultimate load is reached (Point c).

At the wall's ultimate load resistance, a continuous crack (or multiple continuous cracks) would form by splitting the units directly above and below the cracked head joints causing line failure, or by breaking the bond between the bed joints and the units in torsion, resulting in stepped failure. If stepped cracking occurs, the wall would be able to resist lower loads (after the ultimate load has been reached) through friction between the bed joints and the units. In contrast, line failure results in a rapid loss of capacity (Drysdale *et al.*, 1994). This behaviour can be observed from the difference in the Portion c-d between the load-deflection plots.

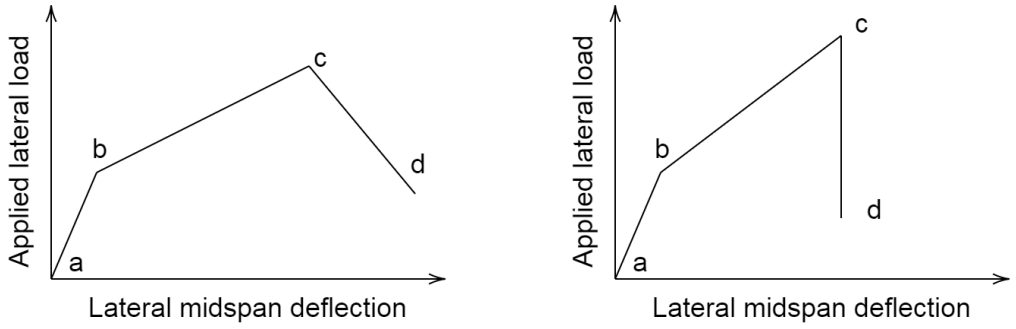

(a) Stepped failure (b) Line failure

Figure 3.5: Idealised load-displacement plots of horizontal flexural walls. Adapted: (Drysdale *et al.*, 1994, p. 296)

Vertical, uni-axial compressive stress contributes significantly to the load-displacement behaviour of walls in horizontal flexure. It is argued (Drysdale *et al.*, 1994, p. 296) that the beneficial effects of pre-compression are only realised in stepped failure. In this case, the torsional strength of the bed joints increases, resulting in a greater ultimate moment capacity and the friction within the bed joints is increased after the ultimate capacity has been reached. This was confirmed by a study performed by Samarasinghe and Lawrence (1994) that investigated the response of small masonry specimens subjected to combined torsional shear and compression.

Analytical models produced by Willis (2004) proposed that compressive stress may reduce the initial cracking load as well as the capacity of masonry that reaches its ultimate load resistance in line failure. This is due to the behaviour observed in conventional clay brick masonry where the units are usually stiffer and stronger than the mortar. If this type of masonry is subjected to axial compression, the units and the mortar will expand laterally as it is compressed vertically. Since the mortar is less stiff than the units, it would undergo more lateral strain than the units if it were in isolation. Since the mortar is bonded to the units (which restricts its expansion), the mortar in the bed joints exerts a biaxial tensile stress on the masonry units beneath and above it. To conserve force equilibrium, the units subject the mortar in the bed joints to compression Drysdale *et al.* (1994).

In this way, compressive stresses contribute to the tensile forces induced by horizontal bending and reduce the horizontal load required to produce line failure as seen in Figure 3.6(b). Alternative masonry walls can be constructed with mortar that is stiffer than the units it binds. In this scenario, a vertical compressive load would induce triaxial compression in the units and uniaxial compression and bi-axial tension in the bed joints (Sarangapani *et al.*, 2002) as seen in Figure 3.6(c). In this case it could be argued that the line failure capacity could increase with increased vertical axial compression, if the tensile capacity of the units remained greater than that of the mortar despite the mortar's greater stiffness.

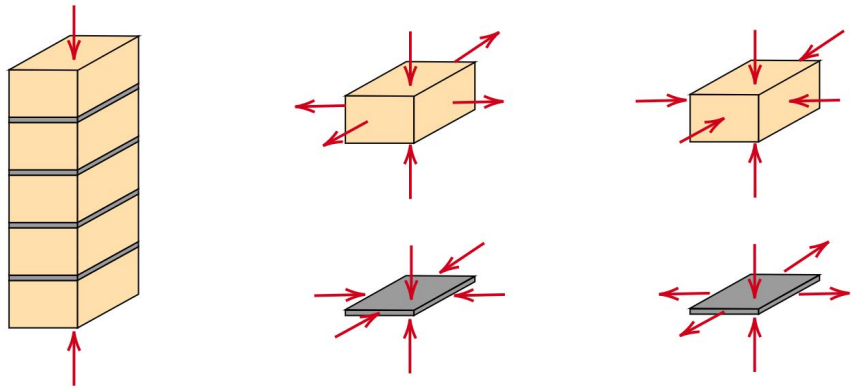

(a) (b) (c)

Figure 3.6: (a) Masonry prism in uniaxial compression, (b) stress state with units stiffer than mortar, (c) stress state with mortar stiffer than units. Adapted: (Wu *et al.*, 2013, p. 145)

3.1.3 Biaxial Flexure

In practice, most masonry walls are supported against lateral, OOP loads by both their vertical and horizontal edges. Comparable, consistent testing on masonry walls in biaxial flexure only began in the 1970's and was concerned mainly with the application of a uniform pressure load to clay brick and concrete block masonry walls supported on three or four sides (Baker *et al.*, 1985). Based off such work, Lawrence (1983) identified three distinguishable stages that walls undergo when subjected to a uniform pressure load: the formation of an initial crack, the development of the full crack pattern and the failure of the wall (characterised as the wall's ultimate load capacity). It was observed that not all of these stages were distinguishable from the others in every case. Four failure modes were identified as having characteristic load-displacement behaviour that usually corresponded to a set of boundary conditions and resultant cracking behaviour. Figure 3.7 displays idealized test walls that resulted in the failure modes identified and Figure 3.8 displays their force-displacement plots i.e. failure modes A, B, C and D in Figure 3.8 correspond with walls A, B, C and D in Figure 3.7.

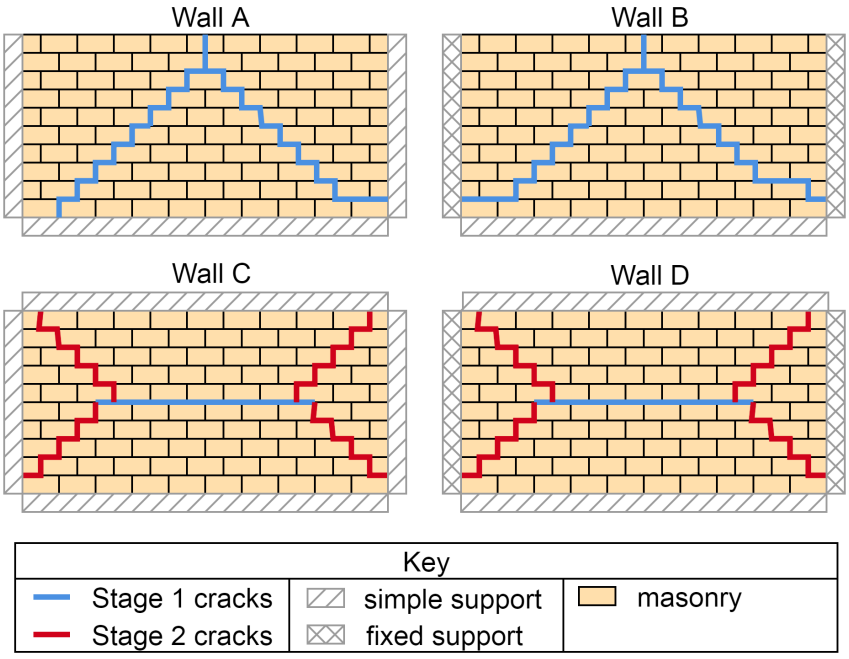

Figure 3.7: Idealized typical crack patterns for biaxial bending Vaculik (2012)

Walls that were simply supported on three sides, such as Wall A in Figure 3.7 were said to be subject to Stages 1, 2 and 3 simultaneously. The full crack pattern develops with the formation of the initial crack so that a mechanism is produced. The resulting load-displacement plot in Figure 3.8(a) shows no abrupt change in slope until failure.

Walls of a similar configuration, but with fixed vertical supports with a simply supported base and fixed vertical edges such as Wall B would produce a similar crack pattern, but would resist more load due to the presence of arching between the vertical supports. This phenomenon is discussed in further detail in Section 3.3.4. Considering the test result shown in Figure 3.8(b), the wall loses a considerable amount of stiffness after 1.7 kPa of pressure has been applied. From this point onwards the initial cracks continue to widen and the remaining capacity is attributed to arching.

Wall C represents walls that are simply supported on four sides. In these cases, an initial horizontal crack would form along a bed joint near the mid-height of the wall. Diagonal cracks form thereafter and failure occurs as the full crack pattern is developed so that Stages 2 and 3 were said to be coincident.

Walls simply supported at their tops and bases, but with moment-supported vertical edges (represented by Wall D) exhibited each failure mode consecutively. The walls would retain some moment capacity after the full crack pattern had developed. This reserve capacity was also attributed to arching.

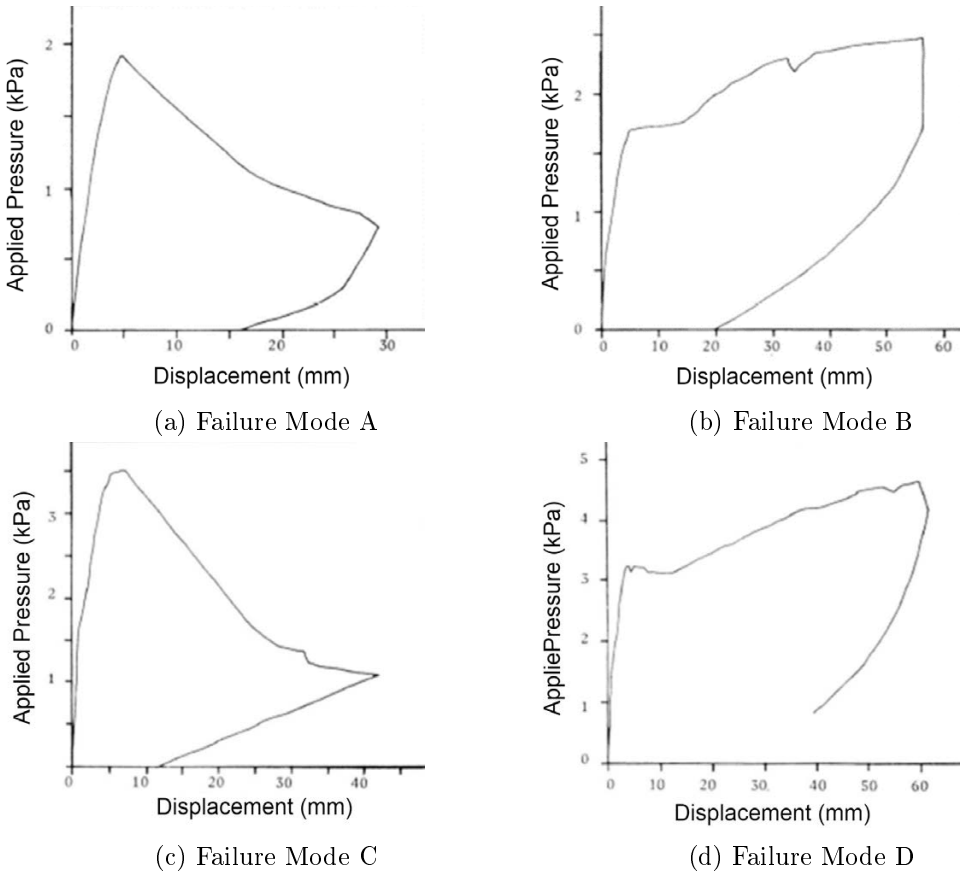

(a) Failure Mode A

(b) Failure Mode B

(c) Failure Mode C

(d) Failure Mode D

Figure 3.8: Typical biaxial force-displacement behaviour (Baker *et al.*, 1985, p. 39)

Diagonal cracks are characteristic of biaxial bending and the strength of a wall in biaxial flexure is dependent on the moment resistance mechanisms present within them. It has been observed in numerous studies [(Lawrence, 1983), (Baker, 1984), (Gairns, 1983), (Anderson, 1976), (Gairns and Scrivener, 1987)], as reported by Candy (1988), that the diagonal cracks in conventional clay brick and concrete block masonry tend to avoid the units, following a stepped pattern through the joints. Assuming this behaviour and considering the effects of bending about each principle axis provides a means of understanding the moment resistance mechanisms along a diagonal crack line. Vertical flexure along the diagonal crack would cause torsion in the head joints and flexure in the bed joints, while horizontal flexure would cause torsion in the bed joints and flexure in the head joints. Masonry resistance to biaxial flexure could be understood as a combination of these effects as seen in Figure 3.9.

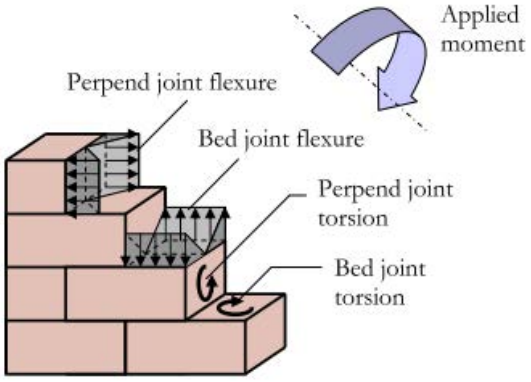

Figure 3.9: Moment resistance mechanisms in diagonal cracks. (Vaculik, 2012, p. 3)

The failure mechanisms induced by diagonal bending act along independent axes on the failure planes. If one considers the effects of simultaneously applied horizontal and vertical moments on a bed joint, the torsion brought about by the horizontal moment could not be superimposed with the flexural stresses brought about by the vertical moment on that joint. Subsequently, initial design methods assumed that there was no interaction between the two mechanisms so that a masonry section in biaxial bending would reach capacity only if the horizontal or vertical components of the applied moment matched the respective moment capacity of the section (Willis, 2004).

This was disputed by Baker (1979*b*) who proposed an elliptical interaction between the vertical and horizontal moment contributions based on the results of tests on small four-brick masonry assemblages as seen in Figure 3.10. Guggisberg and Thürlimann (1988) tested small walls built from hollow concrete blocks subjected to independent vertical and horizontal moments as seen in Figure 3.11 and discovered results that supported Baker's failure criterion. Both studies also investigated the effects of a vertically applied compressive load on biaxial bending and found that it increased the capacity of the masonry irrespective of the direction of the maximum moment.

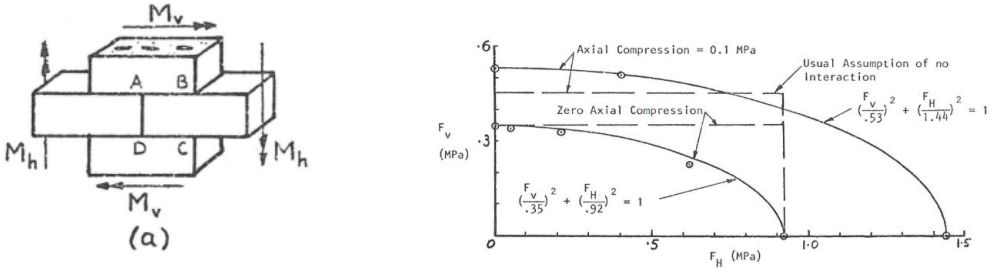

(a) Four-brick biaxial assemblage (b) Elliptical moment interaction

Figure 3.10: Baker's biaxial bending test and corresponding results (Baker, 1979*b*, p. 39)

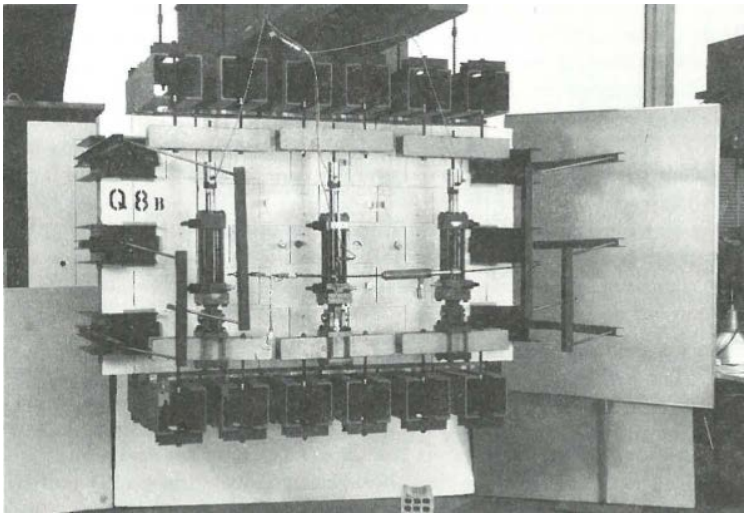

Figure 3.11: Test rig developed by Guggisberg and Thürlimann (1988)

Based on the work of Duarte (1993) and Ng (1996), Sinha *et al.* (1997) proposed a parabolic interaction that implied an increased vertical moment resistance of masonry in biaxial bending as opposed to pure vertical bending, as seen in Figure 3.12(b). This relationship was derived from the results of tests performed on "cross-beam" assemblages as seen in Figure 3.12(a). The central portion of the cross beam was constructed of clay brick and mortar, while the "arms" of the specimen were constructed of a comb-like brick and epoxy resin composite.

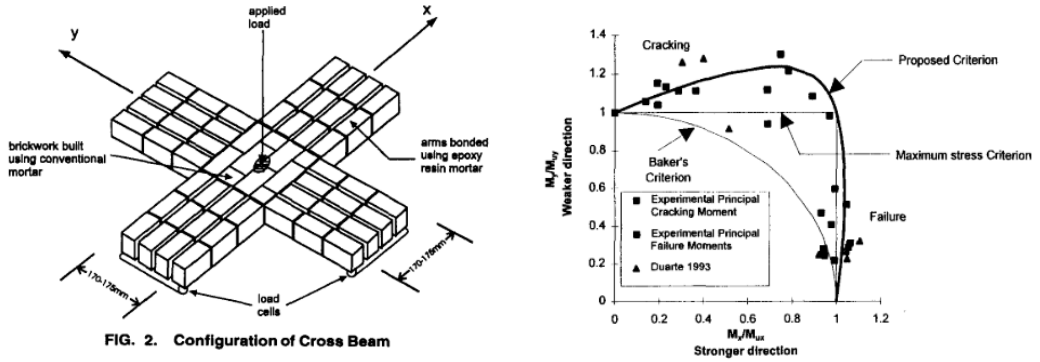

(a) Cross-beam masonry assemblage. (b) Parabolic moment interaction.

Figure 3.12: Test and interaction proposed by Sinha *et al.* (1997, p. 71,74)

Willis (2004) developed an expression for predicting the ultimate load capacity in diagonal bending, considering only the torsion and flexure in the bed joints. Linear-, elliptical- and zero-interaction expressions were compared against experimental data produced with a diagonally oriented four-point bending setup as seen in Figure 3.13. It was found that all three expressions overestimated the capacity of the masonry, but that a linear interaction provided the best fit. Vaculik (2012) further developed

the work of (Willis, 2004) by formulating one mathematical expression that could be used to represent either of the three interaction mechanisms by altering a single parameter as seen in Figure 3.14. The biaxial failure criteria discussed in this chapter are difficult to compare directly as their development has been based on fundamentally differing test setups. Furthermore, each criterion was developed in conjunction with a different analysis technique for assessing the strength of full scale walls. These techniques are presented in Section 3.3.3.

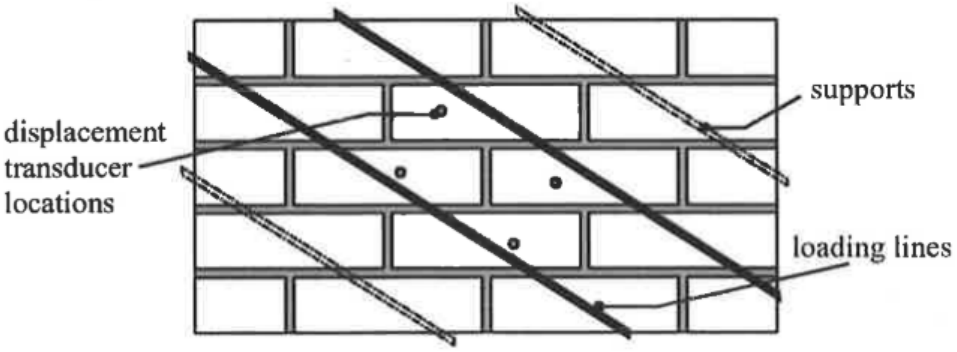

Figure 3.13: Diagonal four point bending test (Willis, 2004, p. 49)

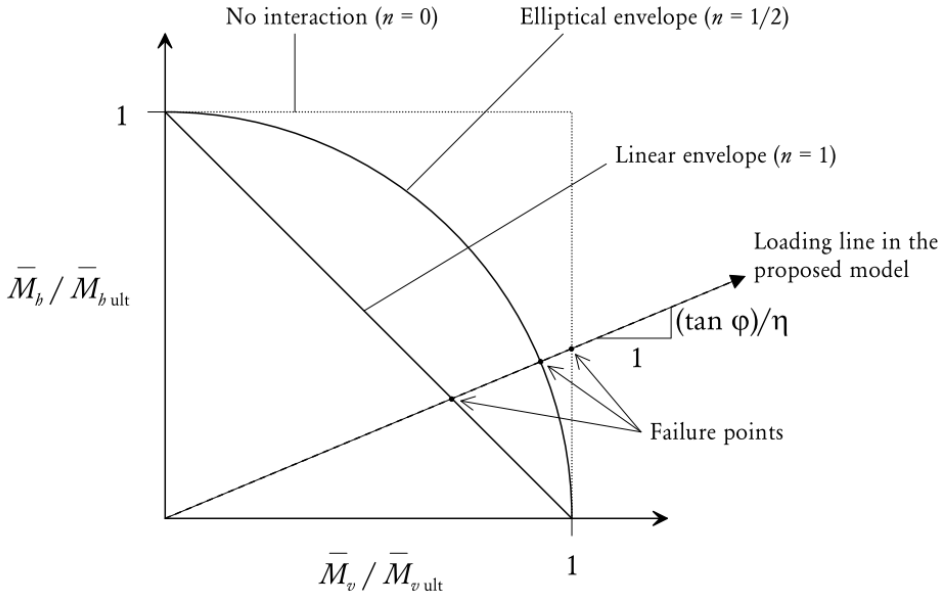

Figure 3.14: Adjustable biaxial bending interaction expression (Vaculik, 2012, p. 137)

3.2 Masonry Flexural Strength Tests

To achieve the objectives of the study, a setup had to be constructed to test masonry walls in flexure so that experimental results could be compared to and used to validate the results of a numerical model. For this reason, existing masonry flexural strength tests were studied. This section presents a brief overview of the most common tests that are employed in determining the flexural characteristics of masonry. The tests are categorized in terms of their size and function.

3.2.1 OOP Wall Tests

Various tests have been performed on full-scale walls. Their main benefit is that they can be used to replicate the behaviour of walls in design scenarios as opposed to strictly determining material properties. This is especially important for investigating the geometrical aspects of masonry walls such as the presence of openings. Observations made during tests and the results thereof can be compared against the applications of analysis techniques, case-studies and standards.

Air-bags have been used to supply load in most OOP tests (Edgell, 2005*b*). With this technique, a bag or a collection of bags is placed between the specimen and a backing board before air is pumped into them at a controlled rate with the use of a compressor. As the bags inflate, they apply a uniform pressure loading to the face of the specimen. The applied load can be recorded by measuring the pressure within the air-bag with a manometer or pressure transducer (Omote *et al.*, 1977). Displacement measurements are usually recorded for the duration of the test so that load-displacement relationships are provided for each specimen.

In some situations, researchers may want to apply a line load or concentrated load to the face of a specimen. This could be to provide a specific bending moment or shear force distribution to obtain material parameters. Often, this type of test is performed to assess the effects of material properties of the masonry units or mortar or the benefits of some form of rehabilitation or reinforcement. Alternatively, a design scenario could be simulated, such as the effect of roof or floor movement induced by earthquake loading. In these situations, hydraulic actuators are typically used to provide a controlled force or displacement. Similarly, displacement and force measurements are usually recorded at key locations on the specimen throughout the test duration. Figure 3.15 displays typical applications of airbag and line load testing.

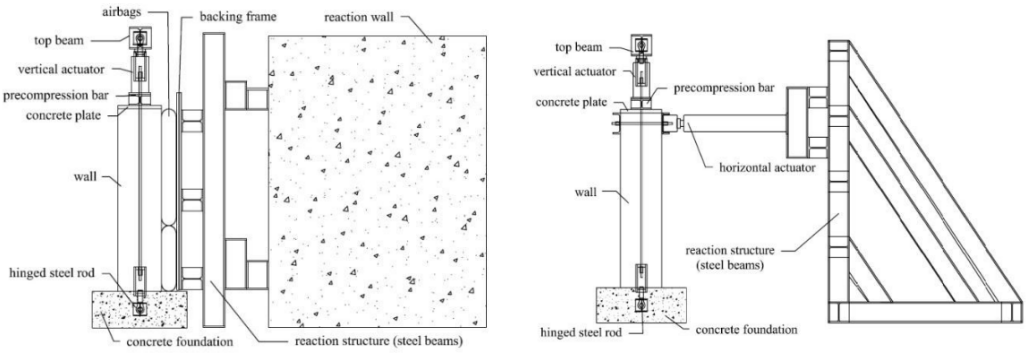

(a) Distributed loading setup (b) Line load setup

Figure 3.15: Full scale walls subjected to air-bag (a) and line load (b) loadings (Costa *et al.*, 2014, p. 4).

3.2.2 Design Strength Flexural Tests

Tests have been developed to determine the flexural strength of masonry as a material parameter. This is achieved by prescribing standard specimen types, construction methods and test procedures. The Eurocode's wallette test, EN 1052-2:2016 and the ASTM E72, Sections 11 and 12 are both examples of standard test methods prescribed for this purpose.

The wallette test subjects a small masonry wall (referred to as a wallette) to four point OOP bending about the desired axis as seen in Figure 3.16. The geometry of the test setup ensures that the portion of the wallette between the inner bearings undergoes a constant maximum moment without being subject to shear forces. In the standard's convention, the type of flexure is named according to the angle of the failure plane with reference to the bed joints. Vertical flexure causes failure parallel to the bed joints, while horizontal flexure causes failure perpendicular to the bed joints. In the interest of brevity, this thesis will use the terms "parallel flexure" and "perpendicular flexure" with reference to these tests.

The test can be performed with the specimen oriented vertically, (as shown in Figure 3.16) or rotated to a horizontal orientation (facing downwards), but vertical testing is recommended. The maximum applied loading and dimensions are recorded for each specimen to determine the flexural strength at failure according to linear elastic bending theory EN 1052-5 (2005). If conformance to the method is satisfactory, the flexural strength results of these tests may be used to determine the characteristic flexural strength of a type of masonry as per Clause 3 of EN 1996-1-1. SANS 10164-1 contains a similar method for the same purpose.

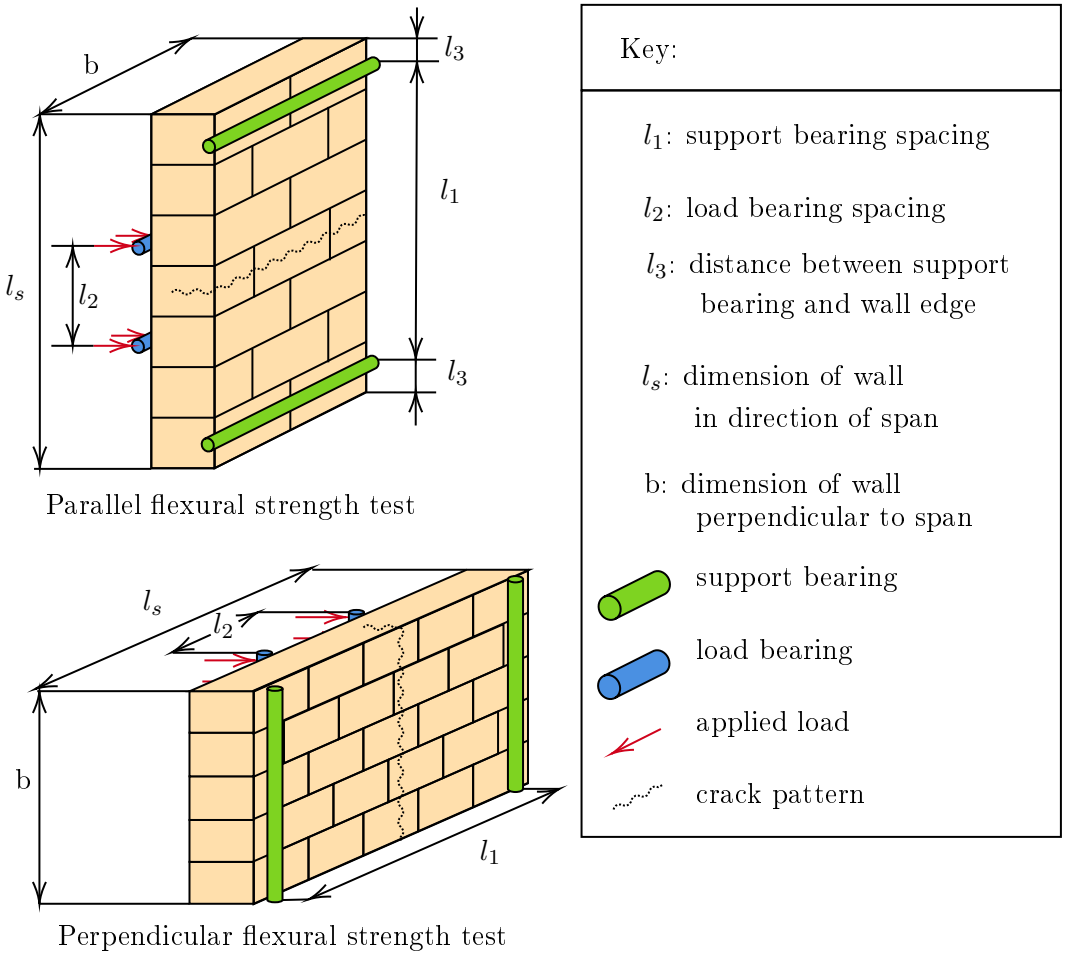

Figure 3.16: Typical flexural strength tests as prescribed by EN 10152-2.

ASTM E72-15 (2015) provides standard test methods for determining the shear, compression and transverse capacities of panels of any construction material. The specimens should be as close as possible to the size of the respective building element with a nominal width of 1.2 meters. Three specimens should be tested for each parameter, unless the specimen is asymmetric in some direction, in which case three specimens should be tested per each differing axis.

Sections 11 and 12 of the standard provide methods for determining the design stresses of panels subjected to transverse loading. Similarly to the European equivalent, it allows testing in the vertical or horizontal orientation. The specimen should be supported at approximately 75 mm away from the nearest edge by steel rollers. The load may be applied as line loads or as a distributed pressure load. The line load method is similar to the one presented by EN 1052-5 (2005) in geometry. If a distributed load is to be applied this can be achieved with the use of the air-bag method or a pressure chamber attached to the face of the specimen.

A cyclic load regime is prescribed. In each cycle, an incrementally larger load is exerted and held and then released. The standard also states that the deflection should be measured at critical states throughout the cycle. This makes the prescribed loading and instrumentation requirements more advanced than EN 1052-5 (2005).

3.2.3 Standardised Flexural Bond Strength Tests

Various standardised bond strength tests have been developed to characterise the flexural tensile stress of the bond between units and mortar. The principle of these methods is to impart a bending moment to stack bonded piers. These are masonry assemblages comprised of bonding one unit on top of the other to form a prism with the same cross-sectional dimensions of the bedface of a unit. Two distinct methods of imparting moment have been identified in standards and can be termed as beam-type tests and bond wrench tests.

3.2.3.1 Beam-type Tests

Beam tests impart a moment by applying transverse loading to the face of a pier as if it were a beam. ASTM E518-15 and Section 6.7 of SANS 10164-1 are both examples of tests where stack bonded piers are tested in this manner. For each standard, the pier is built and left standing vertically until the commencement of the test. At that stage, the pier is rotated horizontally and placed onto supports which are in line with its first and last units. The test described in SABS 0164-1 is a simpler, less exact method, designated only for use as a means of checking the bond strength of masonry during construction, while ASTM E518-15 has been recommended for checking the quality of construction as well as performing experimental research. In each case, the flexural strength is calculated according to linear elastic beam theory including the self-weight of the prism.

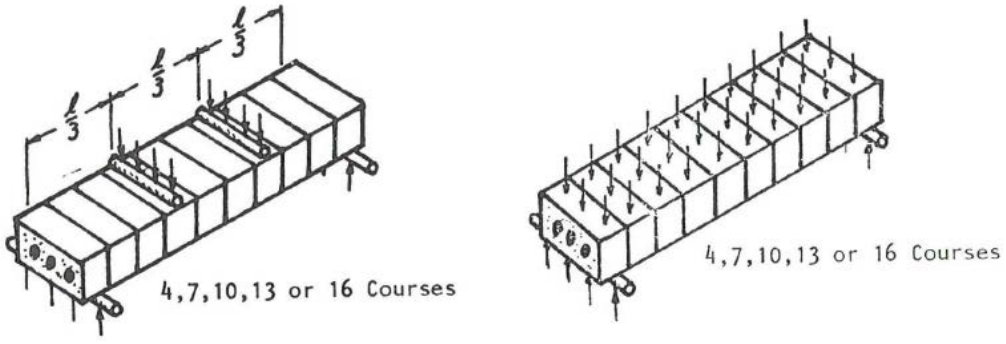

(a) Method A (b) Method B

Figure 3.17: ASTM E518 Test Methods (Baker, 1979a, p. 82)

ASTM E518 - 15 specifies two test methods of loading, referred to as Method A and Method B respectively. Method A subjects the beam to third point loading, while Method B subjects the beam to a uniform loading as seen in Figure 3.17. In both cases, the pier rests on roller supports and in the case of Method A, rollers are also used to apply the load. It is specified that the loading rate should be uniform and cause failure within one to three minutes.

For test prescribed by SANS 10164-1, two masonry units are used as the supports, rather than rollers. Load is applied to the specimen by stacking units onto the middle three bricks of the specimen until it fails. The specimen should be weighed before testing and each brick used to apply load should be weighed before placement. The layout of the test is shown in Figure 3.18 Although this method is more crude than the ASTM equivalent, it is arguably more applicable for use on a construction site.

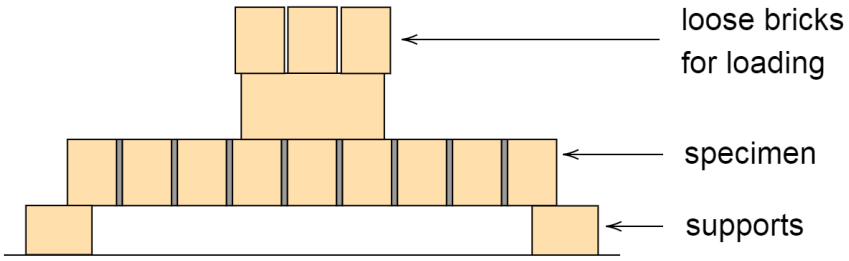

Figure 3.18: Bond strength test according to SANS 10164-1 (1980, p. 50)

3.2.3.2 Bond Wrench Tests

ASTM C1072 and EN 1052-5 both give methods for the determination of bond strength by the bond wrench test. The test procedure is similar in both standards. A stack bonded pier is placed in the testing apparatus, with its base supported on a flat surface. Thereafter, the second unit from the top is clamped to prevent rotation before a lever with a clamping attachment is clamped onto the top unit of the pier. To load the specimen, an increasing vertical downward force is applied to the opposite end of the lever until the top unit de-bonds from the remainder of the pier. This process is repeated by adjusting the specimen or apparatus to test the top unit of the remainder of the specimen until all of the joints have been tested. Figure 3.19 illustrates the essential components of a typical bond-wrench test setup.

Although the principle and action of the tests are similar, the procedures do differ slightly. For example, ASTM C1072 specifies that once both clamps have been fastened, the surface on which the specimen rests should be lowered, while this is not mentioned in EN 1052-5. In each case, the compressive stress and bending moment at the tensile face of the specimen are used to determine the bonding stress. Both standards include the own weight of the wrench as well as the applied force, but EN 1052-5 also takes the own weight of the de-bonded portion into account.

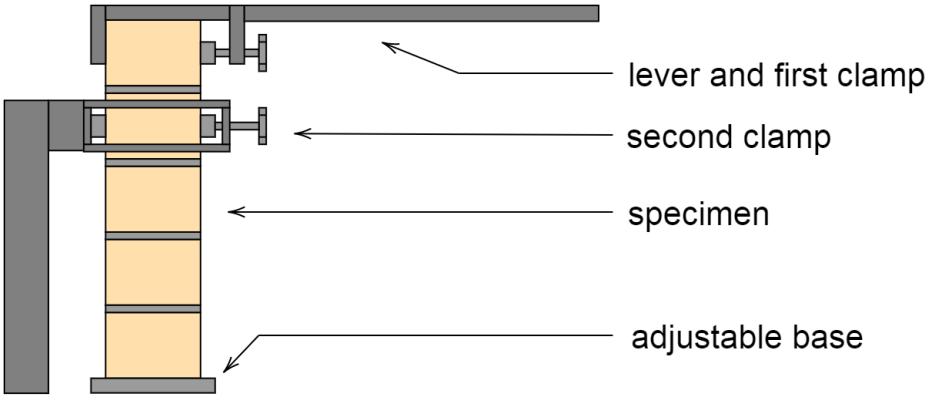

Figure 3.19: Simplified bond wrench setup based on EN 1052-5 (2005, p. 7)

Bond wrench tests only subject one joint of the masonry specimen to flexure. Furthermore, standardised versions of the test only exist for testing the strength of a specimen against vertical flexure since the aim of the test is to measure the strength of the flexural tensile bond between the units and mortar. Although this limits the capability of the test, its results are informative due to the importance of tensile bond in the flexural behaviour of masonry walls. Another distinct advantage of the test is that a greater number of results can be produced from the same amount of material compared to the design flexural strength tests and beam-type tests discussed in Section 3.2.2 and Section 3.2.3.1 respectively.

3.2.4 Smaller Assemblages

Smaller setups have been designed that reduce the size of specimens to a minimum for testing a particular parameter. Some have been developed to test load-resisting mechanisms in isolation, while others purposely induce a combined response to determine the relative effects of each mechanism on the ultimate behaviour of the masonry.

3.2.4.1 Tensile Strength Assemblages

The tensile bond strength of masonry has been investigated in the absence of flexural stress. The crossed couplet test was devised for this purpose and was standardised by ASTM C952. Each specimen is created by bonding two units in stack bond, but rotated 90°relative to the other about a vertical axis. The advantage of this test is that an external compressive action is used to induce tensile stress at the joint. This is achieved by the use of two loading platens that each have three leg protrusions. The specimen is placed so that the bottom face of the top unit rests on the legs of the bottom platen. To load the specimen, the top platen is lowered so that its legs push against the top surface of the bottom brick. Figure 3.20(a) displays a couplet test performed by Schmidt (2020) based on ASTM C952. Despite the carefully controlled conditions stipulated by ASTM C952, the results are typically highly variable (Fried, 1997). The test was withdrawn and replaced by ASTM C1072 in 2018.

Other tests were designed to operate by the application of an external tensile force. Taylor-Firth and Taylor (1990) reduced the length of the mortar bedding to a central portion of a stack bonded couplet and used small beams in the gaps between the units to pry them apart as seen in Figure 3.20(b). Other tests have been developed with fully bonded couplets. These rely on fixing each unit to a tensile testing apparatus mechanically (with bolts or clamps) or with strong adhesives. Despite the range of direct tensile test methods available, there is debate over whether any repeatable, accessible methods exist that are able to apply large uniform tensile stress without introducing bending (Edgell, 2005*a*).

(a) (b)

Figure 3.20: Direct tensile bond strength tests: (a) crossed couplet based on ASTM C952 (Schmidt, 2020), (b) test introduced by Taylor-Firth and Taylor (1990)

3.2.4.2 Shear Strength Assemblages

The torsional shear strength of the bond is an important load-resisting mechanism for masonry in horizontal bending. Recognising this, Lawrence (1983) developed a setup that subjected two bonded couplets to relative torsion. This was achieved by clamping one unit of the couplet and subjecting the other to torque about the centre of its bedded axis with the use of a hydraulic actuator and a lever as seen in Figure 3.21.

Traditional masonry shear tests on small assemblages induce a relative uniaxial translation along the joints between units in an assemblage. The triplet and couplet tests are more popular examples of these and are illustrated in Figure 3.22. These tests are more popular than the torsional shear test, but replicate in-plane behaviour rather than OOP horizontal bending.

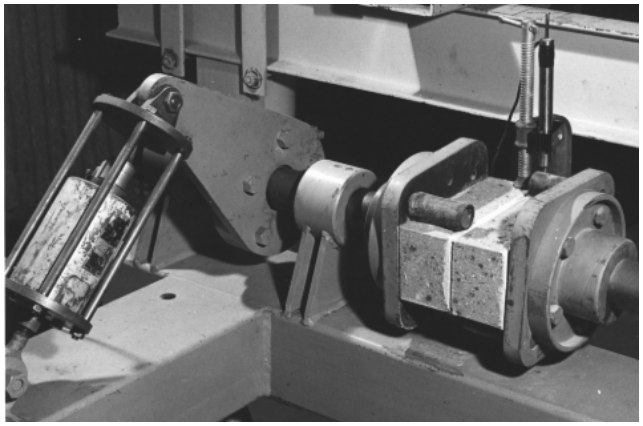

Figure 3.21: Shear torsion test (Lawrence, 1983).

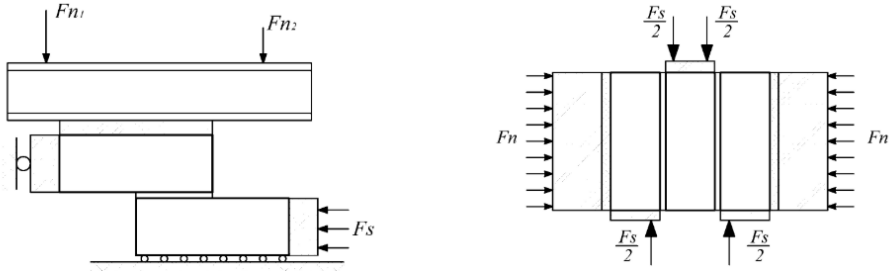

(a) Shear couplet test (b) Shear triplet test

Figure 3.22: Common shear bond strength tests (Lourenço *et al.*, 2004, p. 126).

3.3 Design and Analysis of Walls Subjected to Lateral Loads

Design for walls in vertical flexure and biaxial flexure is discussed. In practice, horizontal flexural walls will always experience some degree of vertical bending and can be attributed to the biaxial flexure category. In South Africa, masonry is designed according to both SANS 10164, which is based on the withdrawn BS 5628 and SANS 51996-1-1, an identical implementation of the Eurocode standard EN 1996-1-1. This is due to the fact that South Africa's masonry codes are undergoing changes to adopt the Eurocode (De Villiers, 2019). Both standards prescribe that walls subjected to lateral loading should be designed by ensuring the applied moment at any point in a wall should be less than or equal to the wall's design moment capacity.

3.3.1 Design Moment Resistance

EN 1996-1-1 specifies that the design moment of resistance in either orthogonal direction (M_{Rdi}) should be calculated as the product of the relevant elastic section modulus (Z_i) and characteristic flexural strength (f_{xdi}), as shown in Equation (3.3.1). Using this notation, i is an index of the failure direction in which values of 1 and 2 indicate bending that would cause failure parallel and perpendicular to the bed joints respectively. The code provides values for f_{xdi} dependent on the unit type and mortar strength and type for common masonry materials. Alternatively, these values can be determined from tests performed according to EN 1052-2 or obtained from existing test data.

$$M_{Rdi} = f_{xdi}\, Z_i \tag{3.3.1}$$

Provision is made for the favourable effect of simultaneous vertical compressive loading by allowing designers to use an increased flexural strength in the vertical direction, known as the apparent flexural strength, $f_{xd1,app}$. This is calculated by adding the compressive stress (σ_d) to the vertical flexural strength as shown in Equation (3.3.2).

$$f_{xd1,app} = f_{xd1} + \sigma_d \tag{3.3.2}$$

3.3.2 Vertical Flexure

EN 1996-1-1 states that standard engineering principles should be used to determine the applied moments within a wall subjected to vertical flexure. Generally, linear elastic beam equations are used to determine the internal applied moments. For this purpose, SANS 10164 provides the standard uniformly distributed beam load equation for calculating applied moments for walls subjected to wind loads.

Vertical flexural walls will be able to resist lateral loading after the initial opening of the crack at midspan (in the case of a wall supported at its top and bottom). As discussed in Section 3.1.1, the wall's own weight and superimposed loads can resist further loading through the stabilising effect. In the case where allowance is made for cracking, the calculation of internal moments becomes dependent on the location of the crack and depth of crack opening. Furthermore, the compressive strength of the masonry becomes a factor in the moment resistance of the section, since the axial and flexural compressive strengths are acting upon an area that reduces as the crack progresses.

3.3.3 Biaxial Flexure

The biaxial bending behaviour of masonry is difficult to predict accurately (Chong, 1993). The problem has seen the application of several fundamental approaches, ranging from purely empirical, such as the crossed strips method (Drysdale *et al.*, 1994, p. 305), to those that are rational, but incorporate some empirical factors. Currently, most masonry codes prescribe some form of rigid plastic analysis for determining the ultimate capacity of masonry panels in biaxial bending. Although the underlying principles of plastic analysis is common to all of these methods, each applies the analysis differently (Vaculik, 2012, p. 115). In this section, the general principle of yield-line theory will be presented. Thereafter, its implementation within the Eurocode 6 and the South African National Standards is discussed. A brief summary of other prominent rigid plastic analysis methods is also presented.

3.3.3.1 Yield-Line Theory

Johansen (1962) developed yield-line theory for the analysis of reinforced concrete slabs. According to the theory, failure occurs once predefined regions of the slab's reinforcing are in a state of yielding simultaneously. The lines along which yielding occurs are known as the yield lines and they divide the slab up into separate parts so that it can be seen as a system of rigid bodies, as seen in Figure 3.23. The geometry of the yield lines (the yield pattern) depends on the slab- and reinforcement-geometry and the boundary conditions along each of the slab's edges.

Once the slab has been subdivided into rigid plates, it is possible to obtain the its moment capacity through the principle of virtual work. This is demonstrated in Equations (3.3.3) and (3.3.4) where the internal and external of work of the system are represented on the left and right hand sides of the equation respectively. For any part of the slab, the internal work can be formulated as the product of the rotation of that part about its support (θ) and the component of the ultimate internal moments in the axis of that rotation (M_i). The external work is the work performed by the applied load, which can be described as the product of the moment of the external force about the axis of rotation and the rotation itself ($M_a\theta$), as in Equation (3.3.3). Alternatively, one can determine the external work by integrating the product of the pressure (p) applied and the subsequent displacement (z) over that part of the slab as in Equation (3.3.4).

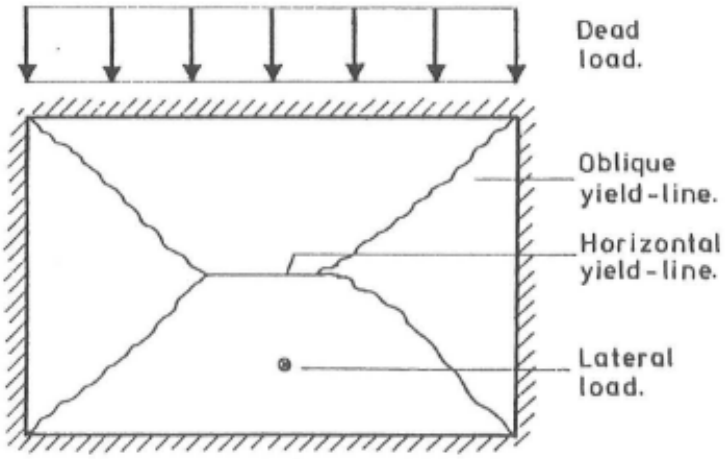

Figure 3.23: Typical yield-line pattern of a concrete slab (Brinker, 1984, p. 8)

$$\sum M_i\theta = \sum M_a\theta \tag{3.3.3}$$

$$\sum M_i\theta = \sum \iint pzdxdy \tag{3.3.4}$$

In the case of reinforced concrete slabs, one can use yield line theory to determine the required moment capacities (and thus reinforcing) for a given applied loading. Simplified means of achieving this have been developed by Johansen. In 1978, yield-line theory was adopted by the British masonry code: BS 5628. The Eurocode 6 superseded BS 5628, but also adopted the same yield-line theory (Maluf *et al.*, 2008; Vaculik, 2012).

3.3.3.2 Biaxial Bending in South Africa

According to EN 1996-1-1, the applied design moments in each orthogonal direction ($M_{Ed,i}$) should be determined from Equation (3.3.5), where i is an index of the failure direction in which values of 1 and 2 indicate bending that would cause failure parallel and perpendicular to the bedding plane respectively. In each case, the applied horizontal pressure (W_{Ed}) is multiplied by the square of the wall's length (l) and a bending moment coefficient (α_i), which is dependent on the wall's geometry and boundary conditions.

The code provides tables for determining α_2, based on the aforementioned parameters, for single-leaf walls with a unit thickness of less than 250mm and set support conditions. These were determined by fitting results obtained by yield-line theory to experimental data (Sinha, 1980; Vaculik, 2012). The complementary coefficient, α_1, is then determined according to Equation (3.3.6), where μ is the orthogonal strength ratio of the masonry as defined in Equation (3.3.7) within which f_{xd1} and f_{xd2} are the characteristic strengths of the masonry as per the aforementioned indices. If bending moment coefficients cannot be obtained from the provided values (due to

non-standard wall geometry), the designer may determine them on the basis of a recognized method of analysis - the code specifically refers to yield-line theory and finite element methods.

$$M_{Ed,i} = \alpha_i \, W_{Ed} \, l^2 \tag{3.3.5}$$

$$\alpha_1 = \mu \, \alpha_2 \tag{3.3.6}$$

$$\mu = \frac{f_{xd1}}{f_{xd2}} \tag{3.3.7}$$

3.3.3.3 Other Analytical Design Methods

Despite the adoption of yield-line theory by the aforementioned standards, its application to the analysis of masonry is theoretically flawed. A key assumption of yield-line theory is that the moment capacities along the yielded regions (or cracks, in the case of masonry) are reached simultaneously. This assumption is not valid in the case of unreinforced masonry due to its brittle nature. As such, it has been found that yield-line theory consistently overestimates the capacity of masonry panels and is the least conservative method for determining the ultimate capacity of a panel (Sinha, 1980; Chong, 1993; Vaculik, 2012). Subsequently, adaptations to the original yield-line theory have been developed to account for these issues (Vaculik, 2012).

In 1978, Sinha proposed an adaptation to the standard yield-line theory by accounting for the stiffness orthotropy of the masonry using the factor k, as shown in Equation (3.3.8). Accordingly, the applied moments are distributed according to the geometry of the wall panel and both the strength and stiffness orthotropies. If k is taken as unity, the method becomes equivalent to yield-line analysis.

$$k = \frac{E_x}{E_y} \tag{3.3.8}$$

Baker and Drysdale proposed the failure line method in 2003. It was adopted into the Canadian masonry code shortly thereafter and was proven to be more conservative than both the yield-line and fracture line methods. This is because the failure line method makes provision for the early cracking of a wall. Depending on a wall's geometry, cracks can form along a vertical or horizontal line before the wall reaches its ultimate capacity. According to the method, that crack can no longer support an applied moment and the cracks that form thereafter carry all of the load. The method is thus analogous to the aforementioned methods with the exception that it ignores the contributions of cracks that form early. For this reason, capacities determined by the failure line method will always be less than or equal to those determined by the yield-line method (Baker *et al.*, 2005).

The virtual work method was developed in Australia and presented by Lawrence and Marshall in three publications 1996; 1998; 2000 and has been incorporated into the Australian masonry code, AS 3700, since 1998. In this method, the crack patterns are not determined through optimization, but by the "natural slope" of the masonry i.e. the diagonal cracks are assumed to travel from the corners of the panel along the mortar joints, always alternating between head joints and bed joints in a stepped fashion. All moment contributions from horizontal cracks are ignored. The moment capacities in each direction are determined independently (including moments that develop along a diagonal crack) (Vaculik, 2012, p. 122).

3.3.4 Arching

Arching is a phenomenon which can increase the lateral load resistance of masonry. This occurs when a masonry wall is built against rigid supports. As the wall displaces, the ends of the unloaded face bear against the supports in compression. Similarly, compression occurs on the loaded face of the wall at the location of the central crack in uniaxial bending. If the supports are rigid enough, the applied lateral loading is resisted through compressive forces known as "arch thrust" as shown in Figure 3.24. The calculations used in the design and analysis of walls subjected to arching are based on the compressive capacity of the masonry, rather than its flexural characteristics.

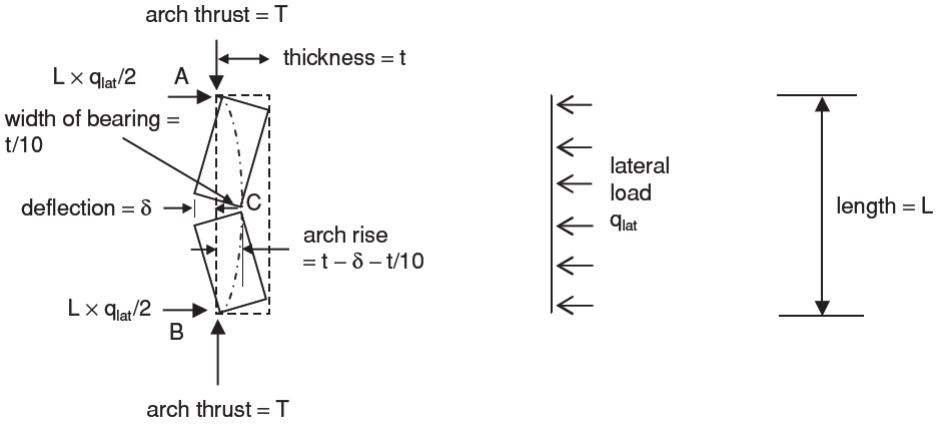

Figure 3.24: Free body diagram of a masonry wall resisting load through arching (Curtin *et al.*, 2006, p. 61)

The maximum allowable lateral load can be determined, by applying moment equilibrium about Point C in Figure 3.24 to give Equation (3.3.9). Assuming that the maximum allowable arch thrust (T) is Equation (3.3.10), where f_d is the compressive strength of masonry in the direction of thrust and that the deflection can be ignored, yields Equation (3.3.11). In EN 1996-1-1, the coefficient is taken as 1 to yield Equation (3.3.12), which may be used if the wall has a slenderness ratio of less than 25.

$$q_{lat}(\frac{L}{2})(\frac{L}{2}) = T(t - \delta - \frac{t}{10}) + q_{lat}(\frac{L}{2})(\frac{L}{4}) \tag{3.3.9}$$

$$T = 1,5\ f_d\ \frac{t}{10} \tag{3.3.10}$$

$$q_{lat} = 1,08\ f_d\ (\frac{t}{L})^2 \tag{3.3.11}$$

$$q_{lat} = f_d\ (\frac{t}{L})^2 \tag{3.3.12}$$

The design lateral strength calculated in this manner can be up to twice as large as that determined by other methods (Drysdale *et al.*, 1994, p. 312). With this in mind it is imperative that the correct conditions for arching can be ensured to prevent unsafe designs. Full contact should be maintained between the wall and the supports throughout the design life and at the point of failure. Furthermore the supports should be able to withstand the required arch thrust forces.

3.4 Concluding Summary

This literature review was conducted to gain an improved understanding on the OOP behaviour of URM, summarize and compare the techniques that have been used to investigate it and introduce the methods that are used to design and analyse URM walls subjected to OOP loads. This provided guidance on which parameters might be most applicable to current study. Furthermore, the considered test setups informed the design of the test setup used to investigate the flexural behaviour of AMU walls in this study.

Chapter 4

Material Constituents and Unit Manufacturing

To meet the objectives of this study, masonry units needed to be manufactured with similar properties to those produced in previous AMU studies conducted by Fourie (2017) and Shiso (2019). The flexural behaviour of AMU walls depends greatly upon the characteristics of the comprising units and mortar. The manner in which these were produced is thus an important aspect of the project. This chapter provides details of the constituent materials that were used to manufacture the units and mortar. Thereafter, their mix designs and manufacturing processes are described.

4.1 Materials

4.1.1 Aggregates

The aggregates used in this project include three types of natural sand, a mechanically derived sand referred to as crusher dust, stone and clay. Due to the long duration of the unit manufacturing phase of the study and the quantity of materials required, different batches of these aggregates were ordered. All of the aggregates were dried before use. The clay contained lumps and required crushing and sieving before it could be added to the CSE and ADB unit mixtures.

The natural sands were sourced from local quarries and are named after their places of origin as Philippi sand and Malmesbury sand. Two distinct types of Malmesbury sand were used however, with one being considerably finer than the other. For this reason, it was decided to name the finer variety "fine Malmesbury". Two batches of Philippi sand were used and will be referred to as Philippi sand #1 and Philippi sand #2. Three batches of the coarser Malmesbury variety were used and are referred to as Malmesbury sands #1, #2 and #3. Two batches of fine Malmesburty sand were used and are referred to as Malmesbury sands #4 and #5.

The crusher dust is produced in a nearby facility by crushing a local stone known as Greywacke. For coarse aggregate, 13mm Greywacke stone was used. The clay, used in manufacturing the ADB and CSE units, was sourced from a local brick manufacturer. Two batches of crusher dust and stone were used and are also named after their respective batch numbers.

A sieve analysis was performed for each of the sands according to SANS 201 (2008), the results of which are available in Figure 4.1. The fineness modulus (FM) was determined as part of the sieve analysis and is provided in Table 4.1 alongside the particle shape and relative density of each aggregate, except for the clay which was not analysed. The relative density was acquired through the methods laid out in SANS 5844 (2014).

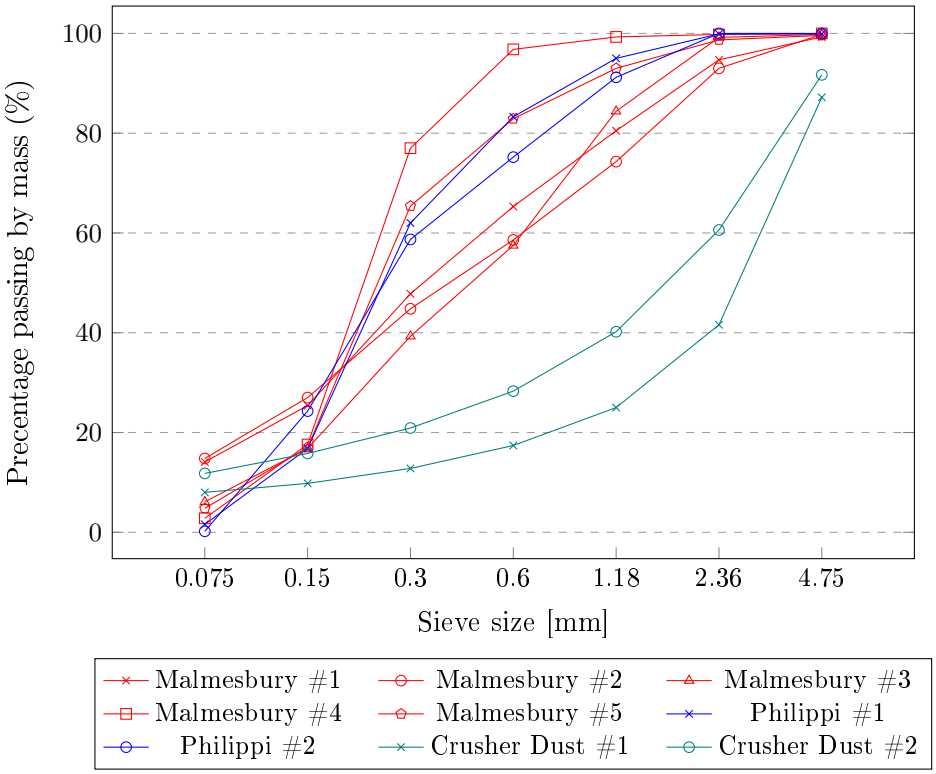

Figure 4.1: Aggregate grading

Table 4.1: Aggregate properties

Aggregate	FM	RD	Particle Shape
Malmesbury #1	1.87	2.56	round
Malmesbury #2	2.02	2.55	round
Malmesbury #3	2.03	2.62	round
Malmesbury #4	1.09	2.61	round
Malmesbury #5	1.44	2.61	round
Philippi #1	1.43	2.61	round
Philippi #2	1.50	2.60	round
Crusher Dust #1	4.06	2.69	angular
Crusher Dust #2	3.42	2.73	angular
Greywacke #1	-	2.74	angular
Greywacke #2	-	2.74	angular

4.1.2 Binders

Two Portland cements, CEM II 52.5 N and CEM II 42.5 N, were used for unit and mortar production. Additionally, fly ash (FA) and ground granulated corex slag (GGCS) were used either as a binder (in the case of the GEO units) or as an extender (in the case of the CON units). Care was taken to ensure that each unit or mortar contained binders derived from one batch only.

4.1.3 Alkaline Solution

Sodium silicate and sodium hydroxide were used to activate the binders of the GEO mix design. The sodium silicate was acquired in liquid from, while the sodium hydroxide was acquired in solid pellets. The sodium hydroxide pellets were dissolved in water for unit manufacturing. A full description of the alkaline solution preparation is provided in Section 4.2.2. Due to the caustic nature of these materials, protective clothing was worn at all times while handling them.

4.1.4 Water

All units and the mortar manufactured in this study required water to allow for hydration of binders and the workability of the fresh mixtures. Local, municipal tap water was used for the duration of the study. This water is potable and considered suitable for construction.

4.2 Unit Manufacturing

Units were manufactured from four kinds of materials: Concrete (CON), Abobe (ADB), Compressed stabilised earth (CSE) and Geopolymer (GEO). After manufacturing units for each type between June and November in 2018, the initial scope of the project increased so that more units were required for testing. To accommodate this, a second set of units was manufactured between April and May in 2019. For the sake of brevity, the first set of units will be referred to as "old", while the second set will be referred to as "new"- for example, the ADB units made in 2018 are called "old ADB" units.

As discussed, these units were developed by Fourie (2017) and a detailed explanation of the considerations that went into the mix designs is available in that thesis. For each unit-type, a set of trial mixes was performed which initially matched the originals. These mix designs were iteratively altered until a suitable mixture was developed. Through this process, the difference in the constituent material properties between the two studies was accounted for. Once the mix design of a unit had been determined, the unit manufacturing process would commence.

Although the preparation of the constituent materials differed substantially between unit-types, the mixing procedures were similar. Firstly, the required amount of each dry material would be weighed off to the nearest 0.02 kg, per batch of units, and decanted into a 50L pan mixer. These would be mixed for approximately 2 minutes before the wet ingredients were added. Thereafter, the wet mixture would be mixed for an additional 3 minutes to ensure an even distribution of the constituents. It was found that after adding water, some dry materials tended to stick to the corners of the mixing pan. To counteract this, the mixing process was halted for approximately 1 minute after adding the water so that the corners and bottom of the pan could be scraped. Once this had been achieved, the mixing was allowed to continue so that the wet ingredients were mixed for a total of 3 minutes.

Once the materials were sufficiently mixed, the units were formed out of the fresh mixture. Two different methods were used to form the units. The CON, CSE and ADB units were formed by compressing a specified mass of the mixture with a manual earth block press, displayed in Figure 4.2. For this method, the required mass of mixture to create each unit was weighed and placed into smaller containers. All of the filled containers of a batch were then covered loosely with polyethylene sheets and transported to the block press.

Figure 4.2: Manual earth block press

To form a unit, the mixture from one small pan would be loaded into the block press chamber in layers. Each layer would be levelled off before proceeding with the next. Figure 4.3 displays one of the containers, filled with CSE mixture, being decanted into the block press chamber. Once all of the mixture from one container had been emptied and levelled off in the chamber, the lid of the press was placed over the chamber and the unit was compacted. The finished unit would then be removed from the block press and placed nearby to set or cure.

Figure 4.3: Container of CSE mixture

The size of the units created by this method were set by the dimensions of the chamber, which produced units that were 290mm long, 140mm wide and 116mm high. The block press applied a single, upward compaction effort to the bottom bed face of the unit in the chamber. In general, the compaction effort of a block press can be described as static or dynamic (Venkatarama Reddy, 2012). In this case, a static compaction effort was applied.

The GEO units were formed by filling wooden moulds with the fresh mixture. The moulds were designed and constructed so that the casting face of the units would correspond with the front or back face of a unit that was laid on its bed face. The dimensions of the mould produced units that matched the dimensions of those produced by the block press.

Some important aspects of the manufacturing processes were unique to each unit-type and warrant detailed attention. The mix design, material preparation, manufacturing procedure and curing methods for each unit will be discussed in more detail in the following sections.

4.2.1 Concrete (CON) Masonry Unit

The CON units were manufactured by mixing the constituents according to their proportions in Table 4.2. The different aggregate batches used in the old and new CON mixtures are indicated in brackets alongside their respective quantities. These correspond with the names displayed in Table 4.1. This convention will be kept for the remainder of the chapter. The exact mix proportions prescribed by Fourie (2017) were adopted for the old CON units. The water content of the new CON units was reduced, after trial mixes revealed that the mix consistency would be too loose. In this instance, a mixture with too much water or insufficient cohesion resulted in a unit that would slump after it was pressed. This also made the unit difficult to handle in its wet state.

Table 4.2: Old CON and new CON mix proportions

Constituents	Old (kg/m^3)	New (kg/m^3)
Malmesbury	607 (1)	607 (3)
Crusher Dust	1316 (1)	1316 (2)
CEM II 42.5	144	144
Fly Ash	48	48
Water	212	193
Total	2327	2308

(*) Aggregate batch numbers

Fourie (2017) found that 10.5kg of wet mixture should be apportioned to each unit. The same was adopted for this study and it was found that a mixture of sufficient volume to produce seven units could be processed by the mixer per batch. The CON mixture was the wettest and loosest of the three units that were formed with the block press. This made it challenging to move the formed units from the block press without deforming or damaging them.

Immediately after forming, the units were placed on a table close to the block press, to set for 24 hours, as seen in Figure 4.4. Care was taken to minimize the deformation caused by moving and placing the fresh blocks. In this regard, two wooden paddles were used to move the units from the press. This was achieved by tilting each unit to rest on one paddle it was being carried.

Although the units were placed carefully, it was found that the action of lifting them and setting them down would still cause some of the units to slump. To counteract this, a mould consisting of two right angled parts was used to correct the shape of the wet unit as seen in Figure 4.5. The height of the mould corresponds with the correct unit height and the inner width of the closed mould corresponds with the width of the unit. The top of the longer sides of the mould were marked at a length of 290mm from the corners so that when the mould was closed up to this point, as demonstrated in Figure 4.5, an inner dimension of 290mm was created.

Figure 4.4: Paddles and mould used to form the CON units

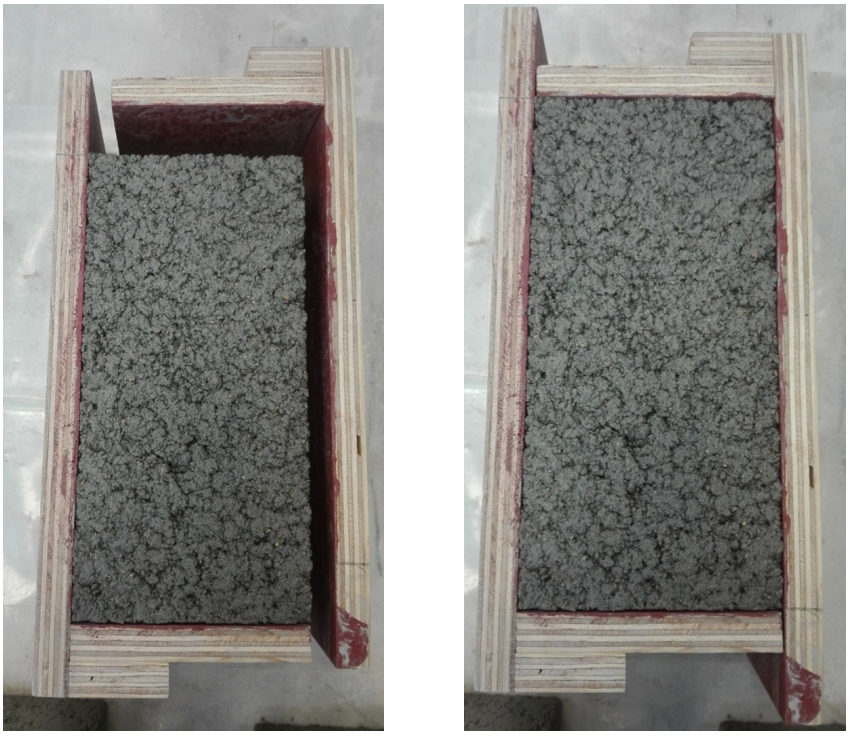

(a) (b)

Figure 4.5: Moulding of CON units after placing

The day after forming, the units were placed in curing tanks. By this stage, they were sufficiently set to manoeuvre by hand. The curing period of the unit depended on its use. A sample of old units was subjected to 28-day characteristic tests in 2018 (as described in Section 5.2). The remaining units were left to cure until two weeks before the construction of the walls and wallettes began. At that stage, the units were stacked loosely on the laboratory floor to dry. This ensured that moisture from the units would not alter the water content of the fresh mortar and that the units would be easier for the masons to handle during construction.

4.2.2 Geopolymer (GEO) Unit

After a set of initial trial mixes with the original GEO mix design proved unsuccessful, a dedicated investigation was performed by Schmidt (2020), to develop a reliable mixture. The old GEO mix design was based on that investigation, with only the water content adjusted to suit the batch of materials in the study.

Trial mixes undertaken before the manufacturing the new GEO units in 2019 revealed that the old GEO mix design resulted in a mix that was too wet with the original water content. Reducing the water content resulted in the mixture segregating due to insufficient cohesion between the paste and the aggregates. The significant difference in the behaviour of the fresh mixture was attributed to the use of FA that was sourced from a different supplier as well as the usual variability of aggregates between batches.

The mix design was corrected by increasing the proportions of the fine aggregates and FA. The required water quantity was ascertained by weighing off and adding water in intervals until the consistency of the mix proved satisfactory. This was performed on small trial mixes of two units. Both mix designs are provided in Table 4.3.

Table 4.3: Old GEO and new GEO Mix Proportions

Constituents	Old (kg/m^3)	New (kg/m^3)
Malmesbury	$700^{(2)}$	$750^{(3)}$
13mm Greywacke	$1000^{(1)}$	$1000^{(2)}$
Slag	100	100
Fly Ash (FA)	350	400
Sodium Silicate (SS)	70	70
Sodium Hydroxide Solution (SHS)	90	90
Water	120	76
Total	2430	2486

$^{(*)}$ Aggregate batch numbers

Before mixing of a batch of GEO units commenced, the sodium hydroxide solution (SHS) was created by adding sodium hydroxide (SH) pellets to water in a SH:water mass ratio of 0.4. The water and SH reacted exothermically, so that the fresh solution was hot. Trial mixes performed by Schmidt (2020) revealed that mixing GEO with the hot, freshly dissolved SHS, resulted in it setting before all the constituents could be mixed sufficiently to achieve homogeneity. To prevent this, the SHS was left to cool for 2 hours, at which point it would reach ambient temperature.

Once the SHS had cooled, the remaining constituents were weighed and decanted into containers. As per the other AMUs, the dry materials were decanted into a 50l pan mixer and mixed for 2 minutes before the liquid constituents were added. Afterwards, the SHS was added, followed by the sodium silicate (SS) and most of the water. The remaining water was then used to rinse the SS and SHS containers, so that the SS and SHS that had adhered to the inside of their containers was loosened and added to the mix. Due to the quick setting time of the fresh GEO, mixing was halted as soon as the mixture was deemed homogeneous. This generally occurred 2 minutes after adding the wet constituents.

The units were formed by casting the wet mixture into moulds as shown in Figure 4.6. The fast setting of the units proved to be challenging as two people were required to empty the mixture into moulds before it set. In both the old GEO and new GEO mixes, a total of six units were cast per batch. Cylinders were also cast in this manner to test the GEOs secant modulus of elasticity. Only one cylinder was cast with each batch of old units, while two cylinders were cast per batch of new GEO units. The filled moulds were placed on a vibrating table and vibrated for approximately 30 seconds while the exposed mixture was smoothed to the edge of each mould. The short vibration duration was adopted after discovering that the stone would segregate from the matrix and begin to sink at longer durations.

Figure 4.6: GEO units setting in their moulds

The fresh units and cylinders were left to set for 24 hours before being de-moulded. They were then moved to a climate-controlled room to cure after being removed from their moulds. The temperature of the room was kept at 25°C and a humidity of 65% was maintained throughout the curing period. It was noted that the units developed a soft crystallised coating in the curing environment, as displayed in Figure 4.7. This was also observed by Shiso (2019) and Schmidt (2020).

This is believed to be efflorescence, which is a known phenomenon in FA-based geopolymers (Provis and Van Deventer, 2009). Since sodium hydroxide (NaOH) was used as the alkali activator in this study, the efflorescence is most likely composed of sodium carbonate hydrates ($Na_2CO_3 \cdot nH_2O$), as described by Zhang *et al.* (2018). This type of efflorescence has been correlated to a loss of compressive strength and modulus of elasticity. Studies investigating the prevention and reduction of efflorescence have found that heat-curing may reduce it, while the addition of slag reduces the rate at which it occurs, but does not effect its potential to form Zhang *et al.* (2013).

Figure 4.7: Coating that developed on the GEO units in their curing environment

No approach to reduce efflorescence was adopted in an effort to ensure that the units were as similar as possible to those produced by previous studies of the project group. All units and cylinders remained in the curing environment until the day of testing, for unit and cylinder tests. For wall construction, the units were removed the day before, to ensure that construction could be performed swiftly. While the units were being transported to the construction area, a brush was used to remove the aforementioned coating.

4.2.3 Compressed Stabilized Earth (CSE) Unit

The CSE units consisted of Philippi sand, clay soil, CEM II 52.5 N cement and water. The clay was crushed and sieved through a 2.36mm aperture sieve. The dry constituents were mixed in the same proportions specified by Fourie (2017), for both old and new mixes, but the water content differed for each, as displayed in Table 4.4.

Table 4.4: Old CSE and new CSE Mix Proportions

Constituents	Old (kg/m^3)	New (kg/m^3)
Philippi	$1198^{(1)}$	$1198^{(2)}$
Clay soil	798	798
CEM II 52.5 N	200	200
Water	264	225
Total	2460	2421

$^{(*)}$ Aggregate batch numbers

The water content of the CSE was determined by testing the optimum moisture content (OMC) of the dry constituents according to SANS 3001-GR30 (2015). The OMCs calculated by this method were 11.3% and 9.2% for the old and new mixtures respectively. It was found that the mixture was slightly too stiff and dry for use in the block press at these moisture contents. The final moisture contents were adjusted to 12% and 10.2% for the old and new mixes respectively.

The OMC and final moisture content of the old CSE mixture was adopted from Shiso (2019) as his materials were sourced from the same batches, while the OMC and final moisture content of the new CSE mixture were determined as part of this study.

It was found that the 50l pan mixer could handle a 7-unit batch of the old mixture and an 8-unit batch of the new CSE mixture. After water was added to the dry materials, large clumps of the mixture would form due to its clay content. These were broken by hand while the mixing was stopped to scrape the mixing pan and again before the units were formed in the block press. The amount of fresh mixture apportioned to each unit was 9.4 kg.

Since the behaviour of the fresh material and the ultimate strength of the unit was dependent on the water content of the fresh CSE, great care was taken to prevent excessive evaporation. The mixture was covered immediately after being weighed off and each batch of units was formed as quickly as possible with the earth block press. The loose CSE mixture needed to be compressed to fit within the block press chamber. The material was thus added into the chamber in layers and each layer was compressed gently before adding the next. The CSEs required the highest compaction effort of the three pressed AMUs.

As a result of the degree of compaction applied, the dry consistency of the materials and the cohesion provided by the clay, the CSE units were the easiest to handle, of the pressed units, in the fresh state. After compaction each unit was placed on a table close to the block press by hand. Once a batch of units had been formed, the units from that batch were covered carefully with a polyethylene sheet to create a humid curing environment.

The units were sprayed with a light mist of water every 24 hours for 7 days after they had been formed. The mist was applied so as to moisten the units without causing pools of water to form. This process allowed hydration of the cement particles within the units. While spraying the units, the plastic covers were removed, but were put back in place immediately afterwards. After 7 days, the units were stored in a climate-controlled chamber with a temperature of 25 °C and a humidity of 65% as displayed in Figure 4.8. The units used for characteristic tests remained in the chamber until the day of testing, while those used to build masonry specimens were removed the day before construction.

Figure 4.8: CSE units in the curing chamber

4.2.4 Adobe (ADB) Unit

The ADB mix design developed by Fourie (2017) was adopted directly for the old ADB units. Attempts to use the same proportions with the batches available in the lab in 2019 resulted in a mix that was too wet. The units formed from this mixture contained too many voids. Schmidt (2020) attributed this to a lack of fines in the new batch of aggregates. To incorporate more fine particles, a blend of aggregates containing equal proportions of Malmesbury, Philippi and fine Malmesbury sand was used. In both instances, the water content was determined incrementally with the aim of producing a unit that had the correct consistency for use in the block press. This mix design was adopted for the new ADB mixture. The final mix designs are displayed in Table 4.5.

Table 4.5: Old ADB and new ADB Mix Proportions

Constituents	Old (kg/m^3)	New (kg/m^3)
Malmesbury	809 [2]	539[3]
Malmesbury (fine)	-	539[4]
Philippi	809[1]	540[2]
Clay soil	534	534
Water	275	145
Total	2427	2297

[*] Aggregate batch numbers

The clay soil used for the ADB mixture was sieved to a nominal size of 1.18mm to minimize the presence of impurities. This was deemed important as clay acts as a binder in the ADB mixture and is the sole contributor to the cohesion of the unit.

The old and new ADB units were manufactured in 7- and 8-unit batches respectively. Similarly to the CSE mixture, clumps would form in the mixing pan after the addition of water and these would be broken up by hand. The mass of material apportioned for each ADB unit was 9.3kg. As with the CSE, the ADB was covered with polyethylene sheets in between mixing and forming.

In practice, ADB units are usually formed by hand compaction using so-called ladder moulds, as discussed in Section 2.3.1. Fourie (2017) adopted this method, but avoided compacting the units by hand and simply added material to each mould until it was full. This method was found to be undesirable, as it was found difficult to hand-compact units consistently, leading to units being produced with different densities and sizes. This would have contributed to the variability of Fourie's ADB unit results (2017).

Shiso (2019) abandoned the aforementioned method of forming in favour of the earth block press and the same decision was adopted for this study. The aim of using the block press, in this instance, was to create ADB units in as uniform a manner as possible, but without using enough compaction effort to add considerably to the strength of the units.

The fresh ADBs were weak and required careful handling after compaction. To this end, the paddles that were used to move the CON units were also used to transport the ADB units. The ADB units were left on a nearby table to air-dry within the laboratory until the day of testing or construction. Figure 4.9 displays curing ADB units. The units in the foreground had been pressed before those in the background and are lighter in colour due to their decreased moisture content after drying.

Figure 4.9: ADB units

4.3 Mortar Manufacturing

Cement-sand mortar was used to manufacture the masonry specimens. Although cement-lime mortars or cement-soil mortars might have been used as alternatives, cement-sand mortars are typically used in the construction of LIH in South Africa and have been used in previous AMU studies at Stellenbosch University (Fourie, 2017; Shiso, 2019).

Since the flexural characteristics of a masonry wall are heavily dependent on the properties of its mortar, two mortars of differing strength classes were used. This would allow comparisons to be drawn between AMU masonry specimens built from different mortars and potentially provide greater insight into the effects of mortar strength on the flexural capacity of masonry. Mortars are typically classified according to their 7-day compressive strength values. The weaker and stronger mortars were designed to exhibit 7-day characteristic compressive strengths of 7MPa and 20MPa respectively. Consequently, the mortars will be referred to as "7M" and "20M" mortars.

The mortar mix designs were determined through a series of trial mixes. For each iteration, the sand-cement ratio was adjusted and enough water was added to provide the mortar with a flow value of 200mm, when assessed according to the standard EN 1015-3 (1999). The binder used was CEM II 42.5 N cement and fine Malmesbury sand was used as the aggregate as it is typically used for mortar production by local masons.

The first trial mixes were manufactured with Malmesbury sand #4 and the mortars used to construct the CON and CSE masonry specimens contained this aggregate. Due to unforeseen circumstances, that batch of sand became unavailable. For this

reason, a second fine Malmesbury sand from a different batch (Malmesbury #5) was obtained. A second set of trial mixes was performed to obtain comparable 7M and 20M mortars with this sand. The goal was to achieve similar flow values and compressive strengths to the first mortars, by keeping the water/cement ratios constant and altering the sand/cement ratios. After successful trial tests, the new mortars were used to construct the ADB and GEO masonry specimens. The final constituent proportions by mass, relative to 1 kg of binder, are provided in Table 4.6. The mortars used to construct each unit-type's masonry specimens are also indicated in Table 4.7.

Table 4.6: Mortar constituents in mass proportion

Constituents	7M 1	7M 2	20M 1	20M 2
CEM II 42.5	1	1	1	1
Malmesbury	$4.83^{(4)}$	$5.1^{(5)}$	$2.68^{(4)}$	$2.89^{(5)}$
Water	1	1	0.61	0.61

$^{(*)}$ Aggregate batch numbers

Table 4.7: Mortars used per unit-type

Unit	20M	7M
CON	20M 1	7M 1
GEO	20M 2	7M 2
CSE	20M 1	7M 1
ADB	20M 2	7M 2

An attempt was made to produce a weaker mortar with a 5 MPa 7-day compressive strength as this corresponds to a class II mortar prescribed by SANS 10145 (2011) for load bearing walls subjected to extremely damp conditions. This was abandoned after it was found that the constituent materials chosen could not produce a flowable mixture at the sand:cement ratio required to achieve that strength. The 7M mortar was thus developed in lieu of the 5M mortar. The 20M mortar was chosen as it represents the strongest mortar allowed by the Eurocode, EN 1996-1 (2005). Since South Africa is in the midst of adopting the masonry Eurocodes, this makes 20M the strongest mortar applicable to the South African masonry construction industry.

During the construction of the masonry specimens, the same quantity of mortar was mixed to ensure that the constituent proportions remained constant throughout the study. The total weight of the batches used were 20.1kg and 20.0kg for the 7M and 20M mortars respectively. These quantities were chosen to ensure that the masons could finish each batch of mortar before it required additional water, thereby ensuring that the mortar water content would remain constant between specimens and unit types. To ensure the quality of the mortars used during construction, the flow value of the mortar was assessed according to EN 1015-3 (1999) at random intervals.

4.4 Summary

This chapter was provided to present the manner in which the masonry units and mortar were manufactured. Firstly, the properties of the constituent materials were discussed. Secondly, the mix design, mixing procedure, forming process and curing process was described for each unit type. Lastly, the motivation behind the choice of mortars used was presented along with its mix design and use during the construction of the masonry specimens.

The work conducted in manufacturing the units was necessary for the fulfilment of one of the objectives of the study, namely, to create units that are similar to those developed by previous students in the research project. This objective was pursued with as much effort as the time and nature of the materials and equipment available could provide. Furthermore, the units and mortar were used to construct the masonry specimens which would be tested as the main objective of the study.

Chapter 5

Experimental Design

5.1 Overview

After the units were manufactured, tests were performed on the units, masonry specimens constructed from each unit-type and the mortar used to build those specimens. This chapter outlines the procedures of each test and describes the test setups that were used to obtain the required parameters. An outline of the tests performed on the units and mortars is provided at the start of their respective sections.

The compressive strength, elastic modulus and flexural behaviour of masonry walls were investigated. For clarity, the specimens that were built to investigate compressive strength and elastic modulus will be referred to as wallettes, while the masonry specimens upon which the flexural investigation was performed will be referred to as walls. Two sets of wall and wallette tests were performed for each unit-type. The first set was built with a stronger mortar (20M), while the second was built with a weaker mortar (7M). All tests were performed 7 days after the specimens had been built. The mortar and units used for each masonry specimen are shown in Table 5.1.

It will be noted that only two replications were tested for the flexural wall tests. This was due to two factors. Firstly, due to time and material limitations, only four replications per unit per flexural test-type could be performed. Secondly, since mortar properties have a significant influence on the flexural properties of masonry, the available units were split to incorporate two types of mortars.

Table 5.1: Masonry Specimens

Test Specimens	Mortar	Units	No. Specimens
Parallel Flexural Walls	20M	Old	2
Perpendicular Flexural Walls	20M	Old	2
Wallettes	20M	Old	4
Parallel Flexural Walls[1]	7M	Old	2
Perpendicular Flexural Walls[2]	7M	New	2
Wallettes	7M	New	4
Wallettes	7M	Old	3

[1] New Units were used for the GEO specimens
[2] Old Units were used for the GEO specimens

5.2 Masonry Unit Tests

The compressive strength and elastic modulus of each unit type were tested at two stages. The first set of tests were only performed on the old units at an age of 28 days to characterize them (characteristic tests). These specimens were tested immediately after they were removed from their curing environments. A second set of tests (auxiliary tests) were performed on both old and new units at the time of testing the masonry specimens to determine their constituent properties. In this case, the specimens were tested in the condition they were in at the time of building. Characteristic dry density tests of both the old and new units were performed, but only after the masonry tests had been completed. A summary of the unit tests is provided in Table 5.2.

Table 5.2: Summary of Masonry Unit Tests

Test Performed	Characteristic	Auxiliary
Compressive Strength	Old	Old, New
Modulus of Elasticity	Old	Old, New
Dry Density	Old, New [1]	

[1] performed after the masonry tests

5.2.1 Compressive Strength Test

The compressive strength of the units was determined according to EN 772-1 (2011). Since the specimens were tested in the bedface orientation, both bedfaces of each specimen were ground flat before testing to ensure the loaded surfaces were smooth and perpendicular to the axis of loading. They were then weighed, measured and

placed between two 20mm thick platens in the test apparatus. These components are displayed in Figure 5.1. A quasi-static displacement-controlled loading of 0.75 mm/min was applied to the specimens by means of an Instron Materials Testing Machine (Instron).

Figure 5.1: Standard bed-face compressive strength setup

Alternative setups were used to test the new GEO and ADB units. The latter units proved to be too weak and brittle to grind successfully, but their bedfaces were sufficiently straight and smooth to ensure an evenly applied loading. To account for any skewness between their loaded surfaces, a self-levelling attachment was placed between the top platen of the specimen and the Instron's actuator. In contrast, the Instron did not have the capacity to test the new GEO units to failure. To overcome this, the units were rotated 90° in plan to reduce the loaded area. This had the effect that the load was applied to the centre of each bedface over an area of 140mm x 150mm. Both alternative setups are displayed in Figure 5.2

(a) GEO bedface compression

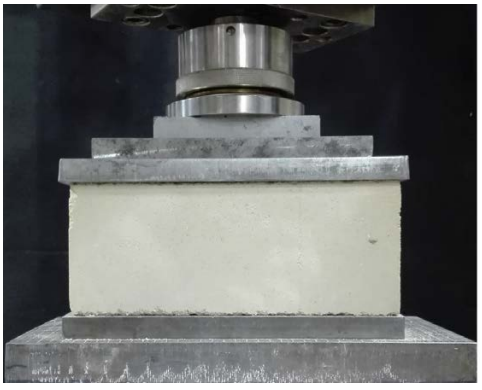

(b) ADB bedface compression

Figure 5.2: Alternative bedface compressive strength setups

After reaching the maximum capacity of each specimen, the Instron would continue loading until the measured load reached half of the specimen capacity. The maximum compressive force, loaded area and mass were recorded for each specimen. While the first two parameters were required to calculate the compressive strength of the unit, the mass of the specimen was recorded for quality control.

5.2.2 Modulus of Elasticity Test

The procedures outlined in EN 12390-13 (2013) were followed throughout the study where possible. It was not possible to follow this standard completely while testing the GEO units and the ADB units, as described later in this section.

Prismatic specimens were sawn out of CON, CSE and ADB units such that their loaded faces coincided with the unit bedfaces. In this way the length of each specimen was identical to the unit height (116mm). To ensure that these specimens adhered to the aspect ratio specified in the code, a square profile of 58mm x 58mm was chosen. The loaded faces of all specimens were ground flat except for the ADB specimens which were too brittle to grind.

Two specimens were sawn out of each unit selected for testing. The first is referred to as a companion specimen and was tested to failure in compression. The modulus of elasticity test was performed on the second specimen and the maximum compressive force applied during this test was chosen as a third of the companion specimen's capacity. After the modulus of elasticity test had been performed the second specimen was also subjected to a compressive strength test.

For all sawn specimens (CON, CSE and ADB), loading was applied to the specimen by a 2MN Instron Materials Testing Machine and an aluminium frame was employed to measure the displacements of each specimen. Four linear variable displacement transducers (LVDTs) (one per each vertical face of the specimen) were attached to two horizontal brackets that would surround the specimen at a spacing equivalent to the required gauge length of 50mm. At the location of each LVDT, a screw was fastened through each bracket into the specimen. The gauge length was ensured by having two struts fastened between the horizontal beams while the frame was being attached. Once the frame was ready, the struts were removed to allow relative displacement between the beams.

Once the frame had been attached to a specimen and the struts had been removed, the specimen was placed within the test apparatus. Initially, the bottom boundary condition consisted of a thick plate resting on top of a 2MN external load cell. The top boundary condition consisted of a metal plate between the specimen and the actuator's loading head. This setup is shown in Figure 5.3. The actuator head was not self-levelling and the results indicated that bending may have been induced within the specimen during the tests. To circumvent this, three tests were performed on each specimen at different in-plan rotations and the resulting elastic modulus was taken as the average result of these tests.

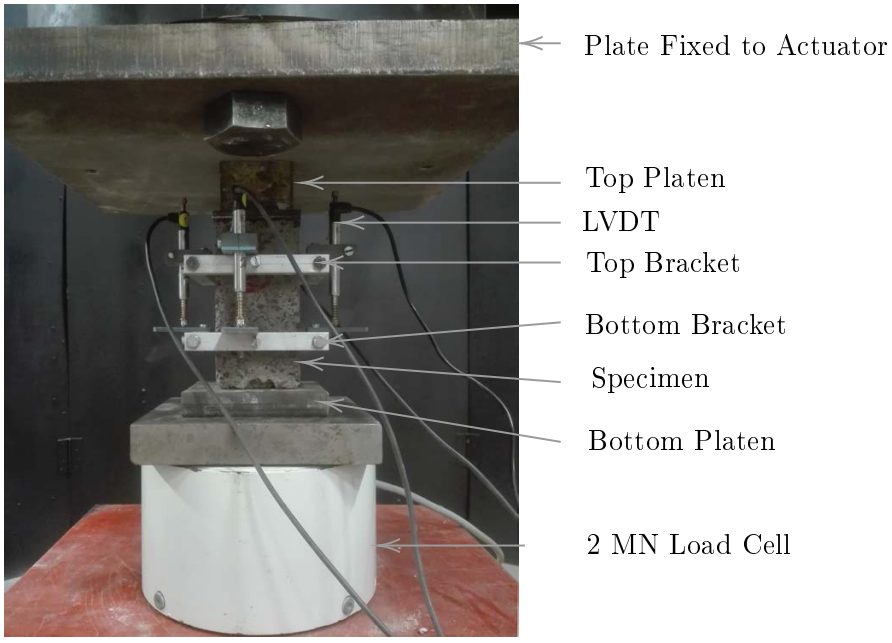

Figure 5.3: Original elastic modulus setup for CON, CSE and ADB specimens

A suitable levelling attachment was found and attached to the actuator head for the second set of tests. With this enhancement, it was only necessary to perform two tests per specimen and measurement issues were rectified by adjusting the LVDTs between tests. A more precise 50kN Load cell (with a higher resolution) and a thicker plate were also introduced as the new bottom boundary condition in this phase. A picture of this improved test setup is provided in Figure 5.4

After a specimen had been placed into the test apparatus and the measurement instruments had started recording, the loading regime was applied. A force-controlled loading was applied to the CON and CSE specimens as specified by method (b) of EN 12390-13 (2013), with one exception. A rate of (0.6 $\pm$ 0.2) MPa/s is specified which corresponds to an applied force in the range of 1345 N/s and 2690 N/s, but a rate of 135 N/s was applied to accommodate the low strength of the specimens. The actuator could not apply a force-controlled loading to the ADB specimens due to the low compressive strength and elastic modulus of the material. Instead, a displacement-controlled regime was implemented based on the companion specimen test results.

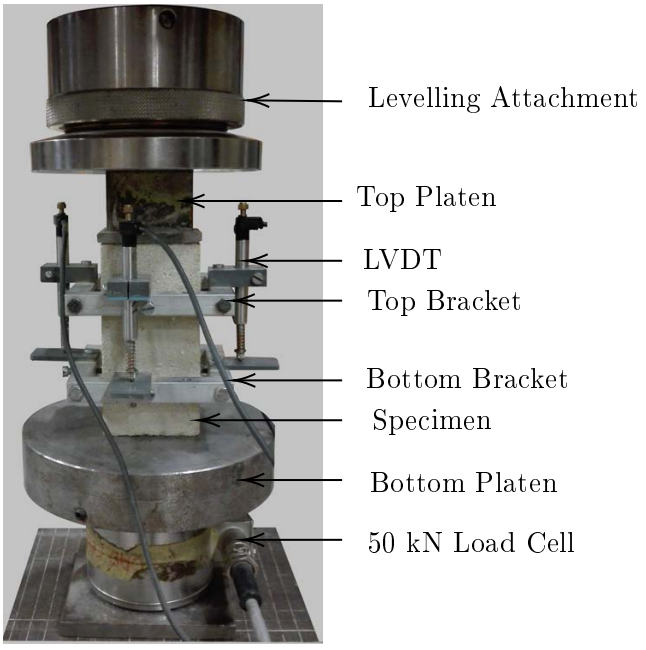

Figure 5.4: Improved elastic modulus setup for CON, CSE and ADB specimens

Due to the extreme hardness of the GEO units, it was deemed infeasible to saw elastic modulus specimens out of existing units. Instead, they were created by casting cylinders during the unit manufacturing process. These cylinders had a diameter of 100mm and a height of 200mm. For the old units, one specimen was cast per batch of units. Three specimens were selected from this set for compressive testing and the average compression result was applied to determine the maximum loading of all the elastic modulus tests. For a more comprehensive set of results, two specimens were cast for every batch of new blocks. In this way, an elastic modulus result was obtained from every batch and the maximum force applied during each test was determined from a companion specimen within the same batch.

As with the other unit-types, a frame was used to measure displacements. Although a different frame was used and only three LVDTs were attached to it, the placement procedure was analogous to that of the other specimens. The actuator that was used to apply load to these specimens was a 2MN KingTest CONTEST. Once the frame had been attached to the specimen, it was placed on top of a platen that rested above a 2MN load cell as seen in Figure 5.5 The actuator of the CONTEST had an in-built self-levelling head and two thick metal platens separated it from the top of the specimen.

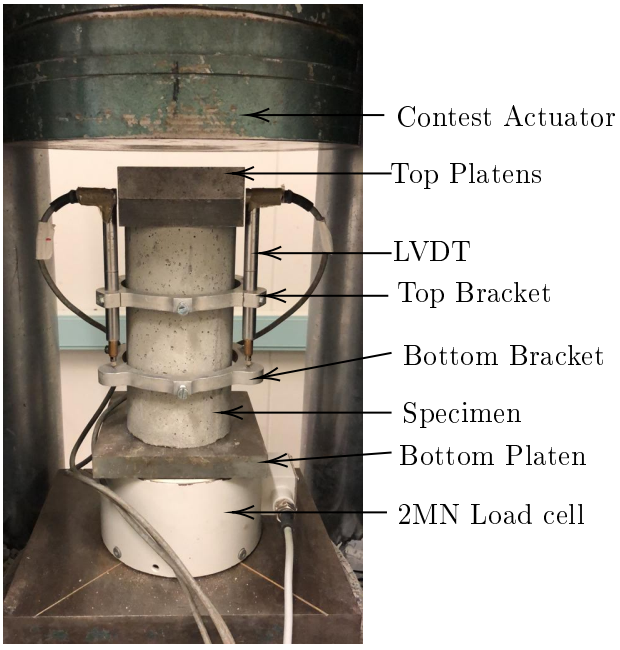

Figure 5.5: GEO elastic modulus test setup

Since the CONTEST did not have a programmable load functionality, the load-regime was applied manually. It was difficult to apply the loading regime as specified by EN 12930-13 (2013) manually, so the prescribed regime was adapted. The maximum load applied during the elastic modulus test was taken as 40% of the companion specimen load capacity. The loading rate applied during the manual tests was set by a dial on the control box. However, the dial settings did not reflect actual loading rates (in kN/s for instance), but were rather rated from 1 to 5. A setting of '1' was adopted for the study, which corresponded to a loading rate of 8 kN/s. This falls outside of the specified range of (18.85±6.28) kN/s.

5.2.3 Dry Density Test

A dry density test was performed according to the provisions of EN 772-13 (2013) for aggregate concrete and manufactured stone units. A sample size of six units was set aside from each set. The volume of each unit was determined by measuring its height, width and length with a measuring tape accurate to the nearest millimetre. Every mass measurement was taken with a scale accurate to 0.1g. Once the volume and air-dry mass of each specimen was determined, the sample of six specimens was placed in an oven that maintained a temperature of 70° Celsius. Every 24 hours, the specimens were removed, allowed to cool for 30 minutes and weighed before being returned to the oven. A mass change of less than 0.2% between consecutive measurements indicated that the specimen had reached its dry mass. The dry density was calculated as the specimen's dry mass divided by its volume.

5.3 Mortar Tests

Tests were performed on the mortars used to construct the masonry specimens to determine the mortar compressive strength, elastic modulus and flexural capacity at 7 days. Each specimen was cast by sampling mortar from the mixing bowl and pouring it into the mould in three equal layers - vibrating for 5 seconds between successive pours. The vibration was applied with a vibrating table. Thereafter, the specimens were cured in accordance with EN 1015-11 (1999), by placing the moulds into polyethylene bags and storing them inside a climate chamber of 65% humidity. After 2 days, the specimens were removed from the mould and stored back into their bags until they were tested.

5.3.1 Consistency (Flow table) Test

The consistency, also referred to as the "flowability", of the mortar was tested during the mortar trial mixes to develop the final mortars for construction and during the construction period itself. The tests performed during the trial mixes were used as a guide to ensure that the final mix designs were sufficiently flowable. Since the final mix designs were kept constant throughout the construction of the walls, the tests performed during that period acted as a means of quality control. Furthermore, these results could be compared to the wall and wallette test results to provide insight into the relationship between mortar consistency and masonry compressive and flexural strength.

The standard EN 1015-3 (1999) was applied to measure and calculate the consistency of the mortar. The apparatus included a conical mould, pallette knife, scoop or trowel, a tamp, a machine capable of providing a jolt (referred to as a flow table) and a ruler or measuring tape. To test a sample of mortar, it was decanted into the mould in two approximately equal layers. Each layer was tamped ten times before the next layer was added into the mould. The final layer was smoothed off to the surface of the conical mould with a pallette knife.

After all of the mortar had been decanted into the mould and levelled off, the mould was lifted off of the mortar slowly. Thereafter, the handle of the flow table was turned so that the machine would impart 15 jolts to the mortar at a rate of approximately 1Hz. The width of the mortar was then measured in two orthogonal horizontal dimensions to the nearest 1mm and the average of these was used to calculate the result. To report on the flow value of a batch of mortar at a particular age, this test must be repeated twice and the average of the two values used. For a result to register as valid, the individual measurements of each test may not differ by more than 10% from the final flow value. In the case of invalid results, the test was repeated until a valid result was obtained.

5.3.2 Elastic Modulus Test

Cylindrical specimens with a height of 200mm and a diameter of 100mm specimens were cast to determine the mortar's elastic modulus. As with the unit tests, their tops were ground flat to ensure an even, horizontal loading surface. Before any specimen was subjected to testing it was first measured and weighed. The same procedure and apparatus used to determine the elastic modulus of the GEO cylinders were also applied to this test. Whenever possible, each elastic modulus test's load profile was determined from a companion specimen of the same batch. If only one cylinder was cast from a batch, the load profile was determined from the companion specimen of a previously tested batch.

5.3.3 Flexural Strength Test

The mortar flexural strength was determined according to EN 1015-11:1999. As specified, prismatic specimens were cast with a square cross-section of 40mm x 40mm and a length of 160mm. Before testing a set of specimens, they were removed from the curing environment and the dimensions and mass of each specimen was recorded. A scale, accurate to the nearest 0.1 g, was used for weighing and a vernier calliper, accurate to the nearest 0.05mm was used to determine the cross-sectional dimensions at each specimen's mid-point. A Zwick Z250 Materials Testing Machine (Zwick) was used to apply a loading to the specimen at third-points. Lines were drawn on the casting face of each specimen to indicate the contact points of the inner bearings. Thereafter it was placed into the apparatus as shown in Figure 5.6 with its casting face oriented horizontally.

Figure 5.6: Mortar flexural strength test

Initially, a force-controlled loading rate of 10N/s was applied to each prism as specified in the code. After inspecting the results, it was found that the Zwick could not apply that test-control accurately. At this stage, the test had already been performed on the CON and CSE mortar. A new displacement-controlled loading rate of 0.04 mm/min was applied to all proceeding specimens and the machine was able to apply this rate satisfactorily. The time, crosshead displacement and applied force were recorded automatically by the Zwick, at a rate of 5Hz. Once a specimen had been tested to failure, it was inspected to determine whether the crack had formed in the zone of constant moment (between the inner bearings). If the crack fell outside of this zone, the result was discarded from the set of flexural strength calculations.

According to EN 1015-11:1999, the specimens should be cast in mould that produces three specimens. The flexural strength of each specimen is rounded to the nearest 0.05 MPa and the mean of the three results, rounded to the nearest 0.1 MPa, represents the flexural strength of the mortar.

5.3.4 Compressive Strength Test

The mortar's compressive strength was determined according to EN 1015-11:1999. Once a set of flexural tests had been performed, a sample of the broken half-prisms was selected for compressive strength testing. A square platen with 40mm side-lengths and a 10mm thickness was placed centrally on the top and bottom of the specimen as seen in Figure 5.7. A self-levelling attachment made contact with the top platen. A loading rate of 400 N/s was applied until failure, where-after the test apparatus was cleaned and the next specimen was placed.

Figure 5.7: Mortar compressive strength test

5.4 Wallette Tests

For each unit-type, three sets of wallettes were built according to unit-mortar combinations shown in table Table 5.3. The compressive strengths (f_{cw}) and the elastic moduli (E_{cw}) of the walls within each set were then determined according to EN 1052-1 (1999).

Table 5.3: Wallette tests per unit-mortar combination

Wall	Old 20M	Old 7M	New 7M
1	f_{cw}	E_{cw} , f_{cw}	f_{cw}
2	E_{cw} , f_{cw}	E_{cw} , f_{cw}	E_{cw} , f_{cw}
3	E_{cw} , f_{cw}	E_{cw} , f_{cw}	E_{cw} , f_{cw}
4	E_{cw} , f_{cw}	-	E_{cw} , f_{cw}

To adhere to the standard, 10 units were used to construct the specimens with 10mm joints to an approximate height of 610mm and length of 590mm. They were built onto steel plates by placing a sheet of polyethylene centrally on each plate before spreading mortar onto each sheet and laying the first blocks on the fresh mortar. To ensure an even, horizontal load-surface, a final layer of mortar was laid on top of the specimen. Once this layer had set sufficiently, the specimens were cured by covering them with polyethylene sheeting. This curing state was maintained until test-day.

On the day of testing, all of the wallettes were uncovered. The same Instron that was used for the unit compressive strength tests in Section 5.2.1 was also used to test the wallettes. All specimens were loaded onto the Instron by overhead crane. To ensure an even load-distribution was applied to the entire loaded face of the specimen, a spreader beam was attached to the Instron's actuator as displayed in Figure 5.8. It was capable of applying a displacement controlled load-rate and the loads recorded during the test were measured from the machine's own load cell. Take note that the LVDTs and brackets shown in Figure 5.8 were not present for the specimens that were only tested for compressive strength.

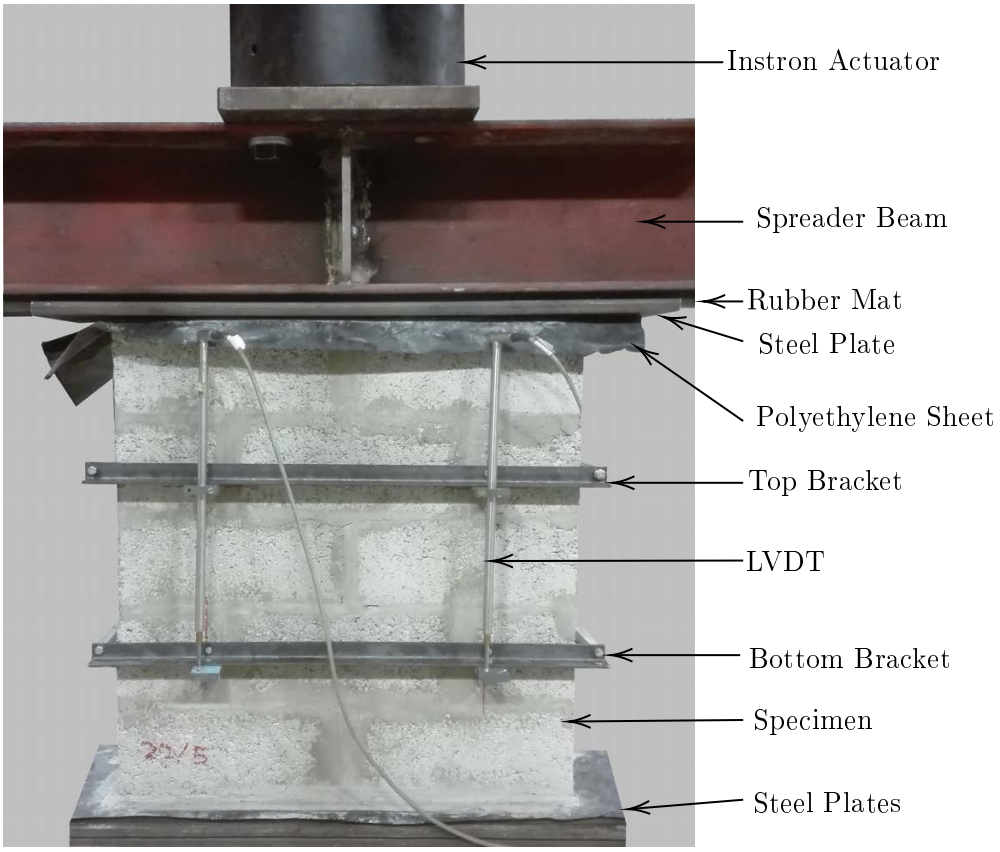

Figure 5.8: Wallette elastic modulus setup

The bottom boundary condition consisted of two steel plates lying flat on top of each other. The top boundary condition was created by placing a polyethylene sheet, steel plate and rubber mats on top of the wallette in that order (bottom to top). Thereafter, the actuator was lowered into position until a pre-load of 1 kN had been reached before it was compressed to failure. Displacement-controlled rates of 0.4, 0.3, 0.25 and 0.2 mm/min were applied to the CON, GEO, CSE and ADB wallettes respectively in an effort to cause failure within a duration of 15 to 30 minutes.

For the Old 20M and New 7M Unit-Mortar combinations, the first specimen was compressed to failure without measuring the displacements on the faces of the wallettes. The maximum compressive capacity was noted before testing the remaining walls. To determine the elastic modulus of the remaining walls, the vertical displacements on each face were measured as specified in EN 1052-1 (1999). This was achieved by attaching an LVDT frame (similar to the those described in Section 5.2.2) to the wallettes before the test commenced.

The frame allowed two LVDTs to measure vertical displacements on each face. The screws that were fastened into the wallettes to hold the frame in place and transfer displacements to the LVDTs were situated 320mm apart horizontally and 210mm apart vertically. This ensured that the LVDTs were given the same horizontal spac-

ing and a gauge length of 210mm. As soon as the compressive force reading reached half of the ultimate compressive capacity of the first specimen, the LVDT frame was removed from the wallette. In the case of the Old 7M wallettes, the frame was removed at half of the average ultimate compressive force of the Old 20M wallettes.

5.5 Wall Flexural Strength Test

5.5.1 Overview

Tests were performed on masonry walls to investigate their flexural behaviour. This section describes the preparation of the specimens that were tested. Thereafter, the test setup that was designed for the purpose of testing the walls is presented as well as the measurements that were taken throughout each test. The European standard, EN 1052-2 (2016) was adopted as a guideline for the test as it would ensure that the results of this study would be as relevant and comparable as possible. Although an effort was made to follow the standard, certain key requirements could not be met. Table 5.4 presents key requirements of the standard and the application of each requirement in this study.

Table 5.4: Key requirements specified by EN 10152-2 (2016) compared to their applications in this study

Parameter	Specification	Application
Specimen Age (days)	28	7
Pre-compression (kPa)	between 2.5 and 5	between 2.4 and 3.2
Replications	5	2
Load Rate	force-controlled: between 0.03 and 0.3 MPa/min	displacement-controlled: as in Table 5.6

The principle of the standard is to apply four-point loading to a masonry specimen so that it fails within a zone of constant moment and zero shear. If the specimen fails within that zone, it's flexural strength can be determined as a function of the total applied force, specimen dimensions and the geometry of the loads and supports. This configuration is favourable (when compared to three-point loading) as the influence of shear stress is removed from the result. Furthermore, since constant flexure is applied over a zone, the stress which causes failure within that zone may easily be determined. Figure 3.16 has been provided to demonstrate typical applications of the standard and to illustrate the terminology that will be used to describe the test.

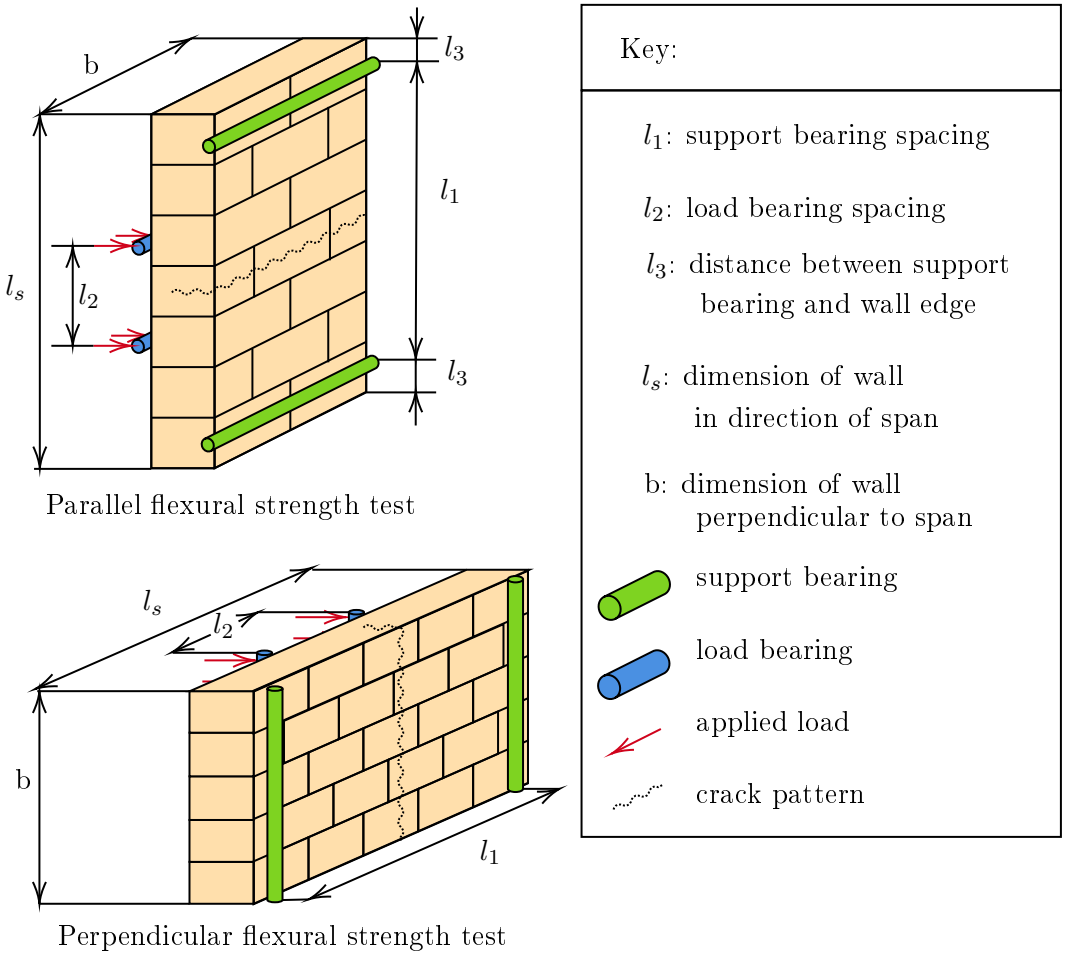

Figure 5.9: Typical flexural strength tests as prescribed by EN 10152-2.

5.5.2 Specimens

A summary of the specimen and test dimensions per test type is provided in Table 5.5. All specimens were built with mortar joints of a 10-15mm thickness and their resultant dimensions are displayed in Figure 5.10 and Figure 5.11.

Table 5.5: Test Geometries

Parameter	Parallel Specimens		Perpendicular Specimens	
	mm	units/spanned joints	mm	units/spanned joints
b	440	1.5 units long	514	4 units high
l_s	640	5 units high	1190	4 units long
l_1	500	4 bed joints	1050	3-4 head joints
l_2	252	2 bed joints	430	2-3 head joints
l_3	70		70	

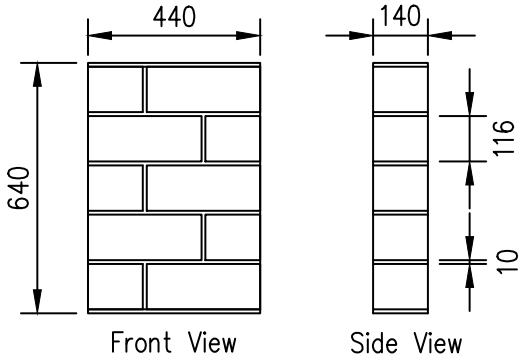

Figure 5.10: Parallel wall dimensions (mm)

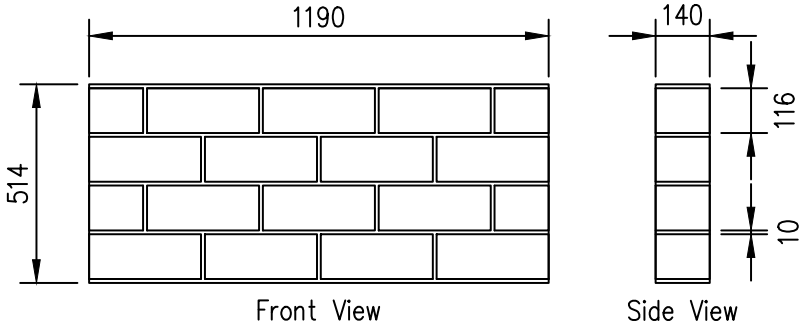

Figure 5.11: Perpendicular wall dimensions (mm)

Since the walls could not be built inside the test setup, they were built onto bases. These allowed walls to be transported to the test setup safely and formed part of each test's bottom boundary condition (discussed in Section 5.5.3). Each base was comprised of a steel member and a slip-plane that was placed between the wall and the steel section to reduce friction between them during tests. Flat steel plates (250mm wide x 16mm thick) were used for the parallel walls and parallel flange channel sections (PFC 260 x 90) were used for the perpendicular walls. For each wall, the slip plane comprised of a 1mm thick HDPE (High Density Polyethylene) layer, coated with mineral oil and covered with a layer of 150 micron polyethylene typically used as damp proof course (DPC). Each wall was mortared to the DPC layer during construction. Figure 5.12 provides a cross-sectional view of a perpendicular wall base.

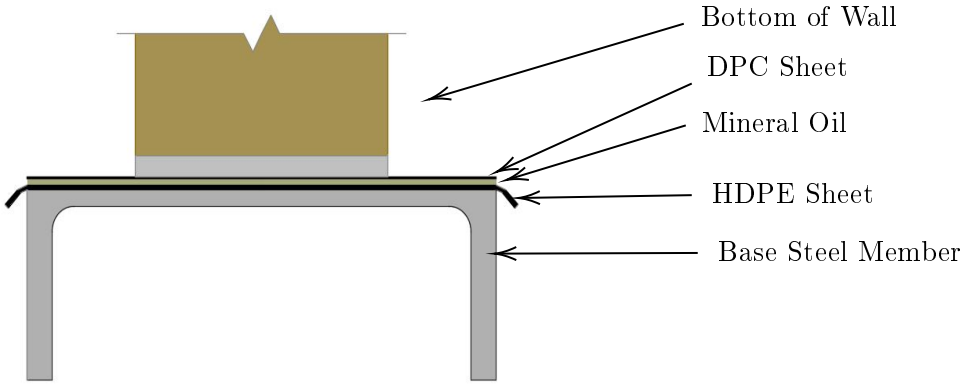

Figure 5.12: Diagram of a perpendicular wall base (not to scale)

After a batch of walls was constructed, a 10mm layer of mortar was spread onto the top of each wall and smoothed flat with a spirit level. Once this layer had set, the walls were covered with polyethylene sheets to cure. A pre-compression was also applied to each wall by placing a wooden plank and weights on top of them. Pre-compressions of 3.2 kPa and 2.4 kPa were applied to the parallel and perpendicular walls respectively.

5.5.3 Test Setup

The applied standard, EN 1052-2 (2016), allows one to test walls in the horizontal or vertical attitude. The latter option was chosen so that they could be tested in the same orientation that they were built in. This is the standard's preferred method and reduces the risk of destroying a specimen before it can be tested.

The load was applied by an Instron hydraulic servo-controlled actuator (Instron), which was bolted to the laboratory's strong-floor. This supplied a displacement-controlled loading to the wall dependant on the wall's unit and mortar type. In each case, a rate was chosen in an attempt to reach failure within 10-15 minutes. Table 5.6 provides the rates that were applied in each case.

Table 5.6: Displacement rates applied to flexural wall specimens in mm/min

Mortar	CON	GEO	CSE	ADB
20M	0.4	0.3	0.4	0.2
7M	0.4	0.3	0.3	0.2

To apply the loads and supports to the specimens at the correct geometries, a test setup was designed and fabricated. Figure 5.13 and Figure 5.14 show the setup in the parallel and perpendicular configurations respectively. The views displayed in these figures were chosen such that the general design of the setup would be clear.

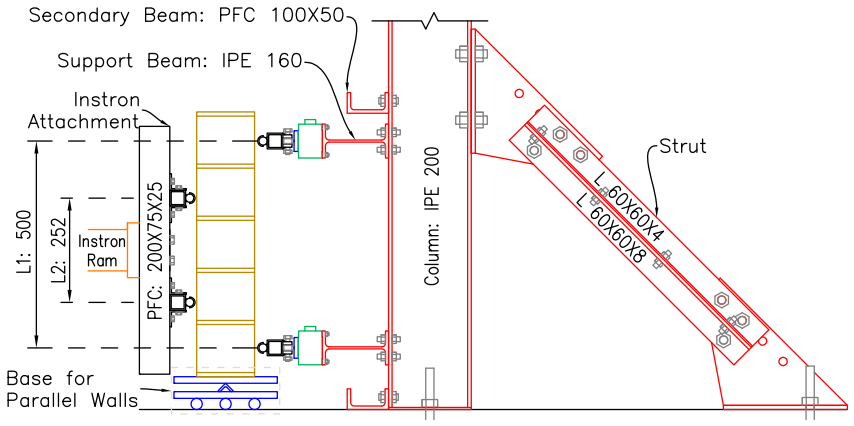

Figure 5.13: Side view of the test setup in the parallel wall configuration

The force produced by the Instron had to be applied to the wall in two line loads. The components that made contact with the specimens are referred to as load bearings. They were constructed by welding 20mm diameter steel rods onto square hollow sections, which were then filled with mortar to prevent local buckling. Plastic irrigation tubing was spliced and slid onto the rods of the bearings to provide an even load application onto the specimen. The bearings were bolted via angle cleats to a parallel flange channel section which was in turn bolted to the head of the Instron's ram.

The combination of these components (excluding the ram) is referred to as the Instron attachment. The bolt holes of the attachment's channel section allowed different load bearing spacings for the parallel and perpendicular tests. Between each type of test, the ram was made to rotate to the correct angle and the load bearings were re-fastened at the required spacing. Depending on the test specimen, shims were placed between the load bearings and the channel section to ensure full contact with the specimen.

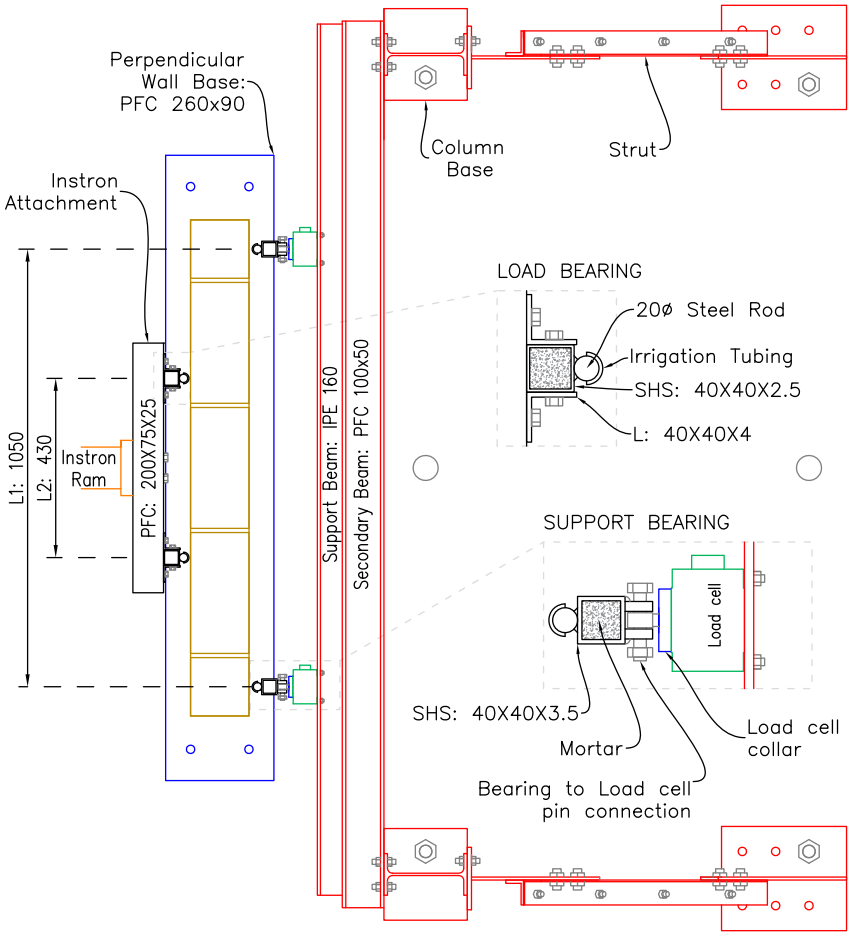

Figure 5.14: Plan view of the test setup in the perpendicular wall configuration

The support bearings (components in contact with the wall on the support side) were similar to the load bearings in cross-section and are also displayed in Figure 5.14. Each support bearing was attached to the beams via two load cells. Four components, henceforth referred to as collar connections, were designed and manufactured for this purpose as shown in Figure 5.15. A make-shift eye bolt formed part of the pin connection of the support bearing and was fastened into the collar connection. In this way, turning the collar connection would force the eye bolt (and therefore the load bearing) towards or away from the wall. This ensured that the setup could handle any skewness in a wall's geometry and that the bearings made full contact with a wall at the start of a test. The support bearings were attached to two horizontal beams. Two columns, bolted to the laboratory's strong-floor, held the beams at the correct height. To provide stiffer horizontal force resistance, a strut was attached to the back of each column and bolted to the strong-floor. To improve the flexural stiffness of the frame, two secondary beams were attached between the columns.

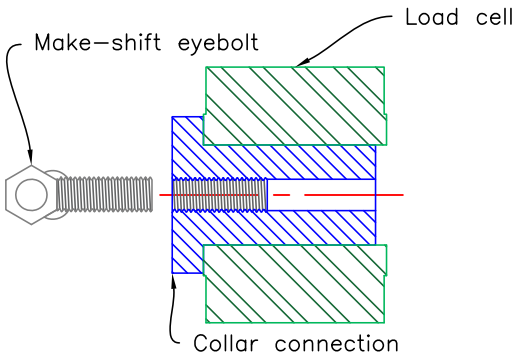

Figure 5.15: Cross-section of a collar connection fitted inside of a load cell

The flexural strength formula provided by EN 1052-2:2016 assumes a simply supported, third-point bending scenario. The bottom boundary condition of each wall type was designed so that the test setup would closely emulate that. This was achieved by designing the bottom boundary conditions such that they would not hinder the flexural deformations that were caused by the applied load. As mentioned in Section 5.5.2, a slip-plane was provided between the bases and the walls to remove frictional restraint along the bottom of each specimen. In the case of the perpendicular walls, this was deemed sufficient in allowing the walls to deform horizontally. However, third-point flexural failure of a parallel wall would cause each of its ends to rotate about a horizontal axis perpendicular to the applied loading. A pivot boundary condition was provided along the central line of the parallel wall's base for this purpose. It consisted of an upturned angle section that was welded onto a steel plate, henceforth referred to as the bottom plate. The bottom boundary conditions of both configurations are shown in Figure 5.16

(a) Parallel test boundary conditions

(b) Perpendicular test boundary conditions

Figure 5.16: Boundary conditions of both flexural test configurations, (a) before test commencement and (b) after test commencement

A second function of the parallel wall bottom plate was to prevent a specimen from tipping over before the bearings had made contact with it. Four threaded holes were cut into the bottom plate so that cap screws could be tightened into the top of the bottom plate. Before a specimen (with it's base plate) was placed onto the bottom plate, the cap screws would be set at the height of the upturned angle (keeping the base horizontal). Before each test commenced and once the bearings had made full contact with specimens, the cap screws were tightened into the bottom plate so that the base would be free to rotate about the pivot point.

Although the specimens could be positioned safely with the use of a crane, fine adjustments to their positions had to be made to ensure that they were situated centrally with respect to the support bearings and load-bearings. Steel rods of 30mm diameter were provided to act as rollers for this purpose. In the case of the parallel walls, they were placed underneath the bottom plate while in the case of perpendicular walls, they were placed below the channel section of their bases.

5.5.4 Measurements

The displacement and load applied by the actuator were measured by its own on-board equipment. To account for the effects of relative displacements and frictional forces within the setup, LVDTs were placed on the loaded side of the wall and load cells were placed on the supported side of the wall. The LVDT positions were adjusted by a set of rods and clamps which were attached to two columns. These

columns were independent from the rest of the test setup so that each LVDT measured displacement relative to the ground. The LVDT arrangement of the perpendicular test setup configuration is shown in Figure 5.17. All of the instrument readings were recorded by a Spider8 data acquisition system. Videos were also taken of the support side of the wall to document where cracks were formed throughout the test. In the case of the parallel wall tests, a video recording was also taken from the side of each wall.

(a) Perpendicular LVDT arrangement

(b) Close-up of LVDT in position

Figure 5.17: LVDT arrangement for the perpendicular test configuration

The positions of all of the LVDTs on each wall are shown in Figure 5.18 and Figure 5.19. A total of 10 LVDTs were placed on the actuator's side of the wall. Four LVDTs (labelled L1a, L1b, L2a and L2b) were positioned behind the ends of the load bearings. Another four (labelled S1a, S1b, S2a and S2b) were positioned in line with the support bearings against the wall's surface. The mid-point displacements were measured by two LVDTs: M_a and M_b. These were also placed directly against the wall's surface. In the case of the parallel walls, they were situated at a height central to the middle row of blocks, while in the case of the perpendicular walls, they were situated just left of the bottom row's central mortar joint. Before each test commenced the LVDT positions were marked and recorded. The four load cells situated behind the support bearings measured the support frame's reaction forces. These were labelled FS1, FS2, FS3 and FS4.

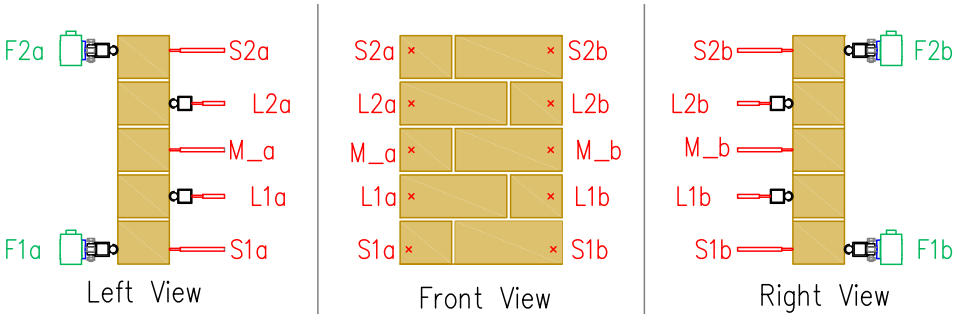

Figure 5.18: Instrument placement on parallel walls

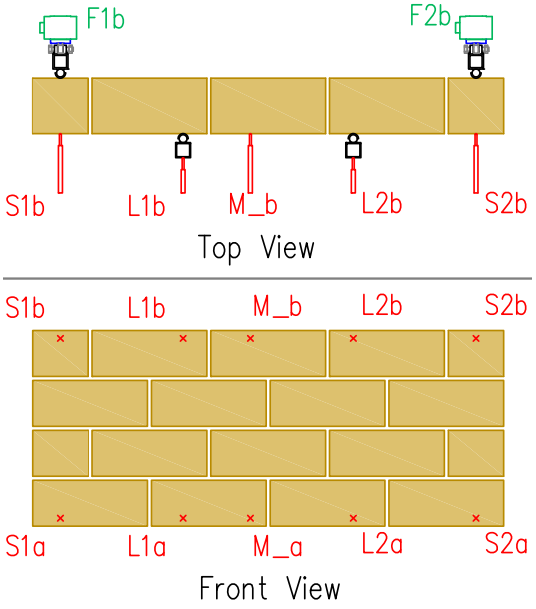

Figure 5.19: Instrument placement on perpendicular walls

5.6 Concluding Summary

This chapter outlines the design of the tests that were conducted during the experimental programme. The tests included compressive strength and modulus of elasticity tests on units, mortar and masonry specimens, unit dry density tests, mortar flow value tests and flexural strength tests on mortar and masonry specimens.

For each test, the specimen preparation, apparatus and test procedure is presented. Although all of the tests are based on existing standard test methods, some modifications were made to account for the wide spectrum of material properties and to ensure the feasibility of the study.

Chapter 6

Experimental Results and Discussions

To fulfil the objectives of this study, experimental tests were performed on alternative masonry units (AMUs), cementitious mortar and masonry specimens constructed thereof. This chapter presents the results of these tests. For each set of results, a discussion is provided on important aspects of the test procedures and general observations are made on the nature of the tests. Thereafter, the results are evaluated according to the objectives of the study and comparisons are made between the different specimen types.

Four types of masonry units were investigated in this study, namely concrete (CON) units, geopolymer (GEO) units, compressed stabilized earth (CSE) units and adobe (ADB) units. This sequence of unit-type will be maintained throughout the results chapter as it generally follows the order of the unit strength. This enables clearer comparisons to be made between specimens. Two types of cementitious mortar were investigated and used to construct the masonry specimens. These were named 7M and 20M after their 7-day characteristic compressive strengths of 7MPa and 20MPa respectively.

The units were manufactured over two periods, as described in Chapter 4. Units produced in the first and second periods are referred to as "old" and "new" respectively. The old and new units within each unit-type exhibited significant differences in their characteristics due to their respective age gaps and the material variation present between the two construction periods. To account for this, the units were allotted to the masonry specimens so that only old or new units were used for each masonry specimen type as described in Chapter 5.

Compressive strength tests, elastic modulus tests and dry density tests were performed on samples taken from the units. These results are presented first. The mortar manufactured during the masonry construction process was sampled and tested for its compressive strength, elastic modulus and flexural strength. These results are presented second in this chapter. Lastly, the compressive strength, elastic modulus and flexural strength determined from masonry specimens constructed from each

unit-type are presented. For clarity, the masonry specimens that were subjected to compressive strength and elastic modulus testing are referred to as wallettes, while those subjected to flexural tests are referred to as walls.

6.1 Unit Test Results

Compressive strength, elastic modulus and dry density tests were performed on samples taken from all of the units studied. These tests were motivated by both the objectives of providing input parameters for numerical modelling and of producing units similar to those investigated in previous studies (Fourie (2017); Shiso (2019)). Furthermore, the results served as a quality control, indicating the variation that existed within the unit-types. For each of these tests, units were sampled from different batches at intervals so that the tested specimens represented the variation present between batches adequately.

For both the compressive strength and modulus of elasticity, 28-day characteristic tests were performed on the old units. These parameters were also investigated on both the old and new units at the time of the wall and wallette tests. For the sake of brevity, the unit tests performed at that stage will be referred to as 'auxiliary' in the text and abbreviated to 'aux' in figures and tables. All units subjected to auxiliary tests were subjected to the same curing conditions as those being used for construction, so that they could most accurately represent the properties of those units. The dry density of the units was investigated for the old and new units of each type after the walls and wallettes had been tested.

6.1.1 Compressive Strength Results

Compressive strength tests were performed on the units in their bed face orientation according to EN 772-1 (2011), as described in Section 5.2.1. The unit compressive strength is a widely tested parameter in studies pertaining to the structural behaviour of masonry. The results not only provide a means of comparing the units developed in this study to those developed by previous researchers at Stellenbosch University, but also allow comparisons to be made against other conventional or alternative units.

The auxiliary tests were performed to determine the compressive strengths of the units within the masonry specimens at the time of testing. These compressive strengths were required as input parameters for the aforementioned numerical model. Furthermore, there is use in comparing the unit compressive strengths to the flexural strengths of the walls from which they were constructed since SANS 10164-1 (1989) and EN 1996-1-1 (2005) provide design flexural strengths for conventional masonry materials, which depend partly on unit compressive strength.

As discussed in Chapter 3, masonry units and the walls from which they are built are stronger in compression than in tension. For this reason, masonry subjected to pure flexural stress is most likely to fail from tensile stresses developed in the units and mortar or from shear and tensile stresses induced between the two. However, walls that undergo arching, as described in Section 3.3.4, resist out-of-plane (OOP) actions through compression. Such walls depend directly on their compressive strength to resist OOP loads. The compressive strength of masonry walls, in turn, is greatly dependent on the compressive strength of the units from which they are constructed.

The mean compressive strengths of the characteristic and auxiliary results are presented for each unit type in Figure 6.1. The mean age (in days) of the auxiliary tests are presented in square brackets above each bar. With the exception of the ADB units, a distinct strength gain is evident between the 28-day and auxiliary results of the old units. This is attributed to cement particle hydration in the CON and CSE units and geopolymerisation in the GEO units. The ADB units did not exhibit strength gain with age since the material reaches full strength upon drying.

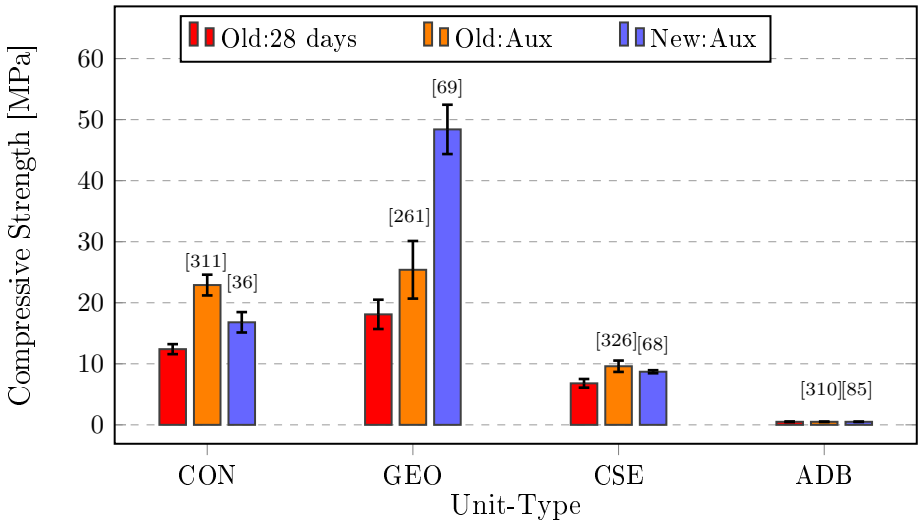

Figure 6.1: Unit compressive strength results

The relationship between old and new units is not constant across unit-types. In the case of the CON and CSE units, the auxiliary results of the new units lie between the 28-day and old unit auxiliary results, this is expected given the material similarity between the old and new units and considering the relative ages of the old and new units. This is not the case for the GEO units whose mix designs differed substantially (as discussed in Section 4.2.2). The effect of this is evident as the new GEO units exhibited a strength of almost double that of their old counterparts. Although the mix designs between the old and new ADB units differed (as discussed in Section 4.2.4), their resulting strengths did not vary significantly.

To ensure reliable results, a minimum of 8 units were selected for the 28-day characteristic tests. However, fewer specimens were available for the auxiliary tests and the number of specimens tested varied between material types. Outliers and results produced from invalid tests were also removed from the sample. This had the effect that the sample size of each result varied per unit-type and time-period of testing. Table 6.1 provides the total sample size of each test result after the removal of outliers and invalid tests. The compressive strengths are presented alongside the coefficient of variation (COV) for each unit-type in Table 6.2.

Table 6.1: Number of specimens per test and unit-type

Test	CON	GEO	CSE	ADB
Old: 28-day	7	8	10	10
Old: Auxiliary	8	9	6	4
New: Auxiliary	4	5	3	4

Table 6.2: Mean unit compressive strength results f_{cu} in MPa

Unit	Old 28-day			Old Aux.			New Aux.		
	$f_{c,u}$	*COV*	*Age*	$f_{c,u}$	*COV*	*Age*	$f_{c,u}$	*COV*	*Age*
CON	12.4	6.6%	28	22.9	7.4%	311	16.8	9.9%	36
GEO	18.1	13.3%	28	25.4	18.6%	261	48.4	8.3%	69
CSE	6.8	10.5%	28	9.6	9.7%	326	8.7	2.9%	68
ADB	0.5	9.7%	28	0.5	7.4%	310	0.5	5.9%	85

As discussed in Section 5.2.1, the new GEO and ADB units were subjected to different testing boundary conditions due to the limits of the testing apparatus. The results of this experiment are thus not strictly comparable between unit types, but are deemed sufficiently accurate for model input and comparison to existing literature. In general, all of the units achieved strengths similar to those obtained by Fourie (2017) and Shiso (2019), except for the new GEO units.

6.1.2 Modulus of Elasticity Results

Unit modulus of elasticity tests were conducted for all unit-types and loosely followed the procedures stipulated by EN 12390-13 (2013). A full description of the test procedure is presented in Section 5.2.2. As with compressive strength, the modulus of elasticity of units is commonly investigated in studies pertaining to masonry.

The modulus of elasticity can be referred to as stiffness and relates the strain of a material to its internal stresses. This makes it a crucial parameter for displacement based numerical models in general and critical for the validation of the model as described in the objectives. In the case of masonry subjected to compressive stresses, the relative stiffness of the mortar and units of a masonry wall can dictate the manner in which it deforms as well as its ultimate capacity. This also effects the capacity of masonry subjected to horizontal flexure, as described in Section 3.1.2

For each unit-type, the average modulus of elasticity in GPa is provided in Figure 6.2. As with the compressive strength graph, the error bars present the sample standard deviation for each data point and the average ages of the auxiliary results are provided in brackets. For the old units, the CON units were the stiffest, followed by the GEO, CSE and ADB in that order. It should be noted that the old GEO units were less stiff than the old CON units even though they performed better in the compressive strength tests. This behaviour was also reported by Fourie (2017) and Shiso (2019). Although the new GEO was the stiffest of all the materials, this was still lower than what would have been expected for concrete at the same compressive stress.

An increase in stiffness with age is observed for the old CON and CSE units, while an apparent decrease in stiffness with age is observed for the GEO units. It should be noted, however, that the mean results of the 28-day tests and auxiliary tests fall within each others standard deviation, making inferences relative to age less valid. As expected, the ADB units were the least stiff material and did not show signs of strength gain with age.

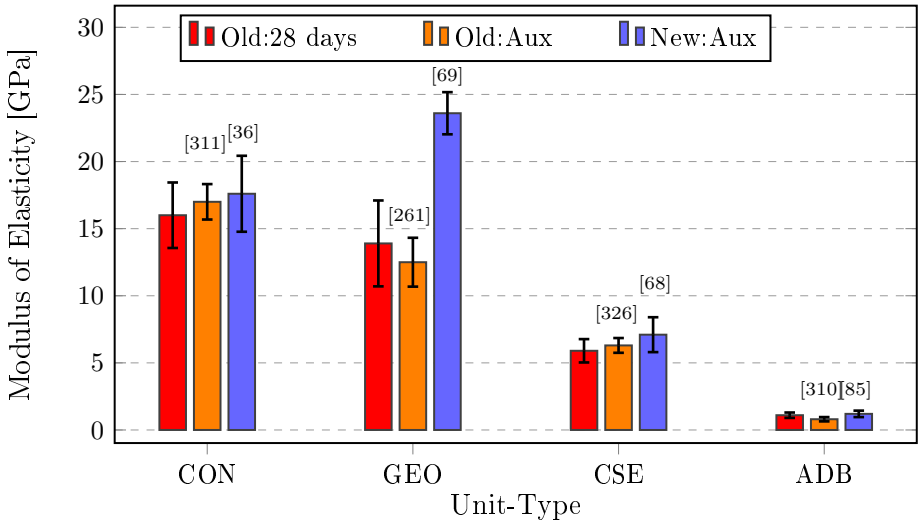

Figure 6.2: Unit Modulus of Elasticity results

Table 6.3 displays the number of specimens tested per unit-type. The initial test programme was designed so that eight specimens would be tested for each. As the programme expanded and new tests were introduced, only four tests were conducted

with the new sawn specimens (CON, CSE and ADB), due to time constraints. As many tests were conducted with old units at the auxiliary testing phase as possible. This lead to a variable number of samples.

A total of twelve new GEO specimens were manufactured for testing since the GEO 28-day tests exhibited the greatest variability. Furthermore, these specimens could be manufactured and tested faster and more reliably than the others as they were produced by casting the fresh mixture into cylinder moulds. The modulus of elasticity specimens of the other unit types were all sawn out of units. This process was time consuming and the resultant specimens were much smaller than the GEO cylinders making them more difficult to handle and test accurately.

The weak compressive strength of the ADB added further difficulty to their test procedure. Some specimens were damaged in the process of attaching the LVDT frame of the test apparatus, resulting in only six valid results being available for the old 28-day results.

Table 6.3: Number of specimens per test and unit-type

Test	CON	GEO	CSE	ADB
Old: 28-day	8	9	8	6
Old: Auxiliary	8	10	6	9
New: Auxiliary	4	12	4	4

The numerical values of the results are displayed in Table 6.4. A high COV was present in most cases. This was also reported by Shiso (2019). The high variability is mostly attributed to the complexity of the test setups that were used as well as the difficulties encountered while preparing and testing the specimens. These issues are described below in the following paragraphs.

Table 6.4: Mean unit modulus of elasticity results E_{cu} in GPa

Unit	Old 28-day			Old Aux.			New Aux.		
	E_{cu}	*COV*	*Age*	E_{cu}	*COV*	*Age*	E_{cu}	*COV*	*Age*
CON	16.0	15.2%	28	17.0	7.8%	311	17.6	16.1%	36
GEO	13.9	23.1%	28	12.5	14.6%	261	23.6	6.7%	69
CSE	5.9	14.9%	28	6.3	8.8%	326	7.1	18.4%	68
ADB	1.1	18.2%	28	0.8	19.9%	310	1.2	19.2%	85

During the tests performed on the sawn specimens (CON, CSE and ADB), difficulties were experienced with applying a level load, evenly over the face of the specimen.

Frequently, bending would occur during the test. This was deduced from LVDTs that recorded displacement in direct opposition to that of the actuator head throughout the test (for instance, the LVDT would indicate tensile strain while the specimen was being compressed) and attributed to the absence of a self-levelling head in the test machine. During some of the tests, an LVDT would not read values that corresponded to the range of movement recorded by the others. This was attributed to the LVDT frame not having a sufficient grip on the unit at that LVDT.

Measures were undertaken to reduce the effects of the uneven load application and sensitive LVDT frame. Three tests were performed for each specimen. Between each test, the specimen would be rotated in place and the LVDT frame would be checked and adjusted if necessary. All three tests would be evaluated to determine the modulus of elasticity of the specimen. This process was followed for each specimen tested at 28-days. For all sawn specimens tested at this stage, no levelling attachment was present.

A suitable self-levelling attachment was acquired during the auxiliary testing phase and was used to test the CSE and ADB specimens, since the CON auxiliary specimens had already been tested. With this improvement, bending in the specimen was much less common. For each specimen, the test was repeated as many times as was required to achieve a result that indicated that the LVDTs were fastened correctly and no bending had occurred.

In comparison, the GEO tests were performed on cylindrical specimens with the CONTEST testing machine, which had an incorporated levelling head. Furthermore, the LVDT frame was easier to handle and would fasten to the specimens more reliably than the sawn specimen LVDT frame would. A few invalid results did occur, however. Again, multiple tests were performed per specimen to ensure that valid results remained.

The results of the tests conducted for each specimen were evaluated and checked according to the requirements of EN 12390-13 (2013). The first check was to ensure that the difference between the strain measured on each LVDT and that of the average strain did not exceed 20% during the second cycle. This would indicate that the test apparatus and specimen were sufficiently level. The second check was to ensure that the strain measured during the second and third cycles did not differ by more than 10% for each LVDT.

A specimen's test results were retained or discarded on the basis of whether they passed both checks and on the availability of valid results (take note that three results were available per specimen as stated above). Although the second check was almost invariably passed, the first check was often failed due to the levelling issues present in the test setup. In cases where all of a specimen's tests failed the first check, the average of those results would be retained. This was done out of necessity for the 28-day characteristic tests for which no levelling apparatus was available. If a specimen had results that passed both checks, the results that passed would be retained, while those that did not would be discarded. For each specimen the modulus of elasticity was taken as the average of the retained results.

Despite the high variability of these results, the auxiliary results were deemed sufficient as input parameters for the numerical model. The general trends of the results were also similar to those observed by Fourie (2017) and Shiso (2019).

6.1.3 Dry Density Results

The dry densities of the units were tested according to the European standard test method, EN 772-13 (2013). This test was performed to compare the densities of the units to those available in literature, for quality assurance and to provide an input parameter for numerical modelling. A total of six units were sampled for each test. All of the tests were performed after the conclusion of the wallette and wall tests.

A graphical representation of the results is presented in Figure 6.3. For the old units, the CON units were the most dense, followed by the GEO, CSE and ADB units. For the new units, however, the GEO was the most dense, followed by the CON, CSE and ADB. This change is caused by an increase in density between the old and new GEO units and a decrease in density between the old and new CON units respectively.

For all unit-types, a difference in density was observed between the old and new units. This is attributed to differences in the mix designs and variability that occurred between batches of material used for the old and new units (as discussed in Section 4.2.2). The GEO units show the most marked difference as the new unit incorporated more fly ash and coarse aggregate than the old.

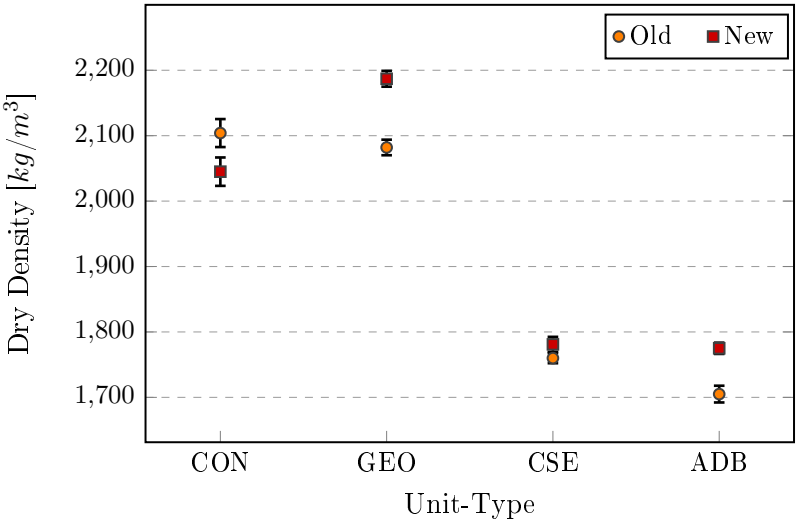

Figure 6.3: Dry density results

For both the old and new units, the results seem to form two groups - one of the denser CON and GEO units and the other of the less dense CSE and ADB units. In general the dry density of a unit should be related to the density of its constituent materials and the amount of voids between the particles present within the unit. The differences between the two groups are probably due to a combination of these factors.

Both the CON and GEO units contain larger aggregates (crusher dust and 13mm Greywacke stone respectively), that have higher relative densities than the fine aggregates. The GEO units were formed by pouring a wet mixture into moulds. This mixture required very little vibration. The CON units were the wettest of the pressed units and no visible voids were encountered in their cross-sections.

The CSE and ADB units did not contain coarse aggregates. Furthermore, their fresh mixtures were the driest of the four materials tested. In each case, compaction was required to form the units. This might have resulted in a greater number of voids throughout the matrix in comparison to the CON and GEO units.

The numerical values of the average dry densities, COVs and average ages of the tested units are provided in Table 6.5. As observed in the table, a large age gap exists between the old and new units that were tested. This age difference might have had an effect on the units which contained contained chemical binders.
The low variability of the results indicated by the COVs in Table 6.5 implies that the units were produced with consistent quality. The fact that the CON and GEO units were the most dense, followed by the CSE and ADB was also observed by Shiso (2019). Although, in his study, the ADB was more dense than the CSE. The same trend was observed by Fourie (2017).

Table 6.5: Unit dry density results $\rho_{g,u}$ in $[kg/m^3]$.

Unit-Type	Old			New		
	$\rho_{g,u}$ $[kg/m^3]$	COV [%]	Age [days]	$\rho_{g,u}$ $[kg/m^3]$	COV [%]	Age [days]
CON	2104	1.0%	428	2045	1.1%	162
GEO	2082	0.6%	321	2187	0.6%	125
CSE	1760	0.4%	416	1781	0.6%	155
ADB	1705	0.7%	387	1775	0.5%	152

6.2 Mortar Test Results

Tests were performed on the mortar to determine its consistency (flow table value) in the fresh state and to determine its elastic modulus, flexural strength and compressive strength in the hardened state. These tests were conducted as quality assurance, as model input parameters and to allow for observations to be made on possible relationships between the mortar properties and the wall and wallette results.

It is important to note that a different batch of the same type of aggregate was incorporated halfway through the study. The mortars used for the CON and CSE specimens differed in aggregate properties and sand/cement ratio compared to those that were used to build the ADB and GEO specimens. The water/cement ratios of the 7M and 20M mortars were kept constant throughout the study in an effort to maintain the same strength characteristics. A more detailed explanation of the mortar manufacturing process and mix designs is provided in Section 4.3.

To allow for observations to be made on the effect of the mortar properties on the masonry specimens, the mortar test specimens were sampled from the same batches that were used to construct the walls and wallettes. The hardened properties of the samples were tested at an age of 7 days if possible to adequately represent the mortar contained in the masonry specimens. This was not achieved in every case, due to the pressures involved with completing multiple tests within a short timespan.

For clarity, the age of the sampled mortar is provided alongside each of the graphical and tabulated results. It should be noted that the mortars are named after the unit types of the masonry specimens they were used to build. In other words, the 20M mortar used to construct the ADB walls and wallettes is referred to as 20M ADB mortar. This does not infer that the mortar itself consisted of ADB (all of the mortars were cement-sand mortars).

6.2.1 Mortar Flow Values

The mortar was sampled intermittently for the purpose of performing flow table tests according to the specifications provided in EN 1015-3 (1999). The methodology used for this procedure is provided in Section 5.3.1.

In most cases, samples were tested as soon as a batch of mortar was being used up, or at some point afterwards. Since the mix designs of both mortar types were kept consistent throughout the study, their resultant flow values may be compared with reference to their ages. Figure 6.4 is provided for this purpose. In this graph, the mortar type is indicated with colour and the the unit-type is indicated by the shape of the marker.

It should be noted that the two oldest readings were taken 20 mins after that mortar had been used up. In other words, the sample had been taken from the builders and allowed to stand before it was tested. Throughout the construction of the walls it was ensured that mortar did not reach an age of one hour before being in used in the construction of specimens, as prescribed by EN 1052-2 (2016).

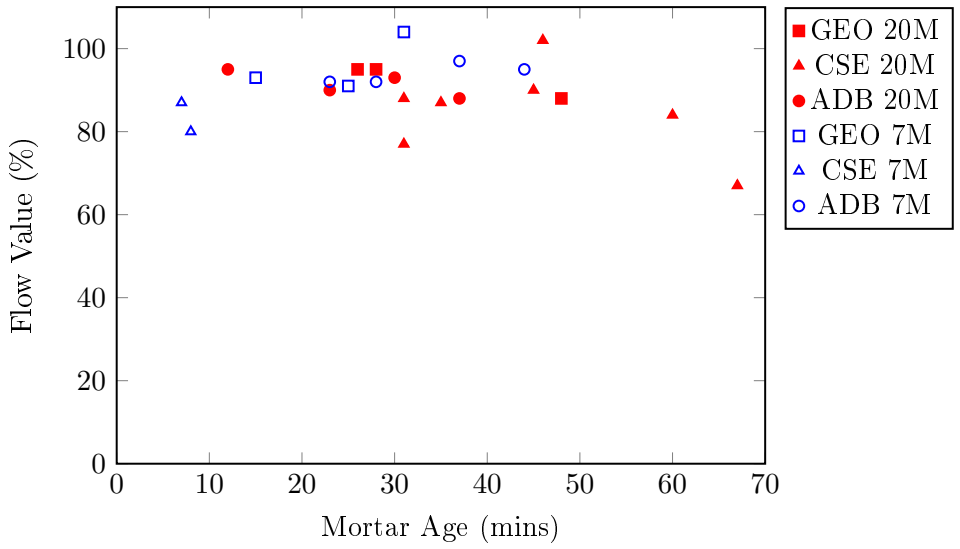

Figure 6.4: Flow Value (%) vs fresh mortar age (mins)

A summary of the flow values (FVs) and of the mortar used to construct walls and wallettes consisting of each unit type is provided in Table 6.6. Here the "Total" row results are calculated on all of the 20M and 7M mortar readings respectively. It can be seen that no measurements were made during the construction of the CON specimens. The CON walls and wallettes were the first of to be built and adapting to the construction schedule proved to be a challenge.

In general, despite the varying ages of the tested mortars, the results are fairly consistent. Table 6.6 shows a total COV of 10% and 7% for the 20M and 7M mortars respectively. Although an average target FV of 100% was not achieved, it should be noted that if all of the tests were performed immediately after mixing higher FVs would arguably have been recorded. Furthermore, the experienced masons who performed the work were satisfied with the mortar consistency.

Table 6.6: Average mortar flow values

Unit	20M		7M	
	FV (%)	COV (%)	FV (%)	COV (%)
CON	-	-	-	-
GEO	93%	4%	96%	6%
CSE	85%	13%	84%	5%
ADB	92%	4%	94%	3%
TOTAL	88%	10%	92%	7%

6.2.2 Modulus of Elasticity

The mortar's modulus of elasticity was tested by following the stipulations provided by EN 12390-13 (2013), with exceptions made with regards to the loading regime applied. A more detailed account of the test procedure is provided in Section 5.3.2 and Section 5.2.2.

The mortar modulus of elasticity was a required input parameter for the numerical model. Furthermore, the mortar stiffness, when compared to the unit stiffness can be used to predict the ultimate modulus of elasticity of a wall in compression. In conjunction, these parameters can also be used to predict the load-displacement behaviour of a wall subjected to horizontal flexure, as described in Section 3.1.2.

Figure 6.5 displays the modulus of elasticity of the mortars used to construct masonry specimens for each unit-type. The ages of the tested specimens are provided in brackets in the figure. No results were available for the mortar used to construct the CON specimens as there was difficulty in producing cylinder specimens in time during construction of the walls and wallettes.

The numerical results of the test alongside the COVs and mortar ages are provided in Table 6.7. Generally, the modulus of elasticity is consistent between unit-types for the 7M mortar. The results of the 20M mortar indicate a consistent stiffness for the GEO and CSE specimens, but a comparitively less stiff mortar for the ADB specimens. This could be attributed to the younger age at which the ADB test was performed.

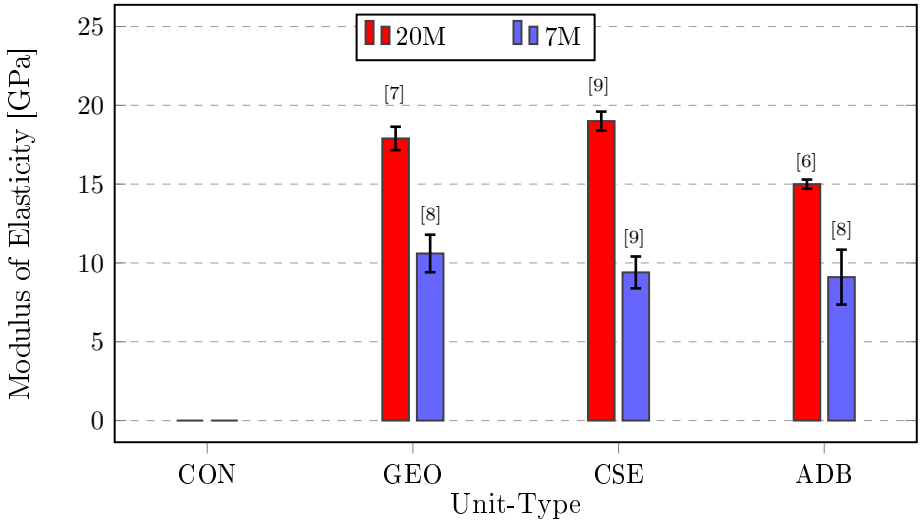

Figure 6.5: Mortar modulus of elasticity results

The number of specimens tested for each result is provided in Table 6.8. The construction and testing of the CSE masonry specimens occurred before that of the ADB and GEO specimens. The results of the CSE mortar revealed an acceptable variability, so that, in the interest of time, fewer modulus of elasticity mortar specimens were cast during the construction of the ADB and GEO masonry specimens.

Table 6.7: Mortar modulus of elasticity, E_m in GPa

Unit-Type	20M			7M		
	E_m	COV	Age	E_m	COV	Age
CON	-	-	-	-	-	-
GEO	17.9	4.2%	7	10.6	11.2%	8
CSE	19.0	3.2%	9	9.4	10.7%	9
ADB	15.0	2.0%	6	9.1	19.1%	8

Table 6.8: Number of specimens per mortar and unit-type

Unit	20M	7M
CON	-	-
GEO	2	2
CSE	5	3
ADB	3	3

The results within each unit-mortar combination showed little variation except for the 7M mortar used to construct the ADB specimens. Of the three 7M ADB mortar specimens, two yielded results of 10.4 GPa and 9.2 GPa respectively, while a third yielded the lowest result of the study at 7.1 GPa. The highest discrepancy between LVDT readings was measured for this specimen. It is likely that the third result underestimates the modulus of elasticity due to a less even load application or less accurate LVDT readings and not due to variation in the material itself.

Taking age into account, the results indicate that mortars with consistent moduli of elasticity were produced throughout the study. Although no results are available for the CON mortar, it was deemed acceptable to estimate its modulus of elasticity based on those measured for the other mortars. For the purposes of quality assurance and providing input data, the mortars and the associated test are deemed acceptable.

6.2.3 Flexural Strength Results

The flexural strength of the mortars was tested according to EN 1015-11 (1999) with the exception that third-point loading was applied. The specimens were 160mm x 40mm x 40mm mortar prisms. The test procedure followed is presented in Section 5.3.3.

As discussed in Section 3.1.2, mortar flexural strength is partly responsible for the ultimate strength of masonry subjected to horizontal flexure. The same could be argued for masonry in biaxial flexure. To this end, the flexural strength of mortar was investigated for the purposes of comparing it the flexural strength of the masonry.

It should be noted that the mortar flexural strength was not a required input parameter for the numerical model. Furthermore, due to the typical variability of the flexural strength of brittle materials the results of this test were not considered as an assessment of the quality of the mortars.

As specified by EN 1015-11 (1999), three specimens were cast and tested for each sample that was taken from a batch. Each specimen result was recorded to the nearest 0.05 MPa and the mean of the specimen results, rounded to the nearest 0.1 MPa was calculated to represent the flexural strength of the sample. During the construction of the walls and wallettes, more than one sample was taken per mortar and unit-type.

For each unit-type, the flexural strengths of the mortars are taken as the mean of the samples. These results are provided in Figure 6.6. The test-ages of the mortars are provided in brackets above each result and the sample standard deviation is provided by the error bars. The numerical values of the flexural strength, COV and age are also provided in Table 6.9.

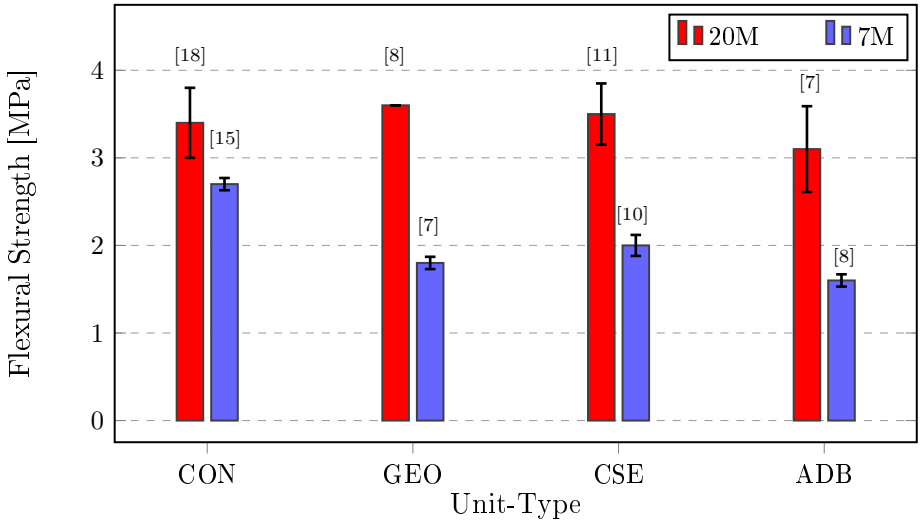

Figure 6.6: Mortar flexural strength results

Table 6.9: Mortar flexural strengths

Mortar	20M			7M		
Unit	$f_{x,m}$	COV	Age	$f_{x,m}$	COV	Age
CON	3.4	11.9%	18	2.7	2.6%	15
GEO	3.6	0%	8	1.8	3.9%	7
CSE	3.5	9.9%	11	2.0	5.8%	10
ADB	3.1	16%	7	1.6	4.4%	8

It should be noted that these values are taken from the mean flexural strengths of each sample tested, with each sample consisting of three specimen results. To provide a better indication of the variation of the test, every valid specimen's result is displayed in Figure 6.7. Here, the mortar type is indicated by the data point's colour, and the shape of each data point indicates a mortar sample (consisting of three specimens). The mortar samples are indicated as "S1", "S2" and "S3" in the legend.

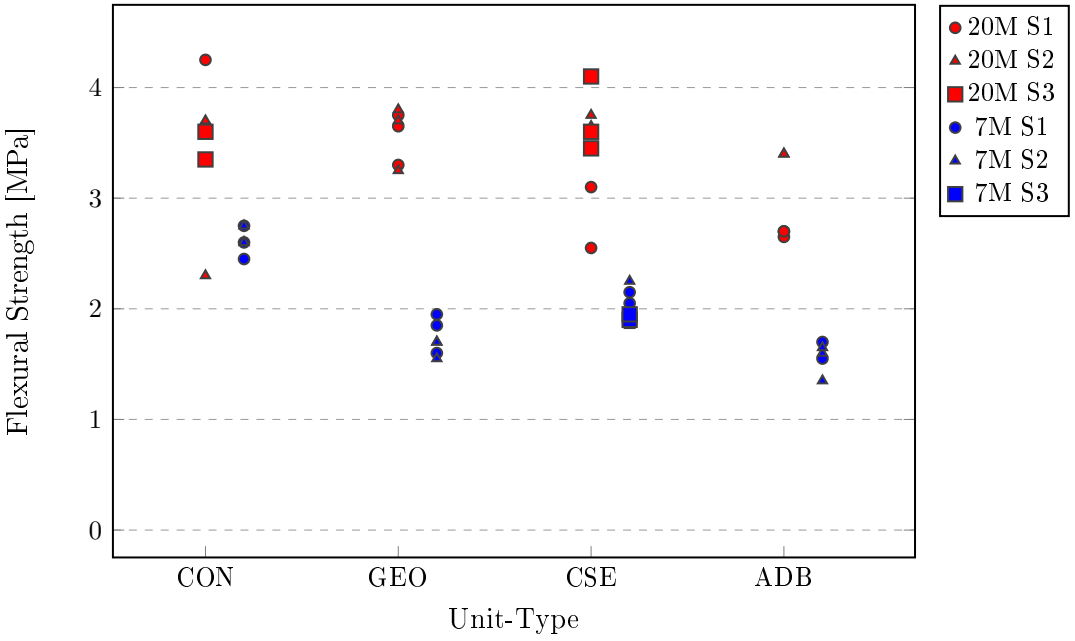

Figure 6.7: Mortar flexural strength

As displayed in Figure 6.7, the specimen flexural strengths were mostly consistent within samples, except for the 20M CON and CSE mortars. Within unit-types, the highest variability between different samples occurs for the 20M mortar. Compared to the 20M mortar results, the 7M mortar results were more consistent between specimens and samples for each unit-type.

Strength-gain with age is not consistently apparent. For example, the 20M GEO mortar, at an age of 8 days is almost equivalent in flexural strength to the CON and CSE mortars with ages of 18 and 11 days respectively. Within the 7M mortars, the 15 day CON result is appreciably higher than the 10 day CSE result, while the 7 day GEO mortar is stronger than the 8 day ADB mortar. The results seem to indicate that the most rapid strength gain for the 20M mortars is achieved before that of the 7M mortars. A more detailed investigation would be required to confirm this.

The flexural strength results of the mortar are deemed sufficient for the purposes of making comparisons to the remaining experimental data of this study. The generally low variability between test specimens within samples indicates that the test procedure was successful. Considering age, the mortar flexural strengths were fairly consistent for each mortar type throughout the study.

6.2.4 Compressive Strength Results

The mortar flexural strength test broke the prism specimens into two halves. After each batch of mortar flexural strength specimens had been tested, the halves were used to determine the compressive strength according to EN 1015-11 (1999). A description of the procedure is provided in Section 5.3.4.

As discussed in Section 3.1, the OOP capacity of a single-storey URM wall is not usually controlled by the compressive strengths of its components, but by the tensile and shear properties of the mortar joints and units as well as the interfaces between them. Although this indicates that the ultimate flexural strength is not directly related to mortar compressive strength, mortars are usually classified according to this parameter and walls that are constructed from different mortar classes do have differing OOP capacities. This is due to the fact that the flexural, tensile and bond characteristics of mortars are affected by their strength classes.

For the purposes of this study, the mortar compressive strength was a required input parameter for numerical modelling. It was the aim that mortars of a consistent 7-day compressive strength would be used throughout the study. The mortar compressive strength test was thus used as a check of whether this had been achieved. Since walls and wallettes were constructed using both 7M and 20M mortars, the effect of mortar class on the compressive strength, elastic modulus and flexural strength could also be investigated.

Figure 6.8 and Table 6.10 display the compressive strengths of the mortars used for each unit-type. The ages of the specimens are indicated in brackets in the graph. The CSE mortar was not tested in compressive strength according to EN 1015-11 (1999) due to time constraints. Since mortar compressive strength values were also recorded during the elastic modulus tests, the cylinder compressive strength of the CSE mortar is displayed in these results and is indicated by the asterisk in the graph.

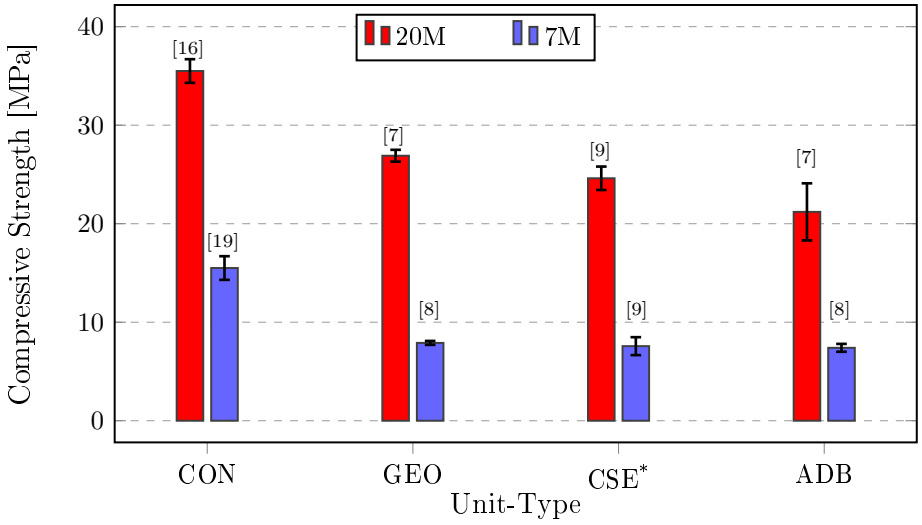

Figure 6.8: Mortar compressive strength results

For each unit-type, the mortar compressive strengths were consistent between batches. Although the 20M ADB results and 7M CSE results had much higher COVs than the others, these were still within acceptable limits. The results recorded from each sample of compressive strength specimens are provided in Table 6.11. It should

Table 6.10: Mortar compressive strength, $f_{c,m}$ in MPa

Unit-Type	20M			7M		
	$f_{c,m}$	COV	Age	$f_{c,m}$	COV	Age
CON	35.5	3.5%	19	15.5	8.0%	16
GEO	26.9	2.1%	8	7.9	2.5%	7
CSE*	24.6	4.8%	9	7.6	12.0%	9
ADB	21.2	13.7%	7	7.4	6.0%	8

be noted that the higher variability that occurred for the ADB 20M mortar is mostly due to variability between batches, while the variability of the CSE 7M mortar is mostly due to variable results in the same batch.

The CON mortars were the first to be tested. For the first two mortar samples, each half produced from the flexural test specimens was used so that 6 compressive strength tests were performed. This was found to be too time-consuming. For the remaining unit-types, only one half from each flexural test specimen was selected so that three compressive strength tests were performed per sample.

Table 6.11: Mortar compressive strength per batch

Mortar	20M				7M			
Unit	Batch	$f_{c,m}$ [MPa]	COV [%]	No.	Batch	$f_{c,m}$ [MPa]	COV [%]	No.
CON	1	35.5	3.5%	6	1	16.0	3.8%	3
	-	-	-	-	2	15.3	9.6%	6
GEO	2	27.0	2.1%	3	3	8.0	2.5%	3
CSE*	2	25.7	1.1%	3	4	7.7	13.5%	3
	6	25.0	-	1	7	7.1	-	1
	12	23.4	1.8%	3	-	-	-	-
ADB	7	18.8	9.2%	3	9	7.4	9.0%	3
	2	23.5	5.2%	3	13	7.4	3.0%	3

The mortars reached their target compressive strengths at an age of 7 days. Those tests performed at later ages produced results that were to be expected with the respective ages. The results indicate that the mortar compressive strengths were sufficiently consistent between unit-types. The low variability of the results per

unit-type indicate that the test method was successful and ensure that these results may be used for the purposes of modelling and comparing parameters.

6.3 Wallette Test Results

The masonry compressive strength and elastic modulus of the unit-mortar combinations were determined according to EN 1052-1 (1999). These tests were performed on single-leaf wallettes with a height of 5 units (measuring 610mm) and a length of 2 units (measuring 590mm). A detailed description of the specimens constructed and the method used to perform these tests is provided in Section 5.4.

Masonry compressive strength is a frequently researched topic and is an important parameter for the design of masonry buildings. The compressive strengths were required as input parameters for the numerical model. Since masonry is usually classified according to its compressive strength and the compressive strengths of its components, these results allow comparisons to be made between the specimens of this study and those in existing literature. Furthermore, common masonry compressive strength models can be compared to these values to determine whether they apply for alternative units.

Since stiffness provides a direct relationship between stresses and strains, this parameter is important for numerical modelling. These results also allow comparisons to be drawn between the stiffness of masonry and its components.

The wallettes are named after their unit-types and mortars. For instance, the wallettes constructed with old units and 20M mortar are referred to as old 20M wallettes. For these and the new 7M wallettes, one specimen was tested for its compressive strength only and three specimens were tested for their modulus of elasticity and compressive strength. For the old 7M wallettes, three specimens were tested for their modulus of elasticity and compressive strength.

Although it was intended to test the wallettes at an age of 7 days, this was not always possible. The age of the specimens at the date of testing is provided in the tables and graphs that present these results.

6.3.1 Compressive Strength Results

The mean compressive strength, COV and age of each set is provided in Table 6.12. The age of each sample differed within unit-types and between unit types. This should be taken into account when comparing wallettes of the same mortar class. A high COV was present for each sample. This also makes it difficult to make comparisons between sets with similar mean compressive strengths.

Table 6.12: Wallette compressive strength, $f_{c,w}$ in MPa

Unit	Old 20M			Old 7M			New 7M		
	$f_{c,w}$	*COV*	*Age*	$f_{c,w}$	*COV*	*Age*	$f_{c,w}$	*COV*	*Age*
CON	11.60	8%	11	10.61	10%	13	7.06	18%	12
GEO	4.88	31%	6	7.01	16%	9	14.81	5%	8
CSE	2.88	22%	9	2.78	25%	9	2.53	17%	9
ADB	0.22	18%	5	0.25	14%	7	0.16	32%	7

The compressive strength of each wallette is provided in Figure 6.9 to better portray the distribution of the results. For wallettes constructed from the old units, the CON specimens were the strongest, followed by the GEO, CSE and ADB specimens. This pattern is also followed for the unit compressive strengths, except that the relationship between the CON and GEO units is reversed. For the new units, the GEO wallettes were the strongest, followed by the CON, CSE and ADB. This pattern is also followed with the unit compressive strengths.

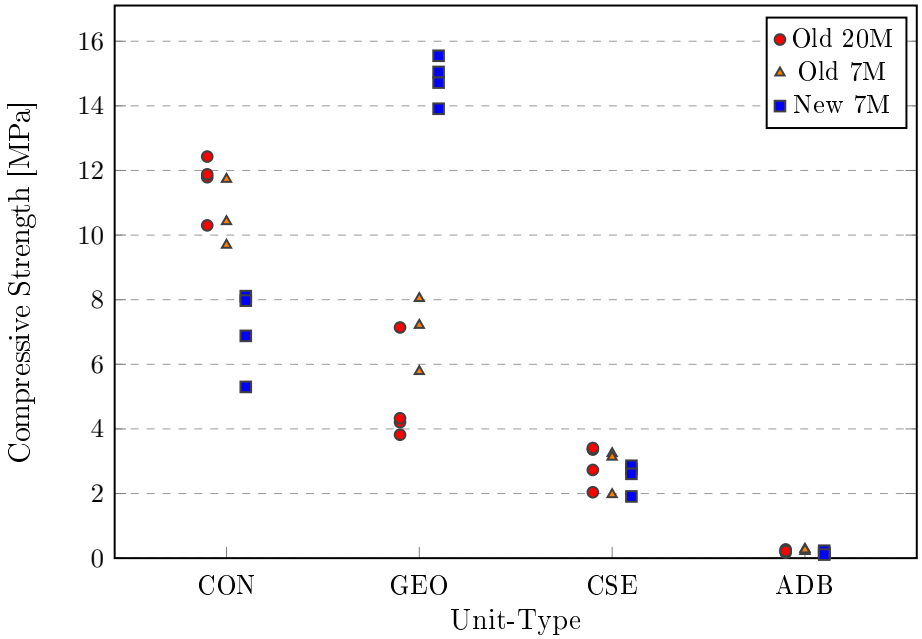

Figure 6.9: Wallette Compressive Strengths

The effect of mortar class on the wallette compressive strength can be observed by comparing the old 20M and old 7M wallettes. For the CON and CSE wallettes, the stronger mortar results in a stronger masonry, while the opposite is true of the GEO and ADB wallettes. It should be noted, however, that the difference between the old 20M and old 7M compressive strengths is small. Furthermore, the COV for each

result was high and only three or four specimens were tested per sample.

The wallette compressive strength results were sufficient for use in the numerical model. Comparisons can be made that highlight the effect of unit compressive strength and mortar strength class. It should be noted, however, that due to the low number of specimens and the high COV of the results, a larger sample would be needed to predict these effects accurately.

6.3.2 Modulus of Elasticity Results

The masonry secant modulus of elasticity was calculated by measuring the differences that occurred in stress and average strain between a quarter and a third of each specimen's ultimate strength. The strains were measured over a gauge length of 210mm and the stress was recorded from the test machine's built-in load cell.

The modulus of elasticity of each specimen is displayed in Figure 6.10 and the mean result, COV and age of each sample is provided in Table 6.13. For the old 20M and old 7M wallettes, the CON specimens were the most stiff, followed by the GEO, CSE and ADB. For the new 7M wallettes, the mean GEO result was the highest, followed by the CON, CSE and ADB. In this case, the mean GEO result was only marginally higher than the CON result.

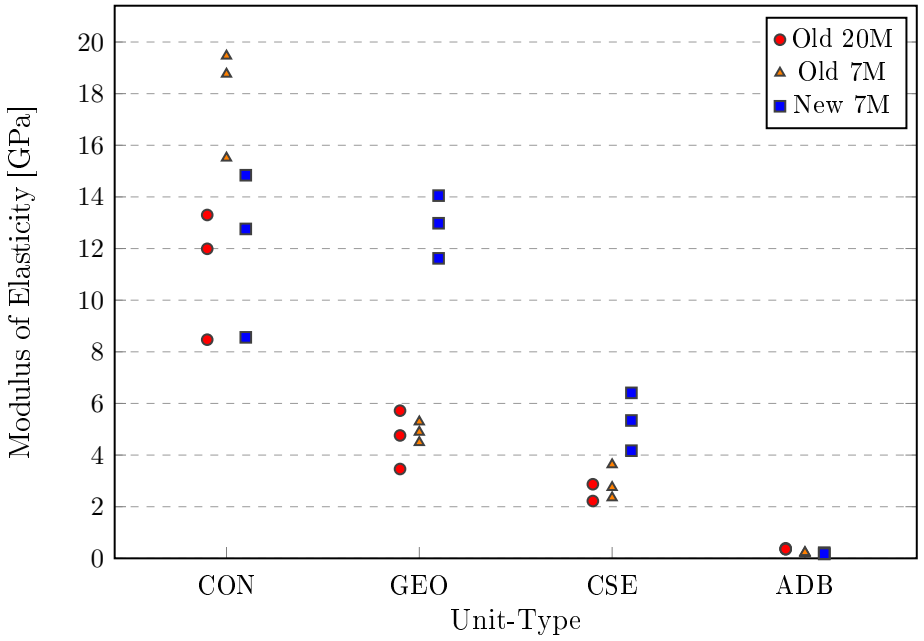

Figure 6.10: Wallette Modulus of Elasticity

Table 6.13: Wallette modulus of elasticity, $f_{c,w}$ in GPa

Unit	Old 20M			Old 7M			New 7M		
	E_w	COV	Age	E_w	COV	Age	E_w	COV	Age
CON	11.25	22%	11	17.91	12%	13	12.05	27%	12
GEO	4.64	24%	6	4.89	8%	9	12.88	9%	8
CSE	2.54	18%	9	2.91	23%	9	5.30	21%	9
ADB	0.37	4%	5	0.21	10%	7	0.19	13%	7

The apparent effects of unit- and mortar-stiffness on that of the wallette stiffness differed for each unit-type. It should be noted that the age at which the tests were performed also differed for wallettes made from the same unit-type for all except the CSE wallettes. This rules out the possibility of developing a predictive model from these results alone. However, it is unlikely that the specimen age differences present in this test would have resulted in the 7M mortar becoming stiffer than the 20M mortar.

For the CON wallettes, the old 7M specimens were markedly stiffer than the old 20M specimens and new 7M specimens, which were similar to each other. The apparent inverse relationship between mortar stiffness and wallette stiffness is unexpected. Furthermore, the results indicate an inverse relationship between unit stiffness and wallette stiffness, considering that the average stiffness of the new CON units is greater than that of the old CON units. It should be noted, however, that the average auxiliary CON unit stiffness results were within one standard deviation of each other.

The new 7M wallettes were strongest for both GEO and CSE groups, but this was more pronounced with the GEO wallettes. This relationship was expected from the unit stiffnesses, although the variability of the CSE unit modulus of elasticity results made it unclear as to whether the new CSE's were stiffer as indicated by the mean unit results. Furthermore, the GEO and CSE wallettes were similar in that mortar stiffness did not have a considerable effect on wallette stiffness, when compared to the effect of unit stiffness.

For the ADB specimens, the old 20M wallettes were nearly twice as stiff as both the old 7M and new 7M wallettes, which were very similar to each other in stiffness. In this case, the compressive strength and the stiffness of the mortars were both much higher than that of the units. Furthermore, the old and new ADB units exhibited similar compressive strengths and elasticities. Considering this, the observed results were expected.

As with the wallette compressive strengths, the modulus of elasticity results were deemed acceptable for the purposes of numerical modelling. The effects of unit-stiffness and mortar-stiffness are evident in the results. Despite this, the varying

ages at which the tests were conducted and the variability of each result makes comparison between some of the samples difficult.

6.3.3 Wallette Test Discussion

A high COV is prevalent in the both the compressive strength and modulus of elasticity results. Masonry is a composite of units and mortar, so that a higher degree of variability might be expected for this test as opposed to the unit tests and mortar tests individually. Furthermore, only three or four tests were performed per sample. Observations made during the tests and upon analysing the data indicated that the test setup itself might have also contributed to the variability of the results.

The top of each specimen consisted of a 10mm layer of mortar which was built to be as level and flat as possible. The top boundary condition consisted of a polyethylene sheet, steel plate and rubber mat which were placed on top of the wallettes in that order. A spreader beam was used to ensure an even load distribution was applied by the actuator to the specimen. A more detailed description and figure of the setup are provided in Section 5.4.

For some of the tests, it was noted that during the first stages of loading, the spreader beam would only make full contact with one side of the top boundary condition. Furthermore, although the top mortar layer was built as flat as possible, it was noted that this was not perfectly achieved as gaps were sometimes visible between the polyethylene sheet and the steel plate. This would have resulted in an uneven load application from the top plate to the wallette. Despite these issues, the top boundary condition was kept constant throughout the testing period. A better alternative to the top boundary condition would have involved mortaring a steel plate to the top of each wallette and placing rubber mats between this plate and the spreader beam. Due to the project timeline and the total number of specimens tested per day, this solution was not feasible for the current study.

For all of the modulus of elasticity tests, four LVDTs were mounted to the specimen to measure displacement. The strain used to calculate the modulus of elasticity was calculated by dividing the average of the LVDT readings by the gauge length of the setup, which was 210mm. However, for most of the tests, at least one LVDT did not measure any displacement over this range. In some cases, this was true for two LVDTs. Since, with each test, the non-responsive LVDT would differ, it is likely that this was due to the insufficient levelling capability in the setup.

In general, straight, vertical cracks were observed on the sides of the specimens. The crack patterns on the wider faces of the specimens varied, but in general, these were vertical or diagonal. In many cases, a specimen would exhibit more severe cracking on one side as opposed to the other, as observed in Figure 6.11, which displays the crack patterns of an old 7M GEO specimen.

Figure 6.11: Tested GEO Wallette

The generally vertical wallette crack pattern was also observed by Fourie (2017) and Shiso (2019). These crack patterns have also been observed by other researchers in tests on conventional clay brick masonry (e.g. Sassoni *et al.* (2014) and Vermeltfoort *et al.* (2007)) and traditional adobe masonry (e.g. Wu *et al.* (2013)).

6.4 Flexural Wall Test Results

The masonry flexural strength of CMU and AMU walls was determined using EN 1052-2 (2016) as a guide. The tests were performed in two configurations: the first caused cracks parallel to the bed joints and the second caused cracks perpendicular to the bed joints. These test configurations will henceforth be referred to as the "parallel test" and the "perpendicular test", respectively. Different wall specimens were built to be tested in each configuration and are similarly referred to as "parallel walls" and "perpendicular walls". A detailed description of the specimens constructed and the method used to perform these tests is provided in Section 5.5.

This test was performed to provide data to validate a numerical model, to enable comparisons to be made between AMU and CMU flexural behaviour and to allow comment to be made on the suitability of AMUs for single storey low-income housing (LIH). To achieve this, the flexural capacities as well as the load-displacement behaviour of each wall was recorded. To allow for qualitative assessment of the results, a video recording of each wall was taken during the test. Similarly, photographs were taken of the tension face of each wall after testing and the crack pattern of each wall specimen was recorded and reproduced in diagrams.

The flexural capacities and load displacement behaviours are presented in separate sections in that order. For each section, the methods used to calculate the results are provided. Thereafter, the results are presented in a series of figures and tables. Descriptions of the results are provided and observational comparisons are drawn for each section. Finally, a general discussion on the suitability of the test and setup is provided.

6.4.1 Wall Flexural Strengths

The wall flexural strength, $f_{x,w}$ (in MPa), was calculated assuming linear elastic bending theory as prescribed by EN 1052-2 (2016). This calculation is presented in Equation (6.4.1) where F_{max} is the ultimate recorded applied force (in Newtons), l_1 and l_2 are the dimensions between the support bearings and load bearings respectively, b is the dimension of the wall perpendicular to the span and t_u is the wall thickness. A diagram of these dimensions is also provided in Figure 5.9. All dimensions are given in mm.

$$f_{x,w} = \frac{3F_{max}(l_1 - l_2)}{2b(t_u)^2} \tag{6.4.1}$$

The force applied to the walls by the actuator was recorded by its own built-in instrumentation. Recordings were also taken of the reaction forces at the supports by four load cells (LCs) situated behind the ends of the supports. The parameter, F, of Equation (6.4.1) was chosen as the maximum of the sum of the reaction forces rather than the maximum force applied by the actuator. This was done in order to prevent the frictional reaction at the bases from contributing to the flexural strength results.

Faulty load cells were mistakenly used for three of the tests. In these instances, the actuator applied force was used to calculate the flexural capacity. The flexural wall results derived from the applied force rather than the reaction force are indicated by an asterisk in the tables of the remaining sections.

According to EN 1052-2 (2016), specimens that exhibit cracking outside of the inner bearings should not be included in the results, since the failure that occurred is not purely in bending. Since the aim of this thesis was not to characterise the flexural strength, these results are included, but annotated with the term "out" in the tables and figures.

6.4.1.1 Parallel Flexural Strength

The parallel flexural strength test was performed for each unit type to determine the vertical flexural capacity of the walls. Only old units were used for the parallel wall tests, except for the 7M GEO specimens which were built from new GEO units.

Each specimen's flexural strength is provided in Figure 6.12 and is designated according to its unit set and mortar type. The data points of specimens that produced cracks outside of the inner bearings are encircled. These results are also tabulated in Table 6.14 along with the ages at which the specimens were tested and the position of the cracks with reference to the inner bearings.

In considering the footnotes of Table 6.14, the bottom boundary condition of the first CSE 20M wall is described as fixed. Before this test, the cap screws that held up the base plate (as described in Section 5.5.3) were not tightened into the bottom plate. The base plate was not able to rotate about its pivot point in this case. For all other tests, the bolts were tightened to allow the parallel wall base plate to pivot.

It should also be noted that no result is presented for the first GEO 20M specimen. This specimen broke while it was being placed into position in the test setup.

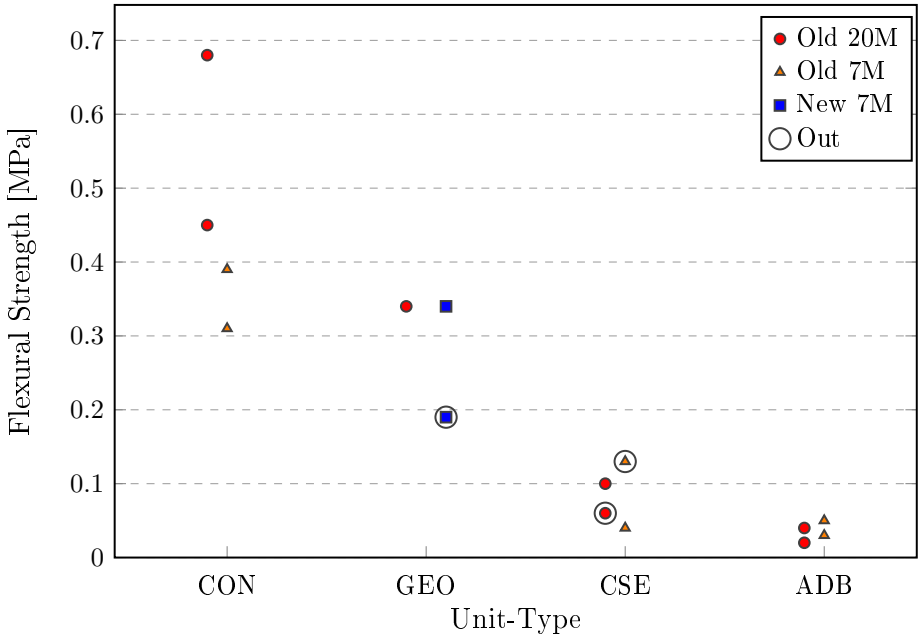

Figure 6.12: Parallel wall flexural strength

Of the walls constructed from 20M mortar, the CON specimens were the strongest, followed by the GEO, CSE and ADB specimens in descending order. For this mortar class, clear distinctions in strength can be observed despite variability within specimens of the same unit-type.

A similar pattern is observed for the 7M walls, but for the GEO and CSE specimens, one test produced cracks outside of the inner bearings. Removing these results from the sample would make the differences between the CON and GEO specimens and between the CSE and ADB specimens negligible.

Table 6.14: Parallel flexural wall results

No.	Unit	20M			7M		
		$f_{x,w}$ [MPa]	*Age* [days]	Crack Position	$f_{x,w}$ [MPa]	*Age* [days]	Crack Position
1	CON	0.45	10	in	0.39	7	in
2		0.68	10	in	0.31	8	in
1	GEO				0.34	7	in
2		0.34[a]	7	in	0.19	7	out
1	CSE	0.10[b]	7	in	0.13	7	mix
2		0.06	7	mix	0.04	7	in
1	ADB	0.03	6	in	0.05	6	in
2		0.02	6	in	0.03	6	in

[a] Calculated from actuator reading
[b] Fixed bottom boundary condition

All of the specimens were tested at an age of 7 ± 1 days, except for the CON 20M specimens, which were tested at 10 days. This difference in age may have contributed to the greater strength of these specimens.

No confident statements on the effect of mortar type can be made for the CON, GEO and CSE specimens due to the difference in age between the CON 7M and CON 20M specimens and the invalid results of the 7M GEO and CSE specimens. Although all four ADB results were valid, the results are too similar to indicate whether mortar strength had an effect on the parallel flexural strength of the specimens.

Six parallel wall crack patterns are presented in Figure 6.13. The crack patterns of the remaining specimens did not have any distinguishing features and are provided in Appendix A. For all crack pattern diagrams, the crack is represented by thick red lines and the measured positions of the inner load bearings and outer support bearings are represented by blue and green dashed lines respectively.

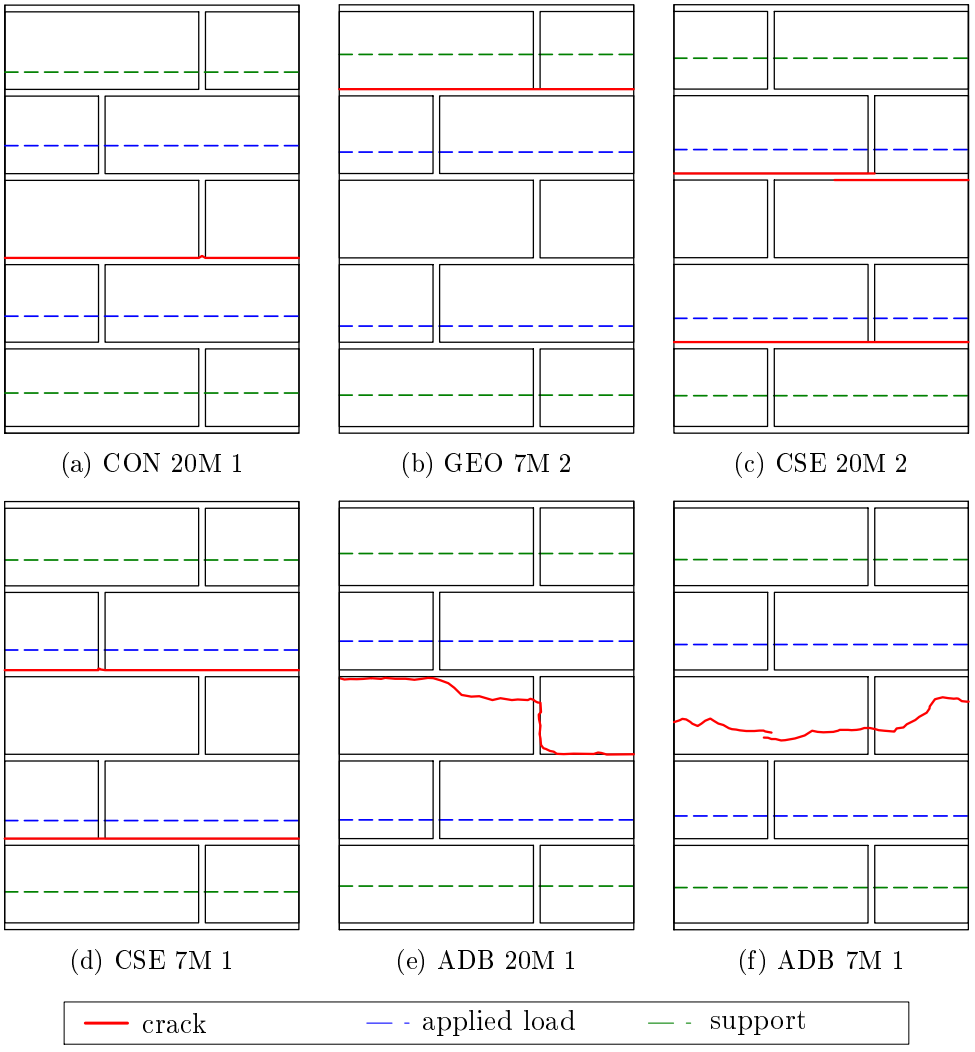

Figure 6.13: Crack patterns observed for the parallel tests

The desired and most common crack pattern is presented in Figure 6.13(a). This pattern was produced by specimen 1 of the CON 20M walls. A straight horizontal crack was formed at the unit-mortar interface below the middle row of units. Some variant of this pattern (a horizontal crack through any interface between the inner bearings) was produced by all of the other nine tested specimens not displayed in Figure 6.13.

Three specimens produced cracks outside of the zone between the inner bearings. Specimen no. 2 of the GEO 7M walls produced one crack that formed at an interface between the upper load and support bearings at the point of failure as displayed in Figure 6.13(b). Since this was the only crack produced, and since its formation coincided with the ultimate load of the specimen, this result should not be considered as valid.

The second CSE 20M and first CSE 7M specimens produced cracks that formed outside of and within the inner bearings. For this reason, their crack positions are designated as 'mix' (as shorthand for mixed) in Table 6.14. In both cases, an initial crack formed between the lower load and support bearings before the final crack was produced within the zone of constant moment as presented in Parts (c) and (d) of Figure 6.13. For both specimens, the lower crack occured well before failure and did not open through the full thickness of the specimens. The formation of the middle-most crack did correspond to the ultimate applied load.

Specimen no. 1 of the ADB 7M and ADB 20M walls produced crack patterns that propagated through the units. This implies that for both 7M and 20M specimens, the unit flexural tensile strength was weaker than or equivalent to the bond strength of the interface. Given the low strength and brittle nature of the ADB units, this outcome was expected. It should be noted, however, that the ADB specimens that failed through the units were stronger than their counterparts that failed through an interface (within the ADB 20M specimens and ADB 7M specimens respectively).

6.4.1.2 Perpendicular Flexural Strength

The perpendicular flexural strength test was performed for each unit type to determine the horizontal flexural capacity of the walls. Old units were used in the 20M walls and new units were used in the 7M walls for all unit-types except for the GEO specimens, where old units were used for both mortar types.

Each specimen's flexural strength is provided in Figure 6.14 and is designated according to unit set and mortar type. These results are also tabulated in Table 6.15 as well as the age of the specimens on the day of testing, the position of the failure cracks with regards to the inner bearings and the type of failure.

Of the 20M walls, the CON specimen was the strongest, followed by the GEO, ADB and CSE specimens. Only one CON 20M result is available as the other specimen was accidentally destroyed before it could be tested. It should be noted that the successful CON 20M result came from a test which was conducted at 9 days (as opposed to 7 ± 1 days).

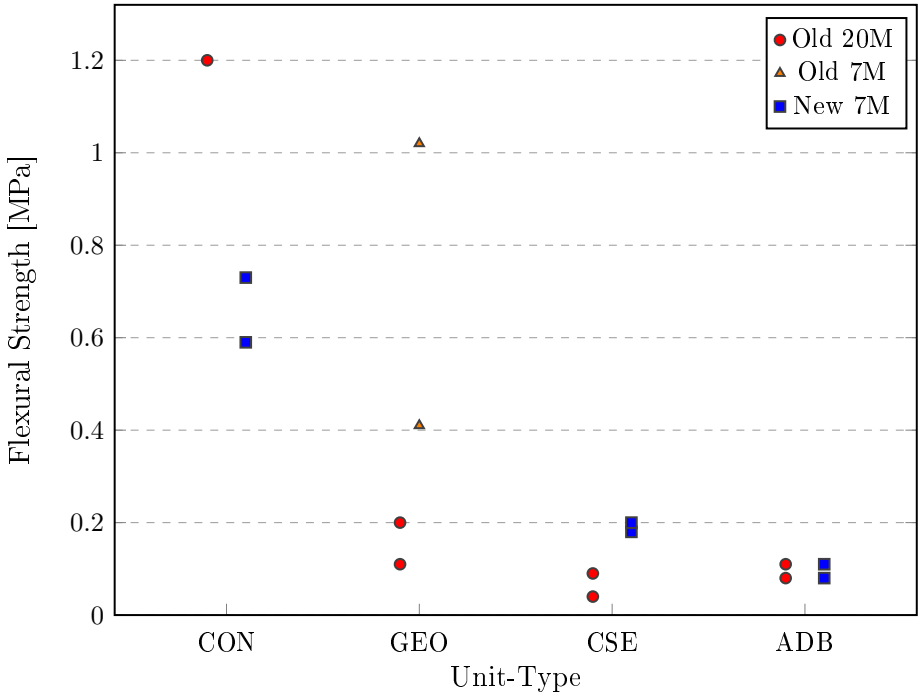

Figure 6.14: Perpendicular wall flexural strength

For the 7M walls, the GEO specimens are the strongest on average, followed by the CON, CSE and ADB specimens. In comparing the 7M CON and GEO results it should be noted that both 7M CON results fall inside the range of the GEO results so that the difference between the two unit-types is not significant.

Within unit-types, an increase in mortar strength class had a beneficial effect on the CON specimens, a detrimental effect on the GEO and CSE specimens and no effect on the ADB specimens. Since the 20M and 7M GEO specimens were all constructed with old units, the observed difference between the 7M and 20M specimens is due to the change in mortar class. For the CON, CSE and ADB specimens, the 20M and 7M specimens were constructed from old and new units respectively. For these specimens, the observed differences in flexural strength between mortar classes are due to changes in both the mortar and unit characteristics between old and new units within unit-types.

The total reaction force measured by the support load cells was compared to the total force applied by the actuator at failure. A discrepancy was found between the two that is thought to have been caused by friction. On average, this force accounted for 1%, 7%, 31% and 38% of the CON, GEO, CSE and ADB specimen actuator readings respectively. In the case of the CSE and ADB specimens this would imply that the bottom boundary condition provided significant restraint during the test.

Table 6.15: Perpendicular flexural wall results

No.	Unit	20M				7M			
		$f_{x,w}$ [MPa]	*Age* [days]	Crack Pos.	Fail. Type	$f_{x,w}$ [MPa]	*Age* [days]	Crack Pos.	Fail. Type
1	CON					0.59	6	in	line
2		1.20	9	in	line	0.73	6	in	line
1	GEO	0.20	7	in	step	1.02	7	mix	mix
2		0.11	7	in	step	0.41	7	mix	step
1	CSE	0.04	7	mix	step	0.18	7	mix	step
2		0.09	8	mix	step	0.20	7	mix	mix
1	ADB	0.08	6	mix	line	0.11[(1)]	6	mix	line
2		0.11	6	mix	line	0.08	6	mix	line

[(1)] Calculated from actuator reading

The crack patterns of six of the specimens are presented in Figure 6.15. Only these six specimens are presented in this section for brevity as they are sufficient for describing the failure types that were observed. A comprehensive collection of all of the crack patterns is provided in Appendix A. It should be noted that only the main cracks associated with the failure strength of the wall are drawn. Typically, smaller cracks were observed at the head joint interfaces before the formation of the final crack pattern.

All of the CON specimens produced line failure (cracking through the units), as shown in Figure 6.15(a), indicating a strong torsional shear bond at the bed joints. Since line failure occurred consistently for these specimens, their strengths were greatly dependent on flexural tensile strengths of their units and mortar. The CON 20M specimens contained mortar that was stiffer and stronger in flexure. Furthermore the compressive strength of the units within these walls was also greater. Since concretes of higher compressive strengths yield higher tensile capacities (Domone and Illston, 2010, p. 151), it is likely that the old units were stronger in tension than the new units. The result of the CON 20M walls being stronger than the CON 7M walls is thus expected.

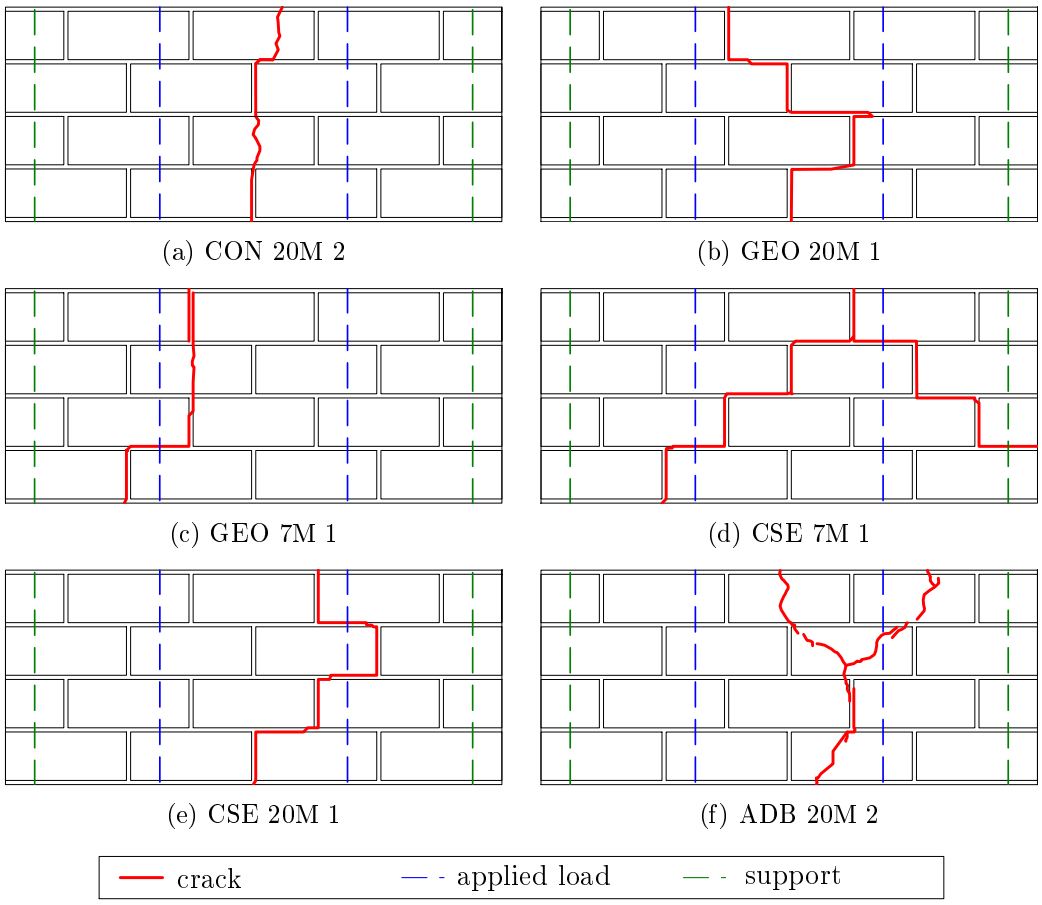

Figure 6.15: Crack patterns observed for the perpendicular tests

All of the GEO specimens exhibited stepped failure, except for the strongest 7M specimen in which cracks propagated through one unit before continuing through the unit-mortar interfaces in a stepped fashion. The greater strength of the 7M specimens is likely due to a stronger bond at the mortar-unit interfaces. This view is supported by the occurrence of the cracked unit in the aforementioned 7M specimen.

Similarly to the GEO walls, stepped failure occurred for all of the CSE specimens except for the strongest 7M specimen, where the crack propagated through one of the units before continuing through the interfaces. As with the GEO specimens, its is likely that the greater strength of the 7M specimens was due to the development of a superior bond between the 7M mortar and the units.

Line failure occurred in all of the ADB specimens. The ADB units were weak in tensile capacity and would split if they were handled roughly. Little difference in compressive strength was recorded between the old and new ADB units and it is likely that their unit flexural strengths are similar. Considering the line failure mode, similar unit strengths and nearly identical flexural strengths of the 7M and 20M ADB walls, one could argue that the flexural strengths of these walls was controlled by the tensile flexural strengths of their units.

In more than half of the walls, cracks appeared within as well as outside of the inner bearings. Examples of this are provided in parts c, d, e and f of Figure 6.15. Variation in the mechanical properties of the units and mortar as well as the bond between the two would have contributed to this behaviour. Design flaws of the test setup might have also been responsible.

If one side of the wall was more heavily loaded than the other, this would explain the formation of cracks between the load and support bearings on one side of the wall, as some shearing action would have been induced between the load bearing and support bearing on one side. To investigate this, the absolute difference between the loads measured at the support bearings was calculated and taken as a percentage of the total reaction load. This can be referred to as the "skewness" of the load.

The load applied to most of the walls had a skewness of less than 10%. Five of the walls exhibited higher skewness values, but three of these five only produced cracks in between the inner bearings. No correlation was found between the skewness of the load and the incidence of cracks forming outside of the inner bearings. This implies that the efforts to maintain an even load application were sufficient for this test. It should also be noted that this mixed crack position behaviour has been observed in at least one previous study: Zhou (2012, p. 153).

6.4.2 Load-Displacement Behaviour

Besides the reaction forces and applied force, the displacements of each wall and the test setup were recorded by LVDTs at key locations for each test. A detailed explanation of how this was achieved is provided in Section 5.5.4. The locations and labels of these recordings are provided again in this chapter in Figures 6.16 and 6.17 for ease of reference.

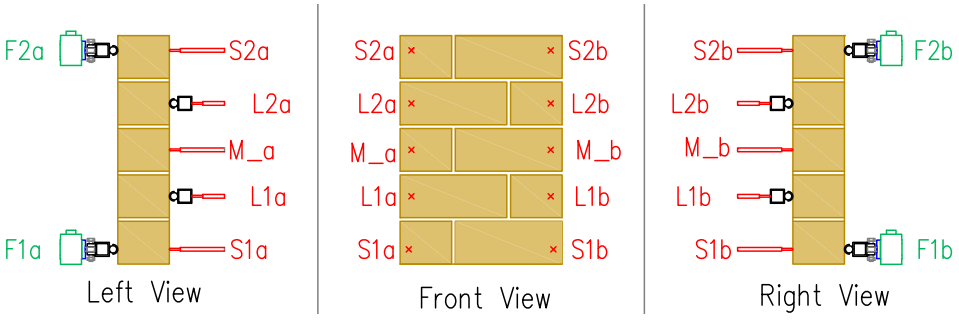

Figure 6.16: Instrument placement on parallel walls

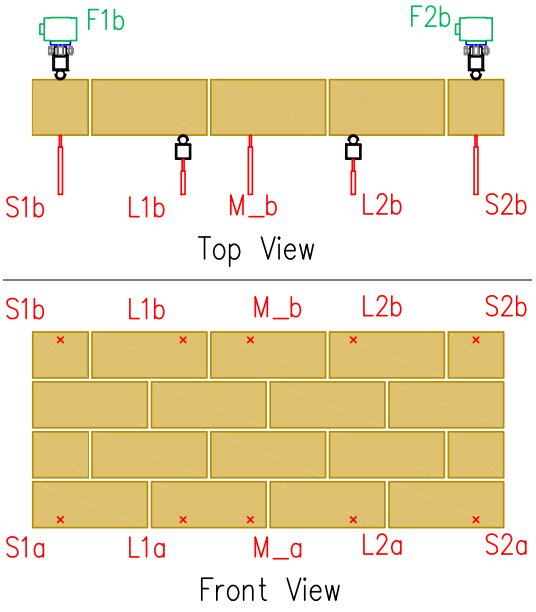

Figure 6.17: Instrument placement on perpendicular walls

The displacements were recorded for the primary aim of producing force vs mid-point displacement plots. The plots provide another means of comparing the flexural test results to those produced by numerical models, other experimental studies and those produced for conventional masonries. For this study, the plots are used in combination with the crack patterns to qualitatively describe the nature of the flexural failures.

6.4.2.1 Midpoint Deflection Calculations

Linear variable displacement transducers (LVDTs) were placed along two lines that spanned the wall. These imaginary lines are referred to as "line a" and "line b" respectively, as indicated by the last letter in the instrument labels of Figure 6.16 and Figure 6.17. Since all displacements were measured relative to the ground, the midpoint deflection along each line was calculated using the support and midpoint displacements. From the support bearing deflections and the measured positions of the readings along the wall, the rigid body displacement of the wall at the midpoint LVDT was determined by linear interpolation. The deflection at each recorded interval was calculated by subtracting the rigid body displacement from the measured displacement. This procedure is illustrated in Figure 6.18.

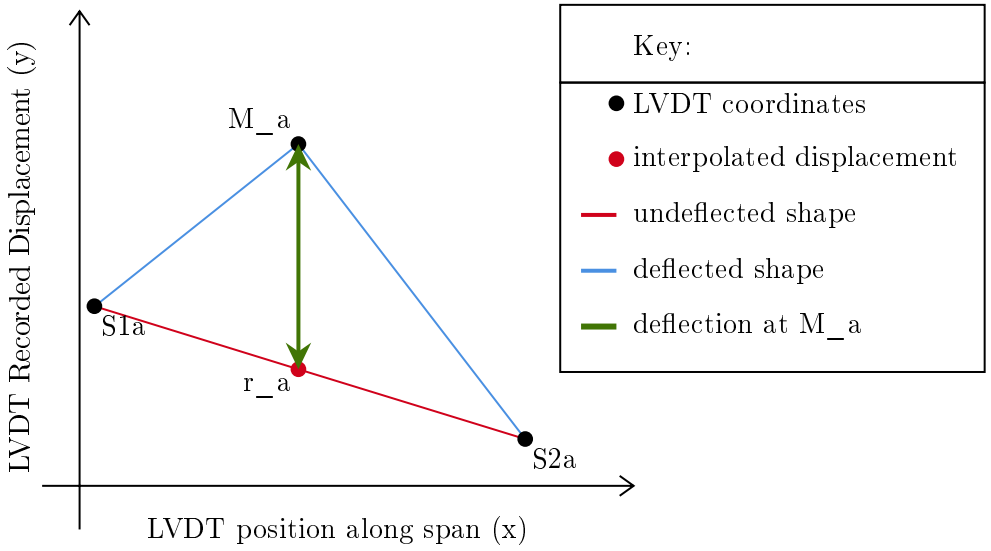

Figure 6.18: Depiction of calculated deflection along line a (not to scale)

The force-displacement plots produced from the calculated deflections indicated that negative midpoint deflection (i.e. deflection towards the actuator) occurred at the start of many of the tests. An example of this is provided in Part (a) of Figure 6.19. In reviewing the data, it was found that the apparent negative deflection always occurred when the wall rotated at the start of the test as it settled against the support bearings. Since rigid-body rotation of the wall about one of the supports would produce a component of displacement tangential to the direction of the applied force, the wall would effectively slide against the LVDT. Although this would occur over a short distance, the sensitivity of the LVDT would allow it to record any bumps or indentations on the walls surface at a precision of 3μm.

To account for this, an adjusted midpoint deflection was calculated. For each wall, the point in time at which the wall had settled against its supports was chosen as the new start time for the adjusted plots. At this point in time, the primary movement of the wall was a translation (instead of rotation) and all of the reaction load cells produced readings. The adjusted deflection was chosen as zero at the adjusted start time and the differences between the deflections between consecutive time steps were added to the adjusted deflection. The recorded force was not altered, so that, in effect, the load displacement plots produced for each line were shifted along the x-axis as shown in Part (b) of Figure 6.19.

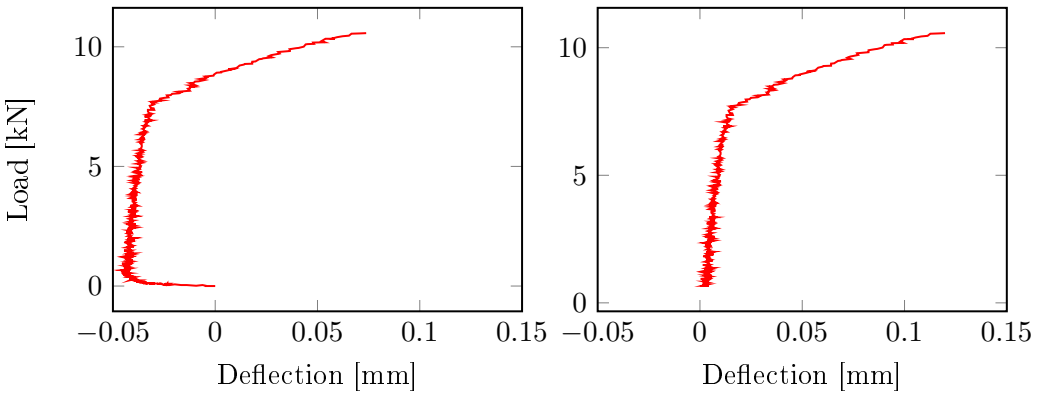

(a) Original (b) Adjusted

Figure 6.19: Adjusted and unadjusted load-displacement plot of the parallel CON 20M wall

6.4.2.2 Load-Deflection Plots and Ultimate Displacements

All of the valid load-deflection plots of the flexural wall specimens are provided in Figures 6.20 and 6.21. The plotted domain of all of the tests is set from 0mm to 1.5mm for comparison of the degree of deflection between all specimens. The range (y-axis) of each graph is set so that the shapes of the plots before failure are clear. The ultimate displacements of the walls are also provided in Table 6.16. In some cases, the displacement was only measured along one line. This is indicated in the notes of Table 6.16

Table 6.16: Midpoint deflections at failure

		Parallel		Perp.	
No.	Unit	20M	7M	20M	7M
1	CON	0.12	0.01		0.12[a]
2				0.18	0.15[a]
1	GEO		0.02[b]	0.19	0.24
2			0.18	0.40	0.13
1	CSE	0.03[b]	0.48[b]	0.59[b]	0.33[a]
2		0.05[b]	0.07[b]	0.82[a]	
1	ADB	0.05[b]	0.09[b]	0.09[a]	0.09[a]
2		0.08[b]	0.02	0.07	0.23

[a] Calculated from line a only
[b] Calculated from line b only

The plots of the parallel walls were generally steep before failure, due to the brittle nature of this test. However, the gradient of the plot reduces significantly before failure in the weaker GEO 7M and CSE 20M and the stronger CSE 7M specimens. The referenced GEO failed outside of the inner bearings. The two mentioned CSE specimens are those that initially produced cracks outside of the inner bearings.

The perpendicular walls deflected further before failure than the parallel walls. This is attributed to the formation of cracks in the head joints before failure, as is common for this test configuration. Furthermore the perpendicular tests were conducted over a greater span. Accordingly, similar strains in both setups would have resulted in a larger deflection in the perpendicular setup.

Usually, perpendicular walls that produce a stepped crack pattern are able to withstand stronger horizontal loads after failure compared to those that produce a line crack pattern. This behaviour is not clearly observable in the results, since only line failure occurred in the CON and ADB specimens and only stepped or mixed failure occurred in the CSE and GEO specimens. All of the CON, CSE and ADB perpendicular walls produced plots that plateaued within a range of 0.5kN to 1kN after failure despite failing according to different crack types. The stronger GEO 20M wall exhibited a higher post-failure strength, but why this occurred is unclear, given that all of the other GEO specimens produced plots that plateaued at a lower load regardless of failure type.

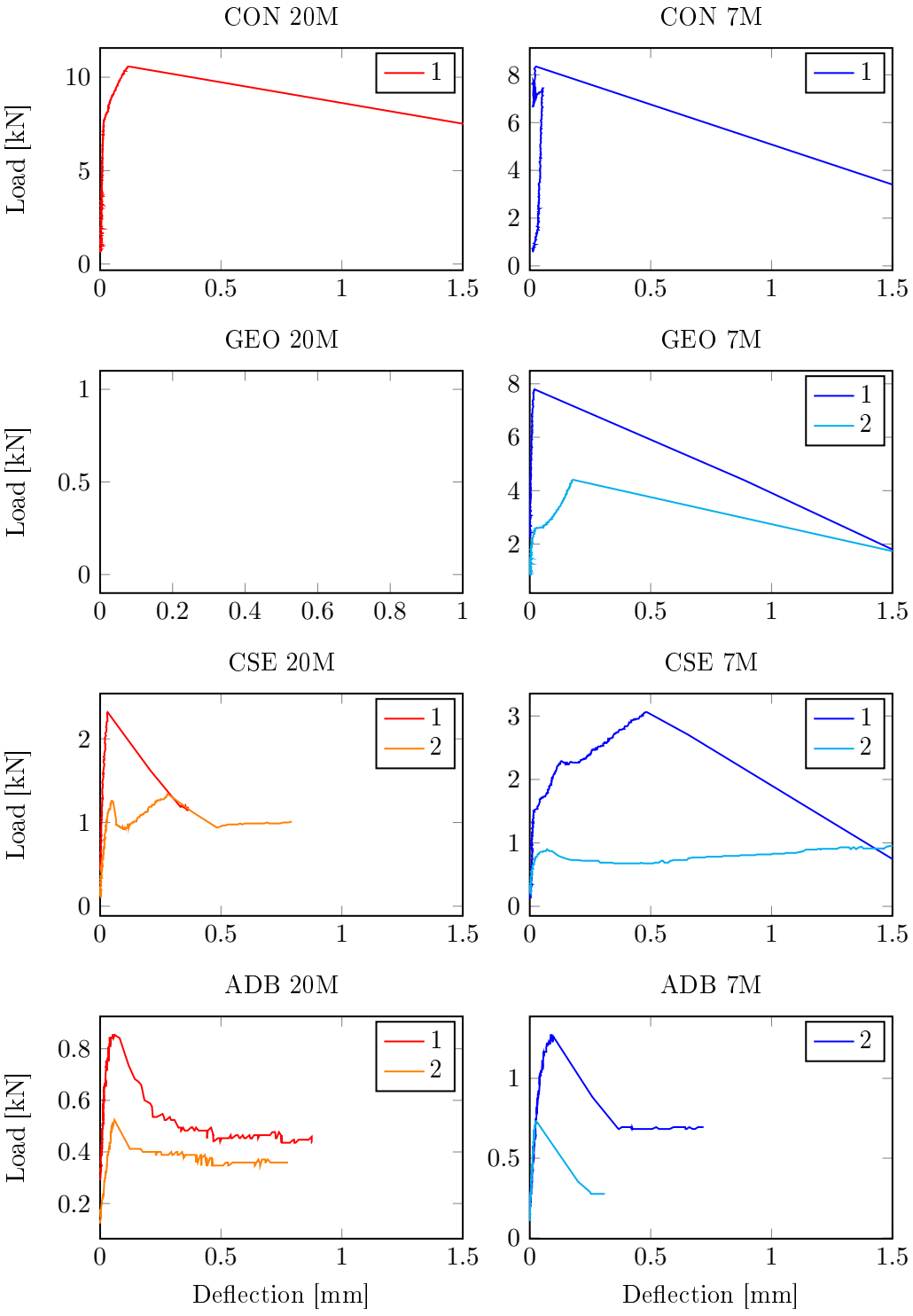

Figure 6.20: Adjusted load-displacement plots of the parallel walls

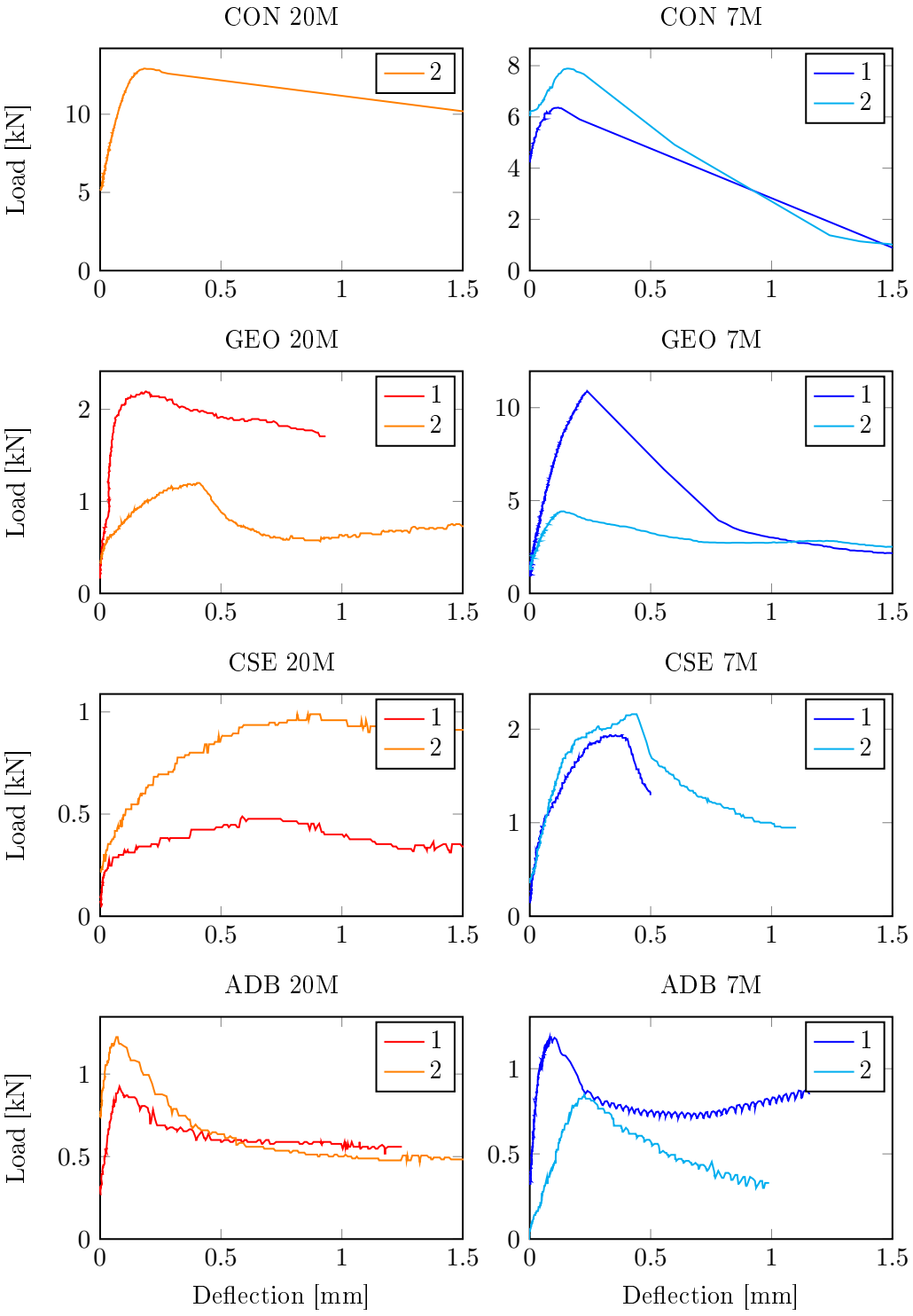

Figure 6.21: Adjusted load-displacement plots of the perpendicular walls

6.4.3 Flexural Wall Strength Model Comparisons

SANS 51996-1-1 and SANS 10164-1 prescribe characteristic masonry flexural strengths that may be used for design in lieu of determining these parameters through testing. It is of interest to compare these values to the experimentally determined results. Doing so provides some context to the applicability of the AMUs as a construction material and allows assessment of the predictive capability of the models used in the standards. The flexural strengths predicted using the models of both standards are provided in Figures 6.22 and 6.23 and Table 6.17.

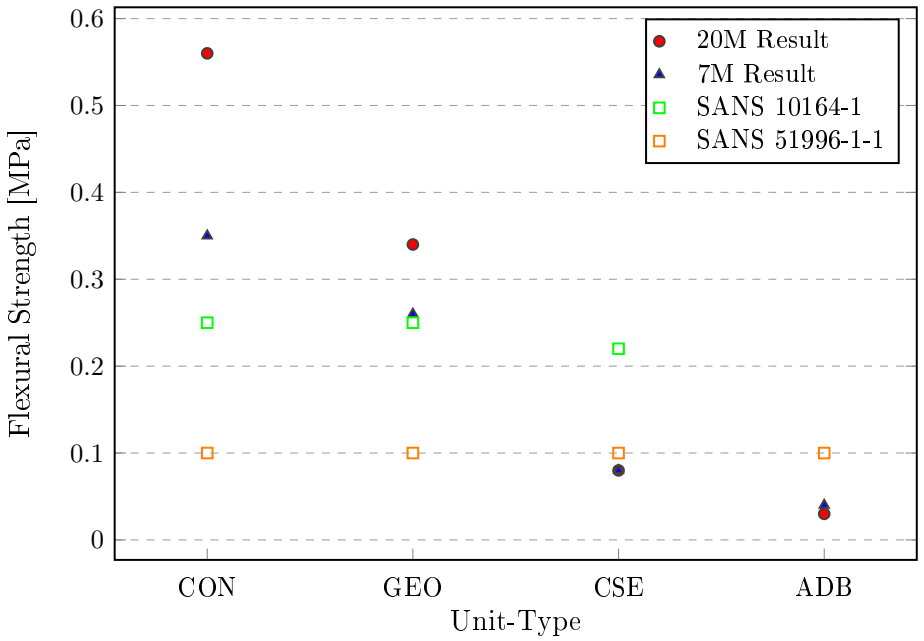

Figure 6.22: Experimentally determined parallel flexural wall strengths vs model strengths

The model provided by SANS 51996-1-1 (Clause 3.6.3 (3) NOTE 2) does not distinguish between unit types and strengths. It does distinguish between mortar classes, but both mortars used in this study fell under the same category. For this reason, it predicted constant parallel and perpendicular flexural strengths. These values grossly underestimated the CON and GEO capacities in both flexural modes. It did provide a good estimate of both mortar classifications of the CSE parallel walls and predicted a design strength that fell between the 20M and 7M perpendicular CSE results. For the ADB walls, the parallel wall strengths were overestimated, while the perpendicular wall results were predicted accurately.

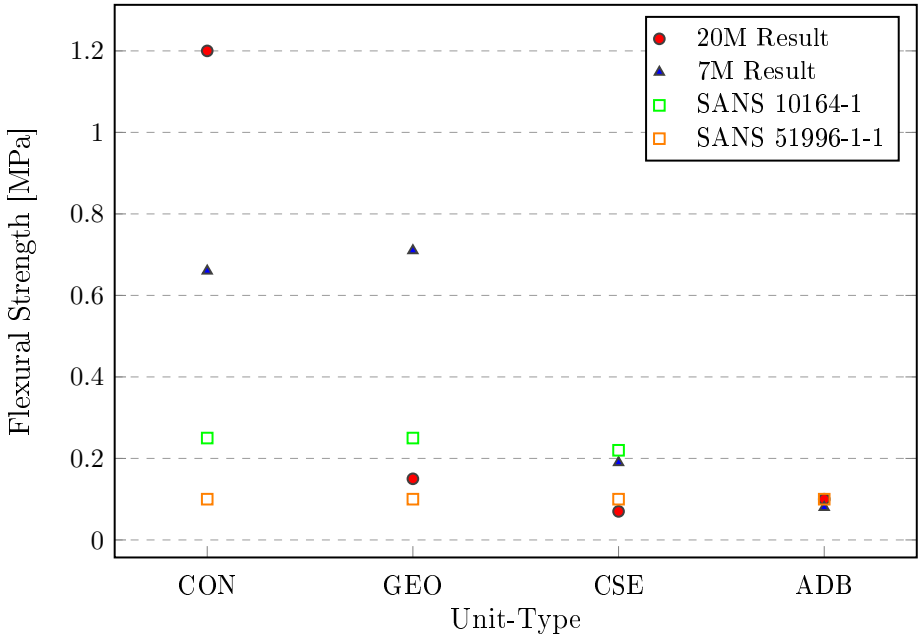

Figure 6.23: Experimentally determined perpendicular wall flexural strengths vs model strengths

The model prescribed in Table 4 of SANS 10164-1 does take unit-type and strength into account. For this model too, however, both mortars used in this study fell under the same category. For the parallel test, the CON 20M result was grossly underestimated. Better predictions were obtained for the CON 7M and GEO results (compared to SANS 51996-1-1). The parallel CSE strengths were overestimated and no value could be specified for the ADB walls as the ADB unit strength fell outside of the range of predictable unit strengths.

For the perpendicular flexural strengths, SANS 10164-1 underestimated both CON results and the 7M GEO result. It only slightly under-predicted the 7M CSE result, simultaneously overestimating the 20M CSE result. Again, no value could be predicted for the ADB specimens.

Although SANS 51996-1-1 provides the aforementioned predicted strengths, these are only provided as recommendations. The code states characteristic wall flexural strengths are nationally determined parameters and hence, should be provided within a National Anex (NA).

The model provided in SANS 10164-1 incidentally is the same as that provided by the British NA to EN 1996-1-1, since both were taken directly from BS 5628-1. This model did not accurately predict the flexural strength results, but did produce a similar trend. It should be noted that the 20M mortar and the stronger CON and GEO units were of compressive strengths far greater than those catered for. Similarly, the ADB units were far weaker than what was catered for in the model.

Table 6.17: Comparison between flexural strength test results and prescribed design strengths.

Mode	Unit	Result		Predictive Models	
		20M	7M	SANS 10164-1	SANS 51996-1-1
Parallel	CON	0.56	0.35	0.25	0.1
	GEO	0.34	0.26	0.25	0.1
	CSE	0.08	0.08	0.22	0.1
	ADB	0.03	0.04		0.1
Perpendicular	CON	1.20	0.66	0.25	0.1
	GEO	0.15	0.71	0.25	0.1
	CSE	0.07	0.19	0.22	0.1
	ADB	0.10	0.08		0.1

With the exception of the ADB specimens, all of the walls exhibited flexural strengths that were greater than or comparable to those predicted by the models. This indicates that walls constructed out of CON, GEO and CSE units could fall within the limits of acceptable design flexural strengths in a South African context. The same could be argued for the ADB perpendicular results, but not the ADB parallel results.

6.4.4 Flexural Wall Test Concluding Summary

The AMU and CON walls were tested in parallel and perpendicular flexure with the use of a test method based on EN 10152-2 (2016). The ultimate flexural strengths, crack patterns and force-deflection plots of the tested walls were provided. The validity of these results was discussed based on the crack patterns produced by and boundary conditions set for each test. Lastly, the flexural strengths were compared to those predicted by models provided in the applicable South African masonry design codes.

Three of the parallel specimens and ten of the perpendicular specimens produced cracks outside of the zone of constant moment. For two of the parallel specimens and all of the perpendicular specimens, these were accompanied by cracks that did form within the zone of constant moment. For this reason, these results are not considered acceptable for the purposes of characterising the flexural strength of the materials. However, the primary aim of the study was to provide experimental data for numerical model validation and not to characteristic design flexural strengths. It is thought that the high occurrence of this behaviour in the perpendicular walls might have been due to an unbalanced distribution of loading between the inner and outer bearings.

Despite these issues, the results provided from the recorded forces and displacements were adequate to enable validation of the out-of-plane behaviour of the numerical model used by De Villiers (2019).

Chapter 7

Conclusions and Recommendations

The aim of this study was to experimentally investigate the flexural behaviour of unreinforced (URM) walls constructed out of alternative masonry units (AMUs). This forms part of a larger study at Stellenbosch University in which other parameters of the same AMUs are investigated. The data produced from the experimental investigation was collected primarily so that it could be applied to validate a numerical model. The achievement of this aim was divided into three main objectives.

The first objective was to manufacture the units to be as similar to the previously developed units as possible. The units in question are: a concrete (CON) unit, that acts as a benchmark conventional masonry unit (CMU), a compressed stabilised earth (CSE) unit, a geopolymer (GEO) unit and an adobe (ADB) unit. Due to an increase in scope, a second set of units was manufactured. The first set is referred to as old units, while the second is referred to as new units. To assess the completion of this objective, 28-day tests were performed on the old units and specimens were sampled from both sets for testing at the time of the flexural wall tests. The latter tests are referred to as 'auxiliary' tests.

The second objective was to design and construct a setup that could test the flexural strength of walls constructed out of AMUs (referred to as "alternative masonry walls"). The final design choice was informed by a literature review. The literature review covered the out-of-plane behaviour of masonry in general, existing flexural strength setups and standardized design and analysis techniques.

The third objective was to assess the flexural behaviour of the alternative masonry walls experimentally, so that the results may be used to validate a numerical model. Two mortars, classified as 7M and 20M (after their target strengths) were used to construct these specimens. Additional unit, mortar and wallette tests were performed to provide input parameters for the numerical model to be validated in a separate study.

In this chapter, conclusions are provided based on the aforementioned objectives. Observations made during the experimental programme are also provided. This is

presented for the manufacturing procedures, auxiliary tests and the wall flexural strength test. Finally, recommendations are provided with regards to improvement of the experimental procedures followed as well as avenues for future research.

7.1 Unit Manufacturing

The mix designs of most of the units were altered from those developed by previous researchers. This was done in order to obtain the fresh characteristics required to handle the mixtures and form the blocks. This was necessary due to variations present in the raw materials occurring between the studies.

The CON, CSE and ADB units were formed with the use of a block press. The CON material was the most difficult to handle after forming as it was the wettest in its fresh state. This lead to the fresh units slumping after they were placed down to set. To reduce variation in unit shape, a mould was used to reshape the units after placing. Conversely, the CSE and ADB units retained their shape well after forming.

The GEO units were formed through casting into moulds. The fresh state of the GEO units proved to be sensitive to small variations in constituent properties. For this reason, the mix designs of the old and new GEO units differed in water, aggregate and fly ash quantities. This resulted in a new GEO unit which was substantially stronger and stiffer in compression than its old counterpart.

7.2 Unit Tests

The unit compressive strength tests were all performed according to EN 772-1 (2011), but modifications had to be made to the boundary conditions of the new GEO and ADB tests due to the high strength of the GEO units and the fragile nature of the ADB units. All of the tests produced COVs within acceptable limits, except for the auxiliary tests of the old GEO units. The high variability of that test is attributed to the sensitive nature of the GEO mix design.

The secant modulus of elasticity test was the most labour intensive of the unit tests. This was due to the sawing which required to produce the CON, CSE and ADB specimens and the intricate nature of the test setups. The setup used to test the CON, CSE and ADB modulus of elasticity specimens was improved by including a self-levelling attachment and replacing the load cell for one with a higher resolution. A force-controlled loading rate was implemented for all, except the ADB specimens. A displacement-controlled rate was implemented for these specimens as the setup was unable to apply a force-controlled loading to a material with such a low stiffness and compressive strength.

The unit modulus of elasticity results were more variable than the unit compressive strength results. This could be attributed to numerous factors. The sawn units were difficult to handle and to test due to their size. For these tests, ensuring that the load was applied evenly and that the linear variable displacement transducers (LVDTs) were secured firmly and correctly was challenging. The GEO test, in comparison, was much simpler and easier to handle. For the sawn units, some of the variability could be attributed to the test setup itself, while the high variability of the old GEO stiffness is due to the variability of that set of units as confirmed by the variable nature of its compressive strength results.

The unit density test was simple to implement and no adjustment to the test was required between unit-types. The variability of these test results was low. This indicates that the units were made with a consistent quality.

Apart from the new GEO units, all unit-types were similar to those produced by other studies conducted in the research group. The compressive strengths and secant moduli of elasticity were within a comparable range and the trends observed in these units were also found in those studies. Although the new GEO unit differed greatly from those produced by Fourie (2017) and Shiso (2019), a GEO unit of similar strength was also manufactured by Schmidt (2020).

The auxiliary unit test results and the dry density results were deemed suitable for use as input parameters for numerical modelling.

7.3 Mortar Tests

For quality control, the consistency of the mortar was tested throughout the construction period. The samples taken during construction were usually sampled from the mortar just before it was discarded to represent the least "flowable" mortar used in the wall and wallette specimens. The flow values (FVs) measured for the GEO and ADB units were consistently higher than 88%, while the minimum FV measured for the CSE mortars was 67%. This is likely due to the fact that the fine aggregate used to manufacture the GEO and ADB mortars were sourced from a different batch than the CON and CSE mortar and the mix designs were adjusted to take this into account.

The mortar modulus of elasticity test was performed using cast mortar cylinders and was relatively simple to perform. A low COV was measured for all of the results except for the 7M ADB mortar. Considering the age differences of the results and the young age at which the test was conducted, the mortar elasticity was found to be sufficiently consistent between unit types.

The mortar flexural strength and compressive strength was performed with square prismatic specimens. Considering the differing ages of the mortars, good consistency was found for the compressive and flexural strength tests for both 7M and 20M

mortars between unit-types. For each unit-type, the variability of these results was sufficiently low for modelling and comparison purposes.

7.4 Wallette Tests

Wallette compression and elastic modulus tests were conducted to produce data for model input parameters. The high variability produced in these results is attributed to a number of factors. The first attributing factor is the composite nature of masonry. The mortar, units and construction process introduce variability to the specimens. The second attributing factor was the test setup. Care was taken to keep the load application even and concentric. However, evidence provided by the LVDT readings (of the elastic modulus test) and observations made throughout the test suggested that these efforts were insufficient.

Despite the high variability clear differences are seen between unit-types and in, some cases, between mortar classes. For the purposes of comparison and for providing numerical model input data, these results are acceptable.

7.5 Flexural Strength Tests

The flexural wall strengths of the AMUs were tested at an age of 7 days with a test procedure based on EN 1052-2 (2016). The test setup was able to perform both parallel and perpendicular tests on specimens constructed out of each unit-type. Two replications were performed per tested unit-mortar combination.

The flexural strengths of the walls were calculated according to EN 1052-2 (2016) with the force parameter taken as the total reaction force to prevent inclusion of frictional forces into the wall strength. For the parallel walls, the CON 20M masonry was the strongest, followed by the CON 7M. In both mortar strength classes, the GEO CSE and ADB followed in descending order of strength.

For the perpendicular walls, the CON masonry was the strongest of the 20M mortar class walls followed by the GEO, ADB and CSE. For the 7M perpendicular walls, the GEO were the strongest, followed by the CON, CSE and ADB specimens. The relationship between the CSE and ADB 20M walls is unexpected, as the ADB units are much weaker than the CSE units. However, the CSE 20M walls failed according to a stepped pattern - through the mortar-unit interfaces, while the ADB specimens produced cracks through the units. This indicates a weak bond strength in the CSE 20M walls.

The crack patterns that formed on all of the walls were recorded. For the parallel setup, cracks always occurred within the inner bearings except for three specimens, where they formed between the inner and outer bearings, in a zone of combined bending and shear. In two of these specimens, the cracks that formed outside of the bearings did not occur at the time of failure. For these specimens, failure was accompanied by the formation of a more prominent crack in the zone of constant moment. Considering that only three of the fifteen tested specimens produced cracks outside of the zone of constant moment, the design, construction and implementation of the setup for these tests is considered successful.

For the perpendicular walls, more variation in crack pattern was observed. In the CON and ADB specimens, cracks propagated through the units in line failure. For both GEO and CSE specimens, stepped failure occurred in all specimens, but one. For both these unit-types, one 7M specimen produced a crack through one of the units before progressing into a stepped failure pattern.

More than half of the perpendicular walls produced cracks which propagated between the inner bearings and outside of the inner bearings. For these walls, part of the crack pattern fell outside of the zone of constant moment and zero shear. Studying the load cell readings revealed that this was not due to an uneven load application. A more likely explanation is that this occurred due to variation in the material properties of the walls. EN 1052-2 (2016) recommends testing more specimens than required in recognition of the fact that this phenomenon occurs frequently (EN 1052, 2016, p. 7). Although improvements might be made to the test programme and setup to improve the odds of producing cracks only within the zone of constant moment (as discussed in Section 7.6), the test setup has not failed to apply an even flexural load.

From the measured displacements, the midpoint deflection at each time step was calculated. These, in combination with the total reaction forces were used to produce load-deflection plots. The plots were adjusted to take the initial settlement of the test setup into account. The parallel wall plots were steeper than those of the perpendicular walls. The three parallel walls that produced cracks outside of the inner bearings also exhibited a loss of stiffness before failure. For the perpendicular walls, those that produced stepped failure deflected more than those that produced line failure, however, no post-failure difference was observable in the results.

The wall flexural strengths were compared to model predictions provided by SANS 51996-1-1 and SANS 10164-1. These models could not accurately predict the flexural strengths of all of the walls based on their mortar class and unit strength alone. With exception to the parallel ADB walls, all of the specimens were stronger than or of an equivalent strength to those predicted by the models. This indicates that walls constructed out of the CON, GEO and CSE units exhibit flexural strengths within the acceptable limits for design in South Africa.

7.6 Recommendations

7.6.1 Test Setup Improvements

Observations made in reviewing the results have led to the proposal of recommendations pertinent to improving the test setups. These recommendations would improve the ease with which tests are conducted, increase the probability of successful tests or reduce the complexity of the results.

- Apart from the GEO specimens, the unit modulus of elasticity tests were difficult to conduct and produced a large number of results that did not conform to the standard requirements. It is recommended that this test be performed on larger specimens, to make the specimens and test setup easier to handle. This would require that the specimens be created in such a way as to mimic the manufacturing process of the units. A further benefit of this approach is the reduction in time and specimen damage associated with negating the need to saw specimens out of the units.

- Since mortar flow value is strongly associated with bond strength, this parameter should be studied closely. It is recommended that the flow value of the mortars used to construct the masonry specimens be tested immediately after mixing to ensure mix design conformity and at the time the mortar is discarded.

- The wallette test setup should be adapted to ensure an even load application. This could involve mortaring the specimen to steel plates during specimen construction and providing rubber mats as boundary conditions on each side of the specimen.

- Moving the walls and wallettes into position for testing was difficult and time-consuming. Setups designed to test small walls and wallettes that are transported into position will benefit from improving the test setups to make this process easier while ensuring safety.

- A significant friction force was produced at the base of the perpendicular wall specimens. An improved boundary condition should be implemented at the base, especially for testing walls of lower flexural strengths. The suitability of other materials for this application should be investigated.

- Ten LVDTs were used to measure the displacements of the walls and the test setup. Although the recordings provided valuable information on the displacement of the wall and the stiffness of the setup, a large portion of the time involved in preparing the setup was spent on attaching and initializing the LVTS. Furthermore, any deflections occurring at the start of the test could not be recorded accurately with the current LVDT configuration. It is recommended that a setup be implemented where one LVDT is attached to the wall to directly measure the midpoint deflection. This could be achieved by attaching the LVDT to a bar which is in turn attached to the supported ends of the wall.

- To lessen the incidence of cracks occurring outside the zone of constant moment in the perpendicular walls, it is suggested that the dimension between the inner bearings be increased to include more units. This would require a larger specimen and test setup.

7.6.2 Recommendations for Future Study

In reading the relevant literature and through observations made during the study, recommendations for future test programmes were obtained.

- It is recommended that a bond wrench setup be developed and that the bond strength of mortar-unit combinations be investigated. Since fewer units are required per result, more replications could be performed per sample and more tests could be achieved over a shorter time-period due to the simplicity of the setup. This would allow a more in-depth investigation into the parameters which affect bond strength in alternative masonry walls.

- The effect of different wall curing conditions on the wall flexural strengths should be investigated.

- The tensile capacity and stiffness of the units is linked to the capacity of perpendicular walls which exhibit line failure. Auxiliary unit flexural tensile tests would provide more insight into the perpendicular wall results.

- To provide sufficient wall test data for characterisation, a more streamlined test programme would need to be implemented so that more flexural wall test replications can be performed per sample.

- The current models that predict biaxial bending strengths have been designed for walls constructed from CMUs. It would be of interest to determine the biaxial capacities of AMUs experimentally for comparison to model predictions.

- Wind and earthquake loads are dynamic in nature. The loading codes which are relevant to this study allow these loads to be applied as static loads if certain requirements are met. It should be noted that these simpler load application methods were devised assuming conventional building materials. The behaviour of alternative masonry walls subjected to dynamic loading should be investigated to determine whether the simplified loading models are applicable to these materials.

References

Act No. 103 (1977). *National Building Regulations and Building Standards Act*, vol. 145. Government Gazette of the Republic of South Africa.

Anderson, C. (1976). Lateral Loading Tests on Concrete Block Walls. *The Structural Engineer*, vol. 54, no. 7, pp. 239–246.
Available at: `http://pascal-francis.inist.fr/vibad/index.php?action=getRecordDetail{&}idt=PASCAL7689011844`

ASTM C1072-13 (2013). *Standard Test Methods for Measurement of Masonry Flexural Bond Strength*. ASTM International, West Conshohocken, USA.

ASTM E518-10 (2010). *Standard Test Methods for Flexural Bond Strength of Masonry*. ASTM International, West Conshohocken, USA.

ASTM E72-15 (2015). *Standard Test Methods of Conducting Strength Tests of Panels for Building Construction*. ASTM International, West Conshohocken, USA.

Baker, C., Chen, B. and Drysdale, R. (2005). Failure Line Method applied to walls with openings. In: *Proceedings of the 10th Canadian Masonry Symposium, Banff, Alberta, Canada*, pp. 1–10. Banff, Alberta.

Baker, C. and Drysdale, R.G. (2003). Failure line design of unreinforced masonry walls subject to out-of-plane loading. Tech. Rep., Centre for Effective Design of Structures Report, Hamilton, Ontario.

Baker, L. (1979*a*). Measurement of Masonry Flexural Bond Strength of Masonry. In: Wintz, J.A. and Yorkdale, A.H. (eds.), *5th International Brick and Block Masonry Conference*, pp. 79–83. The Brick Institute of America, Washington D.C.

Baker, L.R. (1979*b*). A failure criterion for brickwork in biaxial bending. In: *Proceedings of the Fifth International Brick Masonry Conference*, pp. 71–78. The Brick Institute of America, Washington, D.C.
Available at: `http://www.hms.civil.uminho.pt/ibmac/1979/71.pdf`

Baker, L.R. (1984). Concrete Masonry Walls Subjected to Lateral Loads. *Report MRC-ll (for Concrete Masonry Assoc. of Aust.)*.

Baker, L.R., Gairns, D., Lawrence, S.J. and Scrivener, J. (1985). Flexural Behaviour of Masonry Panels - A State of the Art. In: *7th IBMAC*, pp. 27–55. Melbourne, Australia.

Bell, F.G. (1996). Lime stabilization of clay minerals and soils. *Engineering Geology*, vol. 42, no. 4, pp. 223–237. ISSN 00137952.

Brandt, M. (2011). Seismic Hazard in South Africa. Tech. Rep., Council for Geoscience, Pretoria, South Africa.

Brinker, R. (1984). Yield-Line Theory and Material Properties of Laterally Loaded Masonry Walls. *Masonry International*, vol. 1, pp. 8–17.

BS 5628-1 (2005). *Code of practice for the use of masonry, Structural use of unreinforced masonry*. BSI, London.

Candy, C.C.E. (1988). The energy line method for masonry panels under lateral loading. In: De Courcy, J.W. (ed.), *8th International BricklBlock Masonry Conference*, pp. 1159–1170. Elsevier Applied Science, Dublin.

Chong, V.L. (1993). *The behaviour of laterally loaded masonry panels with openings*. PhD Thesis, University of Plymouth.
Available at: `http://hdl.handle.net/10026.1/846`

Constitutional Assembly (1996). *The Constitution of the Republic of South Africa*.

Costa, A., Arêde, A. and Costa, A. (2014). Experimental study of the out-of-plane behaviour of unreinforced sacco stone masonry walls: Comparative analysis of two different test setups. In: *9th International Masonry Conference*, July, pp. 1–9. Guimarães.

Curtin, W.G., Shaw, G., Beck, J.K., Bray, W.A. and Easterbrook, D. (2006). *Structural Masonry Designers' Manual*. 3rd edn. John Wiley & Sons. ISBN 978-0-632-05612-5.
Available at: `https://app.knovel.com/hotlink/toc/id:kpSMDME00N/structural-masonry-designers/structural-masonry-designers`

Dakhane, A. (2016). *Multiscale Engineering Response of Alkali Activated Aluminosilicate Binders*. PhD Thesis, Arizona State University.
Available at: `https://repository.asu.edu/attachments/178537/content/Dakhane{_}asu{_}0010E{_}16636.pdf`

De Villiers, W.I. (2019). *Computational and Experimental Modelling of Masonry Walling towards Performance-Based Standardisation of Alternative Masonry Units for Low-Income Housing*. PhD Thesis, Stellenbosch University.

Ding, Y., Dai, J.G. and Shi, C.J. (2016). Mechanical properties of alkali-activated concrete: A state-of-the-art review. *Construction and Building Materials*, vol. 127, pp. 68–79. ISSN 09500618.
Available at: `http://dx.doi.org/10.1016/j.conbuildmat.2016.09.121`

Domone, P. and Illston, J. (eds.) (2010). *Construction Materials: Their nature and behaviour*. 4th edn. Spon Press, Oxon.

Drysdale, R.G., Hamid, A.A. and Baker, L.R. (1994). *Masonry Structures: Behavior and Design*. Prentice-Hall, Englewood Cliffs, N.J. ISBN 0-13-562026-0.

Duarte, R.B. (1993). *A study of the lateral strength of brickwork panels with openings*. PhD Thesis, The University of Edinburgh.
Available at: `https://www.semanticscholar.org/paper/A-study-of-the-lateral-strength-of-brickwork-panels-Duarte/c46a260df0f52827ce911fce7b9054775cf3fe22`

Edgell, G. (2005*a*). Direct Tension Testing. In: *Testing of Ceramics in Construction*, chap. 3.4.2, p. 120. Whittles Publishing, Dunbeath. ISBN 1-870325-43-5.

Edgell, G. (2005*b*). Full scale testing. In: Edgell, G. (ed.), *Testing of Ceramics in Construction*, chap. 5, p. 157. Whittles Publishing Limited, Dunbeath. ISBN 1-870325-43-5.

EN 1015-11 (1999). *Methods of test for mortar for masonry, Part 11: Determination of flexural and compressive strength of hardened mortar.* European Committee for Standardization, Brussels.

EN 1015-3 (1999). *Methods of test for mortar for masonry - Part 3: Determination of consistence of fresh mortar (by flow table).* European Committee for Standardization, Brussels.

EN 1052-1 (1999). *Methods of test for masonry - Part 1: Determination of compressive strength.* European Committee for Standardization, Brussels.

EN 1052-2 (2016). *Methods of test for masonry - Part 2: Determination of flexural strength.* European Committee for Standardization, Brussles.

EN 1052-5 (2005). *Methods of test for masonry - Part 5: Determination of bond strength by the bond wrench method.* European Committee for Standardization, Brussels.

EN 12390-13 (2013). *Testing hardened concrete - Part 13: Determination of secant modulus of elasticity in compression.* European Committee for Standardization, Brussels.

EN 1996-1-1:2005 (2005). *Eurocode 6: Design of masonry structures - Part 1-1: General rules for reinforced and unreinforced masonry structures.* European Committee for Standardization, Brussels.

EN 772-1 (2011). *Methods of test for masonry units - Part 1: Determination of compressive strength.* European Committee for Standardization, Brussels.

EN 772-13 (2000). *Methods of test for masonry units - Part 13: Determination of net and gross dry density of masonry units (except for natural stone).* European Committee for Standardization, Brussels.

Fourie, J. (2017). *Characterisation and Evaluation of the Mechanical Properties of Alternative Masonry Units.* Masters Thesis, Stellenbosch University.
Available at: `http://hdl.handle.net/10019.1/100880`

Fried, A.N. (1997). A Review of the Techniques To Determine the Tensile Flexural Strength of Masonry. In: *11th International Brick/Block Masonry Conference*, pp. 170–180. Shanghai.

Gairns, D.A. (1983). *Flexural Behaviour of Concrete Blockwork Panels.* Masters Thesis, University of Melbourne.

Gairns, D.A. and Scrivener, J. (1987). The Flexural Stregth of Concrete Block and Clay Brick Masonry Panels. In: *First National Structural Engineering Conference: Preprints of Papers*, pp. 197–202. Institution of Engineers, Melbourne, Australia.

GB 50003-2011 (2011). *Code for the Design of Masonry Structures.* Ministry of Housing and Urban-Rural Development of the People's Republic of China, Beijing.

Glukhovsky, V.D. (1965). *Soil silicates: their properties, technology and manufacturing and fields of application.* Doctoral Thesis, Civil Engineering Institute, Kiev, Ukraine.

Goliger, A., Zuranski, J., Gizejowski, M., Gaczek, M., Retief, J., Kruger, A., Dunaiski, P., Fiszer, S. and Ćwik, M. (2013). Comparative study between Poland and South Africa wind climates, the related damage and implications of adopting the Eurocode for wind action on buildings. *Archives of Civil Engineering*, vol. 59, no. 1, pp. 51–95. ISSN 12302945.

Goliger, A.M. and Retief, J.V. (2007). Severe wind phenomena in Southern Africa and the related damage. *Journal of Wind Engineering and Industrial Aerodynamics*, vol. 95, no. 9-11, pp. 1065–1078. ISSN 01676105.

Grimm, C.T. and Tucker, R.L. (1985). Flexural strength of masonry prisms versus wall panels. *Journal of Structural Engineering (United States)*, vol. 111, no. 9, pp. 2021–2032. ISSN 07339445.

Guggisberg, R. and Thürlimann, B. (1988). Failure Criterion for Laterally Loaded Masonry Walls. In: *Eighth International Brick and Block Masonry Conference*, vol. 2, pp. 699–706. Dublin.

Horn, A. (2006). *Earth building soil analysis and adobe brick making*. Eco Design Architects & Consultants, Cape Town.

Hossain, M.M., Karim, M.R., Hossain, M.K., Islam, M.N. and Zain, M.F. (2015). Durability of mortar and concrete containing alkali-activated binder with pozzolans: A review. *Construction and Building Materials*, vol. 93, pp. 95–109. ISSN 09500618. Available at: `http://dx.doi.org/10.1016/j.conbuildmat.2015.05.094`

Jiao, Z., Wang, Y., Zheng, W., Huang, W. and Zhao, Y. (2019 aug). Bond properties of alkali-activated slag concrete hollow block masonry with different mortar strength grades. *Construction and Building Materials*, vol. 216, pp. 149–165. ISSN 09500618. Available at: `https://doi.org/10.1016/j.conbuildmat.2019.05.007https://linkinghub.elsevier.com/retrieve/pii/S0950061819311663`

Johansen, K.W. (1962). *Yield-line theory*. Cement and Concrete Association, London.

Kelvin, O.O., Edson, M.L. and Golden, M. (2017). Thermal, economic and environmental analysis of a low-cost house in Alice, South Africa. *Sustainability (Switzerland)*, vol. 9, no. 3, pp. 1–20. ISSN 20711050.

Kruger, A.C. (2011). *Wind Climatology of South Africa Relevant to the Design of the Built Environment*. Dissertation, Stellenbosch University.

Kühl, H. (1908). *Verfahren zur Herstellung von Zement aus Hochofenschlacke*. German Patent.

Lawrence, S. and Marshall, R. (2000). Virtual Work Design Method for Masonry Panels under Lateral Load. In: *12th International Brick/Block Masonry Conference*, pp. 1063–1073.

Lawrence, S.J. (1983). *Behaviour of Brick Masonry Walls under Lateral Loading*. Ph.D. thesis, University of New South Wales.

Lawrence, S.J. (1995). The Behaviour of Masonry in Horizontal Flexure. In: *Proceedings of the 7th Canadian Masonry Symposium*, pp. 525–536. Hamilton, Ontario.

Lawrence, S.J. and Marshall, R. (1998). The new AS3700 approach to lateral load design. In: *5th Australasian Masonry Conference*. Gladstone, Queensland, Australia.

Lawrence, S.J. and Marshall, R.J. (1996). Virtual work approach to design of masonry walls under lateral loading. Tech. Rep. DRM429, CSIRO Division of Building, Construction and Engineering.

Lourenço, P.B., Barros, J.O. and Oliveira, J.T. (2004). Shear testing of stack bonded masonry. *Construction and Building Materials*, vol. 18, no. 2, pp. 125–132. ISSN 09500618.

Malkanthi, S.N., Balthazaar, N. and Perera, A.A. (2020). Lime stabilization for compressed stabilized earth blocks with reduced clay and silt. *Case Studies in Construction Materials*, vol. 12, p. e00326. ISSN 22145095.
Available at: https://doi.org/10.1016/j.cscm.2019.e00326

Mallin, M. (2019). Do we realise that buildings are beyond the scope of our codes in many cases? *Civil Engineering : Magazine of the South African Institution of Civil Engineering*, vol. 27, no. 2, pp. 14–17.

Maluf, D., Parsekian, G. and Shrive, N. (2008). An Investigation of Out-of-Plane Loaded Unreinforced Masonry Walls Design Criteria. In: Masia, M. (ed.), *14th Brick & Block Masonry Conference*, pp. 28–37.

Midzi, V., Manzunzu, B., Mulabisana, T., Zulu, B.S., Pule, T. and Myendeki, S. (2020). Probabilistic seismic hazard maps for South Africa. *Journal of African Earth Sciences*, vol. 162, no. May 2019, p. 103689. ISSN 18791956.
Available at: https://doi.org/10.1016/j.jafrearsci.2019.103689

Nagaraj, H.B. and Shreyasvi, C. (2017). Compressed Stabilized Earth Blocks Using Iron Mine Spoil Waste - An Explorative Study. *Procedia Engineering*, vol. 180, pp. 1203–1212. ISSN 18777058.
Available at: http://dx.doi.org/10.1016/j.proeng.2017.04.281

Ng, C.L. (1996). *Experimental and theoretical investigation of the behaviour of brickwork cladding panel subjected to lateral loading*. PhD Thesis, The University of Edinburgh.
Available at: https://www.era.lib.ed.ac.uk/handle/1842/290

Norton, J. (1986). *Building with Earth: A Handbook*. Intermediate Technology Development Group Limited, Rugby, UK.

Olukoya Obafemi, A.P. and Kurt, S. (2016). Environmental impacts of adobe as a building material: The North Cyprus traditional building case. *Case Studies in Construction Materials*, vol. 4, pp. 32–41. ISSN 22145095.
Available at: http://dx.doi.org/10.1016/j.cscm.2015.12.001

Omote, Y., Mayes, R.L., Chen, S.-w.J. and Clough, R.A.Y.W. (1977). A Literature Survey - Transverse Strength of Masonry Walls. Tech. Rep. March, University of California College of Engineering, Berkely, California.

Oti, J.E., Kinuthia, J.M. and Bai, J. (2009). Compressive strength and microstructural analysis of unfired clay masonry bricks. *Engineering Geology*, vol. 109, no. 3-4, pp. 230–240. ISSN 00137952.
Available at: http://dx.doi.org/10.1016/j.enggeo.2009.08.010

Parra-Saldivar, M.L. and Batty, W. (2006). Thermal behaviour of adobe constructions. *Building and Environment*, vol. 41, no. 12, pp. 1892–1904. ISSN 03601323.

Provis, J.L. (2014). Geopolymers and other alkali activated materials: Why, how, and what? *Materials and Structures/Materiaux et Constructions*, vol. 47, no. 1-2, pp. 11–25. ISSN 13595997.

Provis, J.L. and Van Deventer, J.S.J. (2009). *Geopolymers - Structure, Processing, Properties and Industrial Applications*. Woodhead Publishing.
Available at: https://app.knovel.com/hotlink/toc/id:kpGSPPIA06/geopolymers-structure/geopolymers-structure

Purdon, A.O. (1940). The action of alkalis on blast-furnace slag. *Journal of the Society of Chemical Industry*, vol. 59, no. 9, pp. 191–202.

Rigassi, V. (1985). *Compressed Earth Blocks: Manual of Production*, vol. I. Friedr. Vieweg & Sohn Verslagsgesellschaft GmbH, Braunschweig, Germany. ISBN 3528020792.

SABS 0164-1 (1980). *Code of practice - The Structural Use of Masonry: Unreinforced Masonry Walling*. South African Bureau of Standards, Pretoria.

Samarasinghe, W. and Lawrence, S.J. (1994). Behaviour of masonry under combined torsion and compression. In: *10th IB MaC MaC*, pp. 1057–1066.

SANS 10145 (2011). *Concrete masonry construction*. South African Bureau of Standards, Pretoria.

SANS 10160-1 (2018). *Basis of structural design and actions for buildings and industrial structures, Part 1: Basis of structural design*. 1st edn. South African Bureau of Standards, Pretoria.

SANS 10160-3 (2018). *Basis of structural design and actions for buildings and industrial structures, Part 3: Wind actions*. 1st edn. South African Bureau of Standards, Pretoria.

SANS 10160-4 (2017). *Basis of structural design and actions for buildings and industrial structures, Part 4: Seismic actions and general requirements*. South African Bureau of Standards, Pretoria.

SANS 10164-1 (1989). *The structural use of masonry, Part 1: Unreinforced masonry walling*. South African Bureau of Standards, Pretoria.

SANS 10400 (2010). *The Application of the National Building Regulations*. South African Bureau of Standards, Pretoria.

SANS 10400-B (2012). *The application of the National Building Regulations Part B : Structural design*. Pretoria.

SANS 1215 (2008). *Concrete Masonry Units*. 1st edn. South African Bureau of Standards, Pretoria.

SANS 201 (2008). *Sieve analysis, fines content and dust content of aggregates*. 2nd edn. South African Bureau of Standards, Pretoria.

SANS 227 (2007). *Burnt Clay Masonry Units*. 4th edn. South African Bureau of Standards, Pretoria.

SANS 285 (2010). *Calcium Silicate Masonry Units*. 3rd edn. South African Bureau of Standards, Pretoria.

SANS 3001-GR30 (2015). *Civil engineering test methods, Part GR30: Determination of the maximum dry density and optimum moisture content*. 1st edn. South African Bureau of Standards, Pretoria.

SANS 50771-3 (2015). *Specification for masonry units, Part 3: Aggregate concrete masonry units (Dense and lightweight aggregates)*. 1st edn. South African Bureau of Standards, Pretoria.

SANS 50771-4 (2007). *Specification for masonry units, Part 4: Autoclaved aerated concrete masonry units*. 1st edn. South African Bureau of Standards, Pretoria.

SANS 51196-1-1 (2018). *Eurocode 6: Design of masonry structures - Part 1-1: General rules for reinforced and unreinforced masonry structures*. 1st edn. South African Bureau of Standards, Pretoria.

SANS 5844 (2014). *Particle and relative densities of aggregates*. 2nd edn. South African Bureau of Standards, Pretoria.

Sarangapani, G., Venkatarama Reddy, B.V. and Jagadish, K.S. (2002). Structural characteristics of bricks, mortars and masonry. *Journal of Structural Engineering (Madras)*, vol. 29, no. 2, pp. 101–107. ISSN 09700137.

Sassoni, E., Mazzotti, C. and Pagliai, G. (2014). Comparison between experimental methods for evaluating the compressive strength of existing masonry buildings. *Construction and Building Materials*, vol. 68, pp. 206–219. ISSN 09500618.
Available at: `http://dx.doi.org/10.1016/j.conbuildmat.2014.06.070`

Schmidt, M. (2020). *The tensile and shear characterisation of the joint interface of alternative masonry*. Master's Thesis, Stellenbosch University.
Available at: `http://hdl.handle.net/10019.1/107818`

Shiso, E.P. (2019). *In-Plane Structural Response of Single-Storey Unreinforced Walls Constructed Using Alternative Masonry Units*. Master's Thesis, Stellenbosch University.
Available at: `http://scholar.sun.ac.za/handle/10019.1/105889`

Sinha, B. (1980). An ultimate load analysis of laterally loaded brickwork panels. *International Journal of Masonry Construction*, vol. 1, no. 2, pp. 57–61.

Sinha, B.P. (1978). A simplified ultimate load analysis of laterally loaded model orthotropic brickwork panels of low tensile strength. *Structural Engineer*, vol. 56 B, no. 4, pp. 81–84.

Sinha, B.P., Ng, C.L. and Pedreschi, R.F. (1997). Failure criterion and behavior of brickwork in biaxial bending. *Journal of Materials in Civil Engineering*, vol. 9, no. 2, pp. 70–75. ISSN 08991561.

Sorrentino, L., D'Ayala, D., de Felice, G., Griffith, M.C., Lagomarsino, S. and Magenes, G. (2017). Review of Out-of-Plane Seismic Assessment Techniques Applied To Existing Masonry Buildings. *International Journal of Architectural Heritage*, vol. 11, no. 1, pp. 2–21. ISSN 15583066.

Statistics South Africa (2016). *Community Survey 2016 in Brief*. Report No. 03-03-06, Statistics South Africa, Pretoria.

Taylor-Firth, A. and Taylor, I.F. (1990). A bond tensile strength test for use in assessing the compatibility of Brick/Mortar interfaces. *Construction and Building Materials*, vol. 4, no. 2, pp. 58–63. ISSN 09500618.
Available at: `https://linkinghub.elsevier.com/retrieve/pii/095006189090001H`

Thomas, R., Ye, H., Radlinska, A. and Peethamparan, S. (2016). Alkali-Activated Slag Cement Concrete. *Concrete International*, vol. 38, no. 1. ISSN 0162-4075.

Vaculik, J. (2012). *Unreinforced masonry walls subjected to out-of-plane seismic actions*. Ph.D. thesis, The University of Adelaide.

Vaculik, J. and Griffith, M.C. (2018). Out-of-plane shaketable testing of unreinforced masonry walls in two-way bending. *Bulletin of Earthquake Engineering*, vol. 16, no. 7, pp. 2839–2876. ISSN 15731456.
Available at: `https://doi.org/10.1007/s10518-017-0282-8`

Venkatarama Reddy, B. (2012). Stabilised Soil Blocks for Structural Masonry in Earth Construction. In: Hall, M.R., Lindsay, R. and Krayenhoff, M. (eds.), *Modern Earth Buildings - Materials, Engineering, Construction and Applications*, chap. 13. Woodhead Publishing, Cambridge. ISBN 978-0-85709-026-3.
Available at: `https://app.knovel.com/hotlink/khtml/id:kt00C553D1/modern-earth-buildings/stabilised-soil-blocks`

Venkatarama Reddy, B.V. (2009). Sustainable materials for low carbon buildings. *International Journal of Low-Carbon Technologies*, vol. 4, no. 3, pp. 175–181. ISSN 17481317.

Vermeltfoort, A.T., Martens, D.R. and Van Zijl, G.P. (2007). Brick-mortar interface effects on masonry under compression. *Canadian Journal of Civil Engineering*, vol. 34, no. 11, pp. 1475–1485. ISSN 03151468.

Willis, C.R. (2004). *Design of unreinforced masonry walls for out-of-plane loading*. PhD Thesis, University of Adelaide.
Available at: `http://hdl.handle.net/2440/22133`

Wium, J. (2010). Background to Draft SANS 10160 (2009): Part 4 Seismic Loading. *Journal of the South African Institution of Civil Engineering*, vol. 52, no. 1, pp. 20–27.

Wu, F., Li, G., Li, H.-N. and Jia, J.-Q. (2013 sep). Strength and stress-strain characteristics of traditional adobe block and masonry. *Materials and Structures*, vol. 46, no. 9, pp. 1449–1457. ISSN 1359-5997.
Available at: `http://link.springer.com/10.1617/s11527-012-9987-y`

Yang, K.H., Song, J.K. and Song, K.I. (2013). Assessment of CO2 reduction of alkali-activated concrete. *Journal of Cleaner Production*, vol. 39, pp. 265–272. ISSN 09596526.
Available at: `http://dx.doi.org/10.1016/j.jclepro.2012.08.001`

Zhang, Z., Provis, J.L., Ma, X., Reid, A. and Wang, H. (2018). Efflorescence and subflorescence induced microstructural and mechanical evolution in fly ash-based geopolymers. *Cement and Concrete Composites*, vol. 92, no. June 2015, pp. 165–177. ISSN 09589465.

Zhang, Z., Wang, H., Provis, J.L. and Reid, A. (2013). Efflorescence : A Critical Challenge for Geopolymer Applications? *In Concrete Institute of Australia's Biennial National Conference*.

Zhou, Z. (2012). *Development of bond strength in hydraulic lime mortared brickwork*. PhD Thesis, University of Bath.
Available at: `http://opus.bath.ac.uk/29559/`

Appendices

Appendix A

Flexural Test Crack Patterns

A.1 Parallel Crack Patterns: 20M Mortar

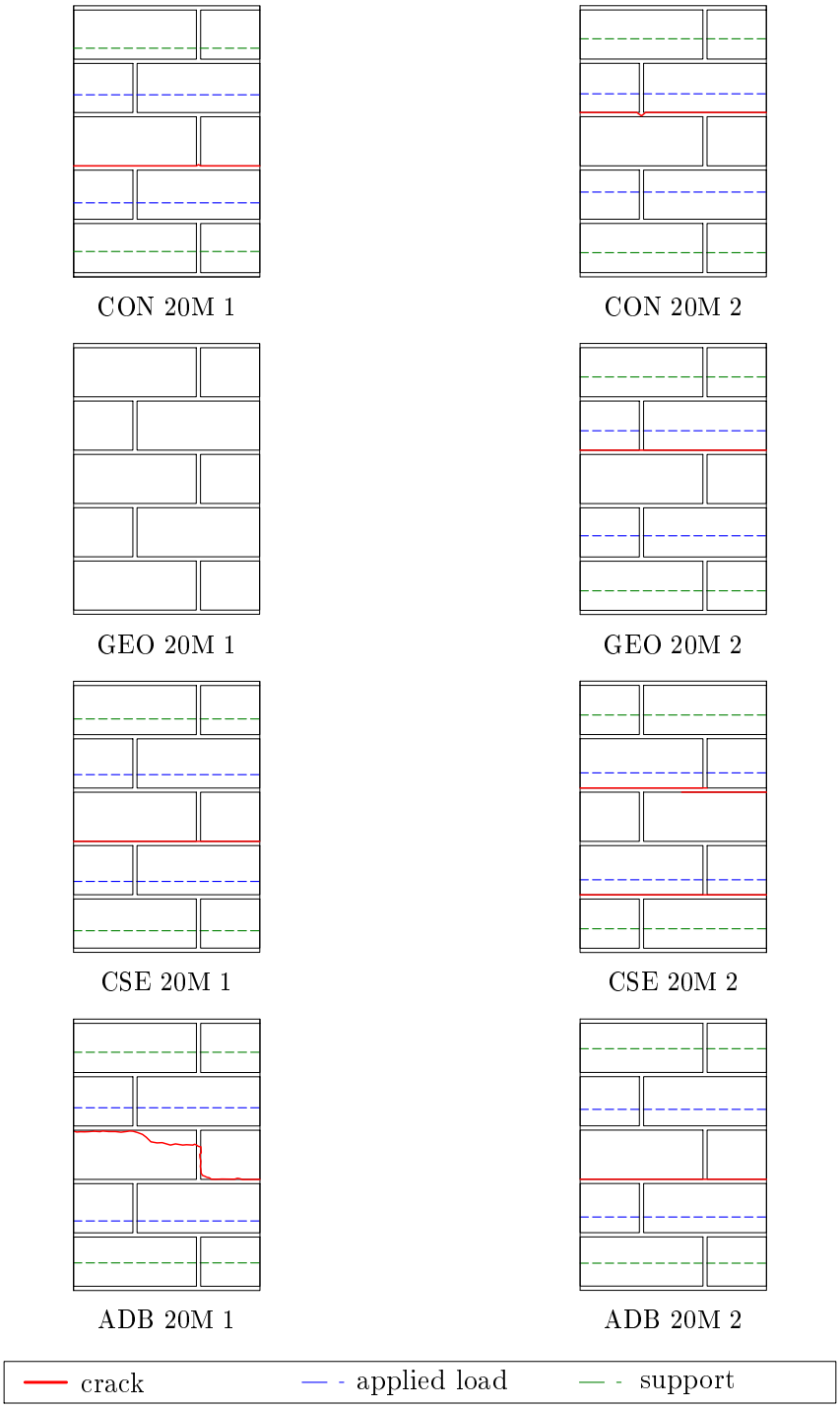

A.2 Parallel Crack Patterns: 7M Mortar

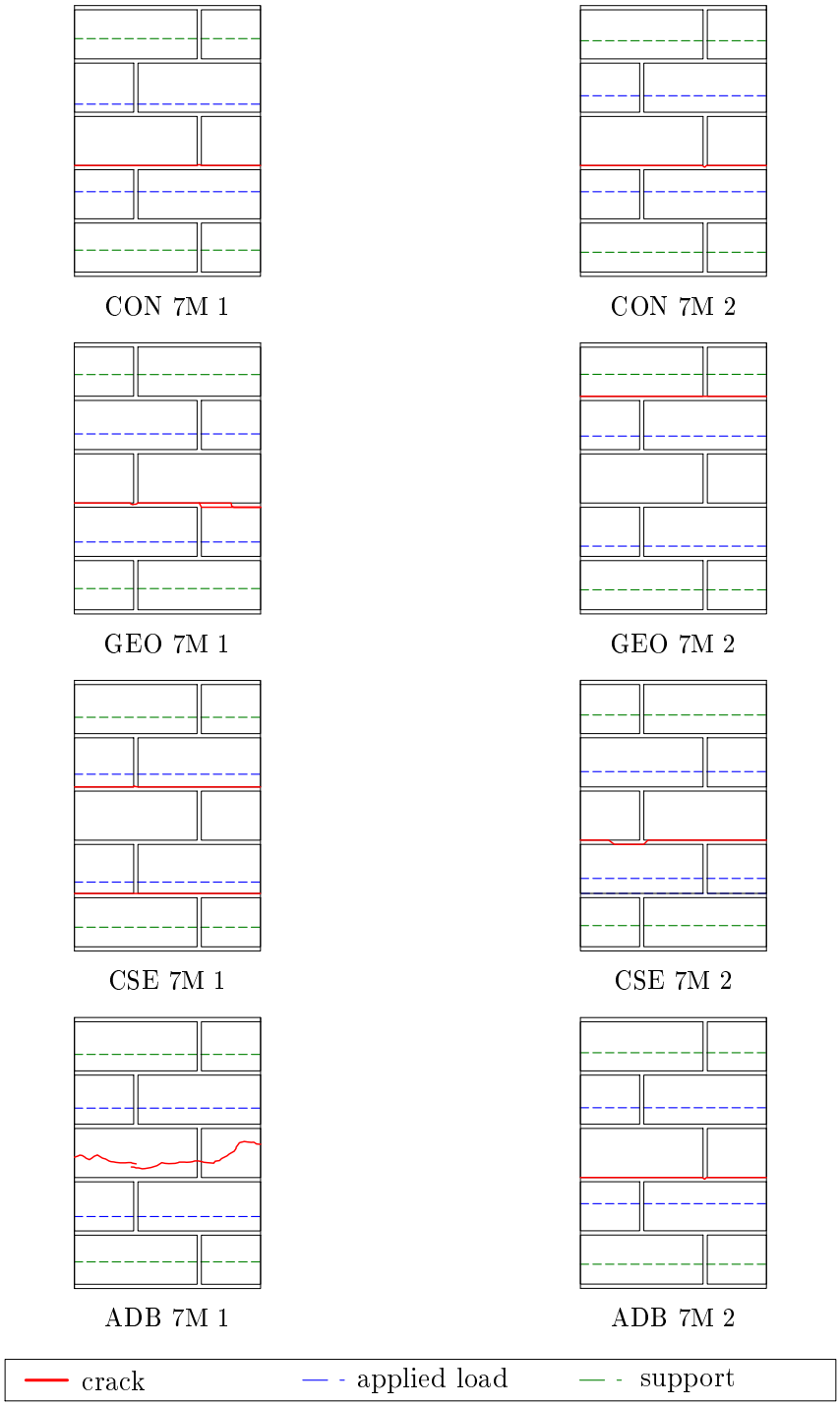

A.3 Perpendicular Crack Patterns: 20M Mortar

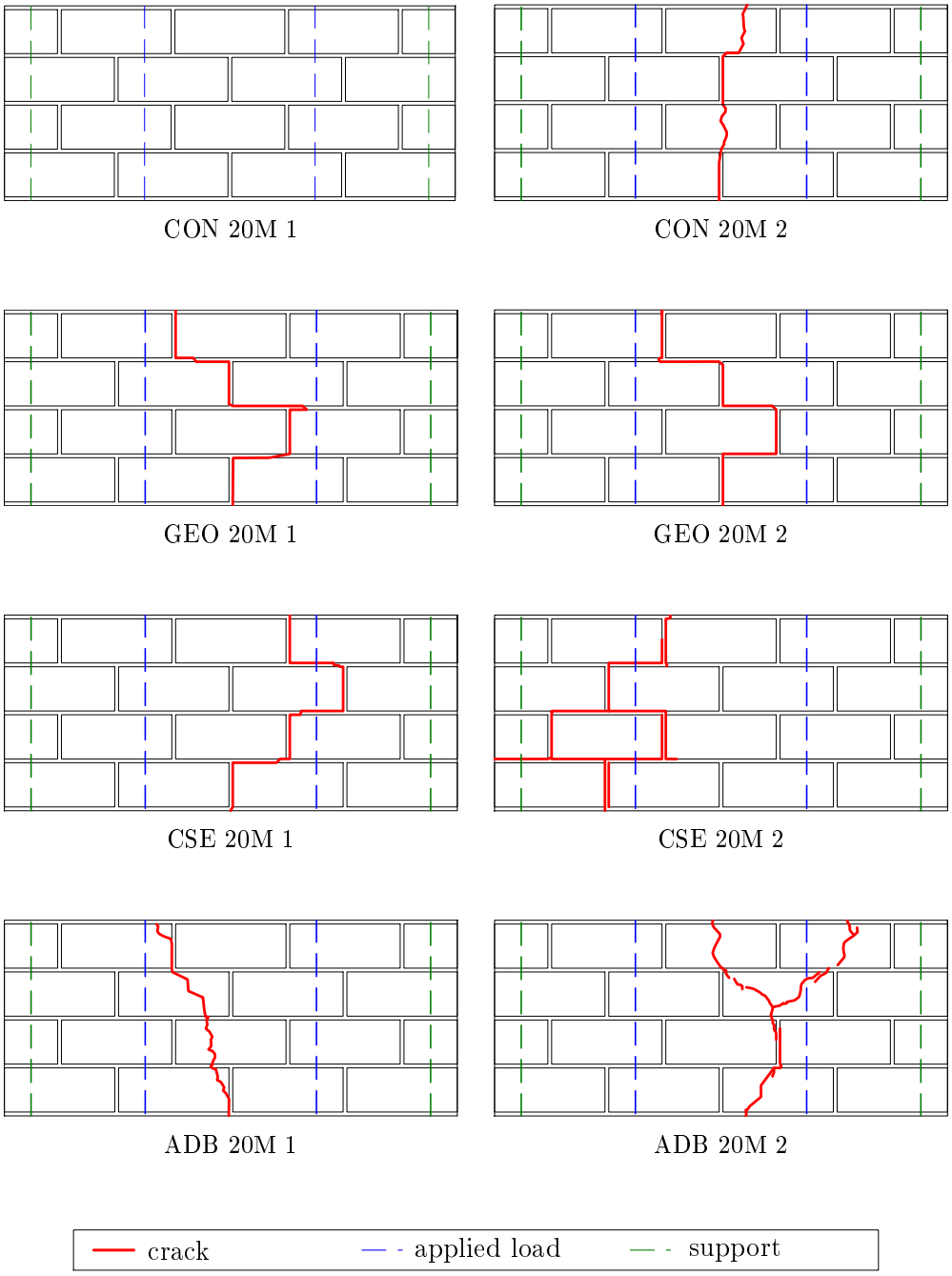

A.4 Perpendicular Crack Patterns: 7M Mortar

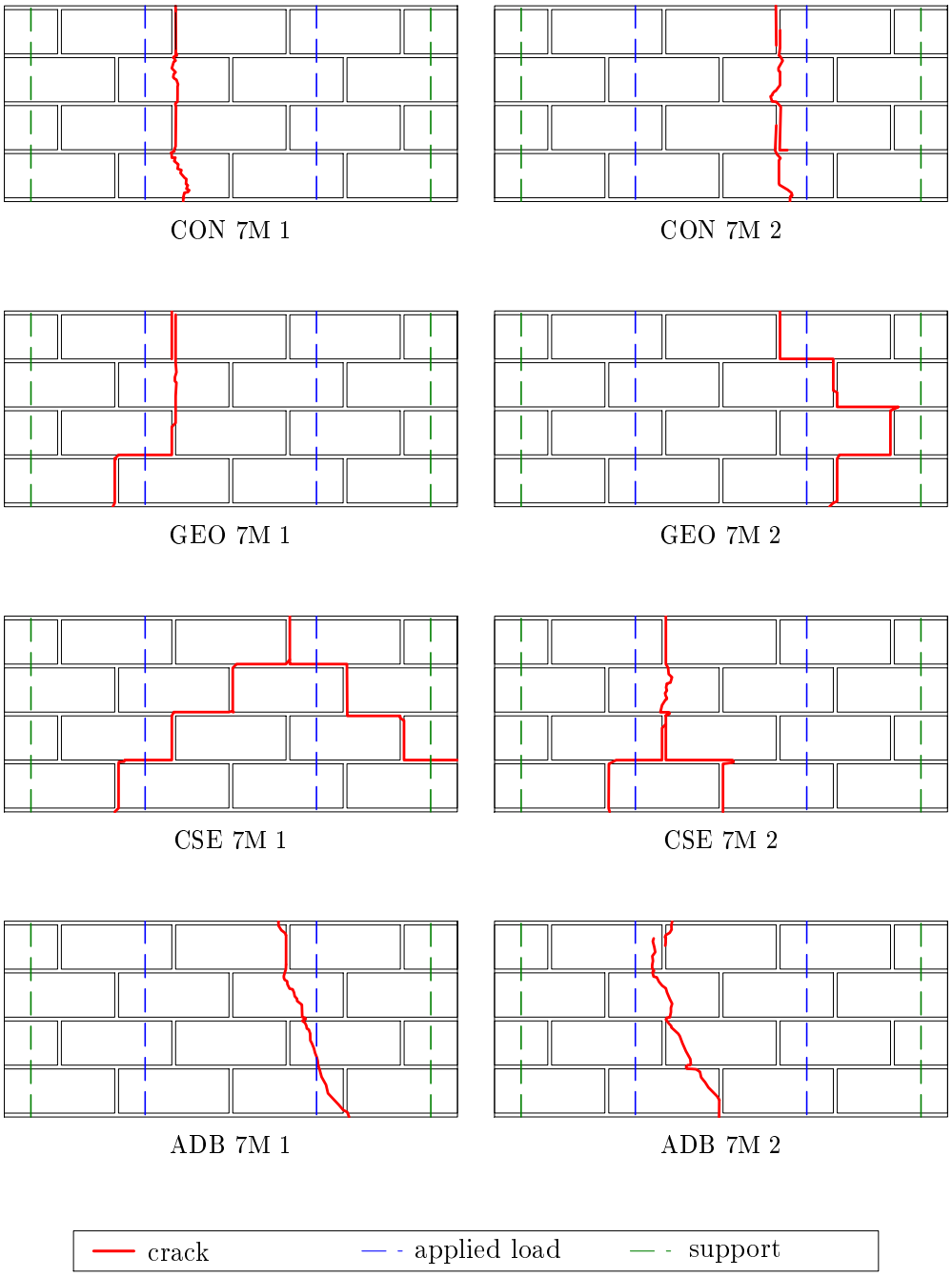

Appendix B

Flexural Test Load-Deflection Plots

B.1 Parallel Wall Load-Deflection Plots

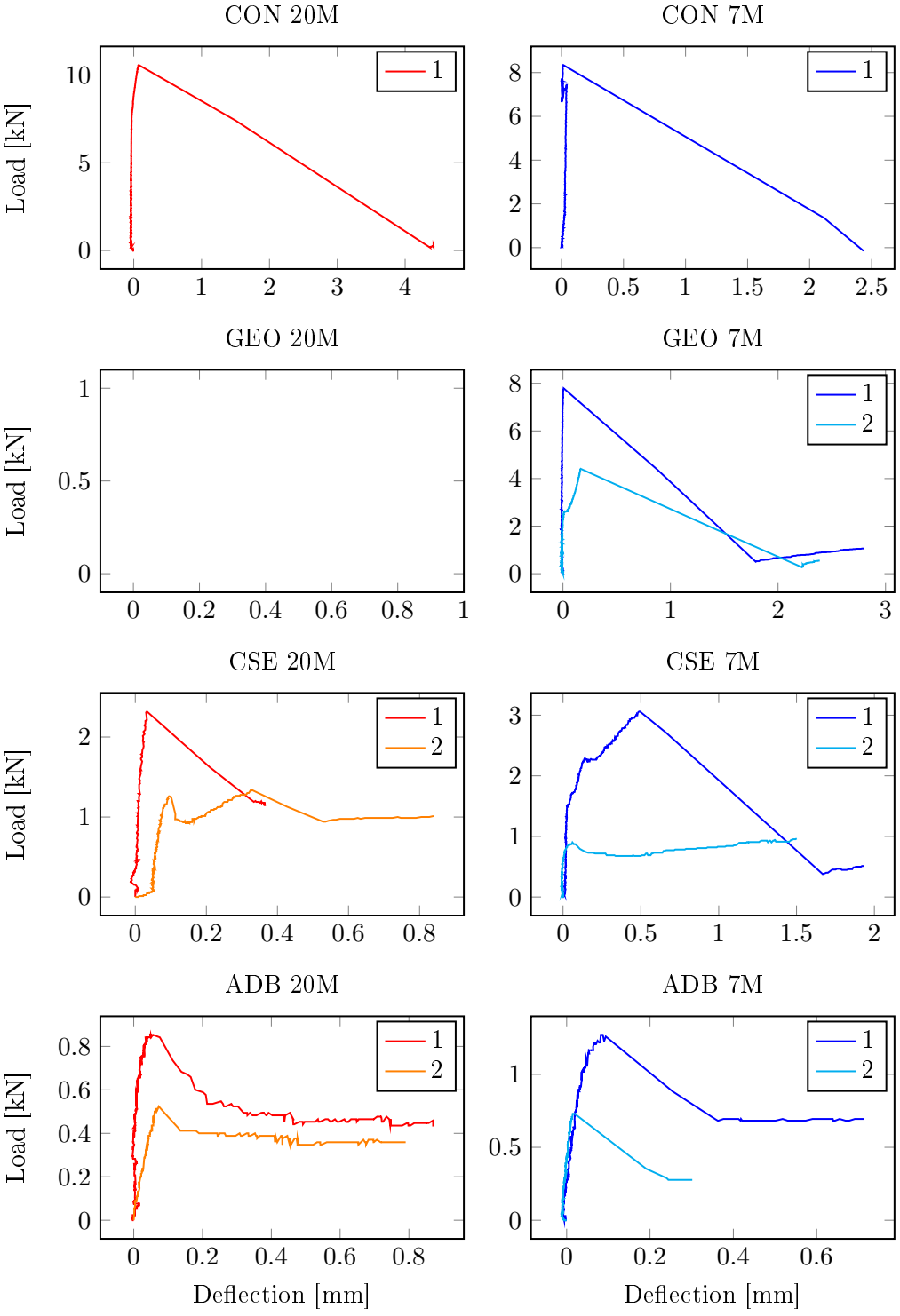

B.2 Perpendicular Wall Load-Deflection Plots